



**Università
degli Studi
di Palermo**

AREA QUALITÀ, PROGRAMMAZIONE E SUPPORTO STRATEGICO
SETTORE STRATEGIA PER LA RICERCA
U. O. DOTTORATI

Dottorato di Ricerca in Scienze della Terra e del Mare
Dipartimento di Scienze della Terra e del Mare (DiSTeM)
SSD GEO/04: Geografia Fisica e Geomorfologia

**Improving statistical methodologies for landslide susceptibility
modelling at regional and basin scale. Applications in the Sicilian and
Salvadoran territory**

LA CANDIDATA
Chiara MARTINELLO

IL COORDINATORE
Prof. Marco Milazzo

IL TUTOR
Prof. Christian Conoscenti

IL CO-TUTOR
Prof. Edoardo Rotigliano

CICLO XXXIV
ANNO ACCADEMICO 2021/2022



**Università
degli Studi
di Palermo**

AREA QUALITÀ, PROGRAMMAZIONE E SUPPORTO STRATEGICO
SETTORE STRATEGIA PER LA RICERCA
U. O. DOTTORATI

Doctoral programme in Earth and Marine Sciences
Department of Earth and Marine Sciences (DiSTeM)
SSD GEO/04: Physical Geography and Geomorphology

**Improving statistical methodologies for landslide susceptibility
modelling at regional and basin scale. Applications in the Sicilian and
Salvadoran territory**

CANDIDATE

Chiara Martinello

COORDINATOR

Prof. Marco Milazzo

TUTOR

Prof. Christian Conoscenti

CO-TUTOR

Prof. Edoardo Rotigliano

Landsliding is a worldwide problem that probably results in thousands of deaths and tens of billions of dollars of damage each year. Much of this loss would be avoidable if the problem were recognized early.

Landslides are generally more manageable and predictable than earthquakes, volcanic eruptions, and some storms, but only a few countries have taken advantage of this knowledge to reduce landslide hazards...

Prof. Earl E. Brabb, 1991

Summary

1.	Introduction.....	3
2.	Theoretical background	6
2.1.	Landslides	6
2.1.1.	Landslide classification.....	6
2.1.2.	Feature and geometry of a landslide	10
2.1.3.	Landslide activity and evolution	14
2.1.4.	Landslides controlling factors.....	17
2.2.	Landslide Susceptibility	18
2.2.1.	General assumptions	18
2.2.2.	Methods for landslide susceptibility evaluation: a general view	23
2.2.3.	Statistic modelling	28
2.2.3.1.	Statistical methods	30
2.2.4.	Validation schemes and tools.....	33
2.2.4.1.	Main validation schemes	33
2.2.4.2.	Main validation tools	35
2.2.4.3.	Cross-validation for model robustness and error mapping	38
2.2.5.	Mapping units and diagnostic areas.....	39
2.3.	Landslide predisposing factors.....	42
3.	Introduction to the applications	50
3.1.	Triggers	50
3.2.	Modelling and validation strategies	52

3.3.	Mapping units and susceptibility mapping.....	53
3.4.	Inventories.....	54
4.	Study areas.....	56
4.1.	El Salvador.....	56
4.1.1.	Regional setting	56
4.1.2.	Main characteristics of the studies sectors.....	63
4.2.	Sicily	72
4.2.1.	Regional setting	72
4.2.2.	Main characteristics of the study sector.....	73
5.	Applications.....	84
5.1.	Predicting the landslides triggered by the 2009 96E/Ida tropical storms in the Ilopango caldera area (El Salvador, CA): optimizing MARS-based model building and validation strategies	84
5.2.	Evaluation of debris flow susceptibility in El Salvador (CA): a comparison between Multivariate Adaptive Regression Splines (MARS) and Binary Logistic Regression (BLR).....	100
5.3.	Investigating limits in exploiting assembled landslide inventories for calibrating regional susceptibility models: a test in volcanic areas of El Salvador	108
5.4.	Optimal slope units partitioning in landslide susceptibility mapping	119
5.5.	Landform classification: a high performing mapping unit partitioning tool for landslide susceptibility assessment. A test in the Imera river basin (northern Sicily, Italy).....	130
6.	Concluding remarks.....	149
	References.....	152

1. Introduction

One of the more important tools which has been developed in the last decades for landslide risk mitigation and planning strategies has resulted from the application of GIS-supported multivariate statistical analysis for producing landslide susceptibility maps.

Stochastic approaches to landslide susceptibility assessment are based on the hypothesis that the new slope failures will occur under the same conditions which caused the past landslides which are (on the field or remotely) presently recognizable. Therefore, recognizing and mapping the past landslides allow preparing inventories which can be exploited to quantitatively assess the spatial correlations between an outcome status (no landslide/landslide or stable/unstable) and a set of predictors, corresponding to those geo-environmental variables assumed as directly or indirectly involved in the morphodynamic causal relations. Stochastic approaches have the great advantage to increase at the most the need for obtaining a quantitative objective susceptibility scoring of the study areas.

Landslide susceptibility assessment through a stochastic approach is typically based on a standardized sequence of steps, consisting of i) preparation of GIS vector/raster layers, including a landslide inventory (the outcome) and a set of controlling factors (the predictors); ii) partition of the area into mapping units and assignment of the status (from the outcome layer) and the factors conditions (from the predictor's layers); iii) setting of a model building and validation strategy; iv) calibration and modelling; v) validation; vi) preparation of the final maps.

A lot of modelling methods have been made available from applied statistics in the recent decades, ranging from inferential to classification based, from Bayesian to frequentists, from bivariate to multivariate, etc. At the same time, different model building and validation strategies are adopted, depending on the type, quality and number of available landslide inventories: Chrono-validation (time partition-based), when both a calibration and a non-coeval validation inventory are available (we calibrate using one and validate using the other); Self-validation (random partition-based), when the single landslide inventory we have is randomly split into calibration and validation subset; Export/Import validation (spatial validation), when a model is calibrated in a training area and validated into a different validation area.

A very relevant component of landslide susceptibility studies is strictly dependent on the way the final maps are prepared and in particular on their final user-friendly design. In fact, despite the very high performing results which can be achieved by means of classification

and regression trees techniques implemented on a pixel-based units partition of the study area, very unmanageable prediction images are typically obtained, with the susceptibility changing in the space of a few meters, and a very black-box susceptibility model which doesn't give to the user any geomorphological reference from understanding the adequacy of the model. In this sense, optimal solutions are investigated to obtain a performing open-box model implemented on geomorphologically reasonable mapping units.

Landslide susceptibility maps allow the user to recognize in a given area the grade of the propensity of new slope failures to occur in each of the mapping units into which is partitioned. Although no indications regarding time recurrence or magnitude are explicitly given in a susceptibility map, a useful hazard interpretation of the susceptibility prediction image can be obtained, considering that landslide volume or mass and their typical velocity can be hypothesized for any given landslide type in the study area, on the basis of the features of the recognized past phenomena. At the same time, the time recurrence of landslides can be roughly estimated from its spatial frequency and known historical records. As matter of fact, low discrimination ordinal of magnitude and time recurrence assessment is largely enough for taking civil protection and land use planning decisions. Besides, landslide susceptibility maps are the basic step in a multilevel approach to complete hazard assessment and early warning system devising, as they allow to restrict to a cost/effective scale a differently unsolvable task.

The research activities which have been carried out during the PhD three years period have been designed to face some of the more relevant topics landslide susceptibility assessment issue poses: optimal mapping units extraction, low-quality landslide inventories managing, new model building and validation strategies designing, comparing and optimizing statistical modelling methods, methods for landslide susceptibility mapping. All the researches were designed so to search for the best trade-off between time/money costs and resolution, precision, reliability and adequateness of the results.

The PhD research activity has been carried out and supported by the SUFRA (“SUscettibilità da FRAna” = Landslide Susceptibility) project, funded by the Regional Basin Authority for the completing of the regional landslide susceptibility maps of Sicily, and the RIESCA project, funded by the Italian Ministry of Foreign Affairs, aimed at capacitating technics and researchers of El Salvador in the issues of Natural Hazards.

The thesis is structured into five chapters: 2 Theoretical background; 3 Introduction to the applications; 4 Study areas; 5 Applications; 6 Concluding remarks.

In the second chapter three main topics are discussed: i) landslides definition and description, with a deep analysis of the controlling factors; ii) theoretical/conceptual view of landslide susceptibility materials and methods; iii) description of main validation schemes and tools.

In the third chapter, an introduction of the main applications carried out during the three years of PhD research is given. In particular, the main topics faced by the applications are reported and a deep description of the importance of the topics is provided.

The fourth chapter is focused on the description of the study areas. An analysis of the main characteristics, including the geomorphological and lithological setting of the areas, is reported.

In the fifth chapter, the main applications related to the research are shown.

In the sixth chapter, the final discussions, and conclusions relative to the research carried out during these three years are discussed.

2. Theoretical background

2.1. Landslides

2.1.1. Landslide classification

According to a simple definition (Varnes 1978), a landslide is “a downward and outward movement of a mass of rock, debris, or earth down a slope, under the influence of gravity”. However, landslides can be considered complex phenomena, the result of the interaction of different factors that determine their characteristics. Therefore, different definitions of landslide are proposed in the literature and, due to the real high complexity of these phenomena, the scientific community has to suggest several classification schemes (e.g., Varnes 1984; Cruden and Varnes 1996; Hungr et al. 2014). In fact, landslides can involve various types of material, according to several movement mechanisms, and can occur in different climatic environments.

Given that, it is not easy (if not impossible) to limit landslides inside a single rigid grid. However, according to the scientific method, the use of a classification system is necessary to minimise ambiguity and deception.

Among the proposed classifications, in this research, the system of Hungr et al. (2014) was exploited. As the authors declare, “*the starting point of the modifications is the 1978 version of the classification (Varnes 1978), taking also into account concepts introduced by Cruden and Varnes (1996)*”, but updating the latter in some aspects, related mainly to: i) the typology of involved material and ii) the movement mechanisms. Besides, the authors suggest that a simple term needs to be assigned to a given landslide type, thus avoiding ambiguity in the definition. For this purpose, the “complex” class of Varnes was deleted, recommending a deeper analysis for this typology for a more specific classification of each phenomenon inside.

The Hungr et al. (2014) classification overcomes the threefold material division proposed by Varnes (1978). The latter considers only the rock, the debris, and the earth as typology, while Hungr et al. (2014) suggest the use of geotechnical material terminology, considered more appropriate and detailed for characterising the mechanical behaviour of the landslides. In particular, the types considered are rock, clay, silt, sand, gravel, boulders, peat, ice, debris, and mud (first column of Table 2.1.1.1).

As reported by the authors, the words “debris” and “mud” do not have clear equivalents in geotechnical terminology but have acquired status in geology and landslide science and have therefore been retained (Bates and Jackson 1984) Debris is a mixture of sand, gravel,

cobbles, and boulders, often with varying proportions of silt and clay. Mud is a similar unsorted material, but with sufficient silt and clay content to produce plasticity (cohesiveness) with high moisture content. Both debris and mud may contain a proportion of organic matter (e.g., Swanston D.N. 1974) and may be gap-graded (“diamictons”). These are materials that have been mixed from various components by geomorphic processes such as weathering (residual soil), mass wasting (colluvium), glacier transport (till or ice contact deposits), explosive volcanism (granular pyroclastic deposits), or human activity (e.g., fill or mine spoil).

The second column of Table 2.1.1.1 is proposed by the authors as supplementary terms for a better description of the main material (if necessary). The third column gives a brief description of the main characteristics of each material, while the last two columns report the corresponding soil classes (the 4th) and the geotechnical indices which allow objectively to determine the case (the 5th).

Material name	Character descriptors (if important)	Simplified field description for the purposes of classification	Corresponding unified soil classes	Laboratory indices (if available)
Rock	Strong	Strong-broken with a hammer		UCS>25 MPa
	Weak	Weak-peeled with a knife		2<UCS<25 MPa
Clay	Stiff	Plastic, can be moulded into standard thread when moist, has dry strength	GC, SC, CL, MH, CH, OL, and OH	Ip > 0.05
	Soft			
	Sensitive			
Mud	Liquid	Plastic, unsorted remoulded, and close to Liquid Limit	CL, CH, and CM	Ip>0.05 and Il>0.5
Silt, sand, gravel, and boulders	Dry	Nonplastic (or very low plasticity), granular, sorted. Silt particles	ML	Ip<0.05
	Saturated		SW, SP, and SM	
	Partly saturated		GW, GP, and GM	
Debris	Dry	Low plasticity, unsorted and mixed	SW-GW	Ip<0.05
	Saturated		SM-GM	
	Partly saturated		CL, CH, and CM	
Peat		Organic		
Ice		Glacier		

Figure 2.1.1.1: Landslide-forming material types (modified from Hungr et al., 2014).

Regarding the type of movement, Hungr et al. (2014) propose six main movement mechanisms, giving a deeper description of specific landslide types, according to the material involved.

Table 2.1.1.2 summarizes the movement types proposed by the authors. Below is a brief description of all main movement mechanisms and a more specific description of the landslide types which have been faced in this research, directly based on the definition of Hungr et al. (2014).

Type of movement	Rock	Soil
Fall	<i>Rock/ice fall^a</i>	<i>Boulder/debris/silt fall^a</i>
Topple	Rock block topple ^a	<i>Gravel/sand/silt topple^a</i>
	Rock flexural topple	
Slide	Rock rotational slide	<i>Clay/silt rotational slide</i>
	Rock planar slide ^a	<i>Clay/silt planar slide</i>
	Rock wedge slide ^a	<i>Gravel/sand/silt slide^a</i>
	Rock compound slide	<i>Clay/silt compound slide</i>
	Rock irregular slide ^a	
Spread	Rock slope spread	<i>Sand/silt liquefaction spread^a</i>
		<i>Sensitive clay spread^a</i>
Flow	Rock/ice avalanche ^a	<i>Sand/silt/debris dry flow</i>
		<i>Sand/silt/debris flowslide^a</i>
		<i>Sensitive clay flowslide</i>
		Debris flow
		Mud flow
		Debris flood
		Debris avalanche
		Earthflow
		Peat flow
Slope deformation	Mountain slope deformation	Soil slope deformation
	Rock slope deformation	Soil creep
		Solifluction

Figure 2.1.1.2: Summary of the proposed new version of the Varnes classification system. The words in italics are placeholders. ^a Movement type that usually reaches extremely rapid velocities as defined by Cruden and Varnes (1996). The other landslide types are usually (but not always) extremely slow to very rapid (modified from Hungr et al. 2014).

- a) Fall: phenomena characterised by the detachment of material from a steep slope or cliff, through discontinuities of different nature. Based on the inclination and morphological characteristics of the base of the slope, the movement of the detached

mass occurs by free-fall and/or by "jumps and bounces", to run out with the disintegration of the mass into blocks of different sizes. Both the two types of falls identified by the authors are analysed in this research:

- 1 Rock fall: detachment, fall, rolling and bouncing of rock or ice fragments. May occur singly or in clusters, but there is little dynamic interaction between the most mobile moving fragments, which interact mainly with the substrate (path).
 - 2 Boulder fall: detachment, fall, rolling, and bouncing of soil fragments such as large clasts in soil deposits, or blocks of cohesive (cemented or unsaturated) soil. The mechanism of propagation is similar to rockfall, although impacts may be strongly reduced by the weakness of the moving particles.
- b) Topples: phenomena characterised by the detachment of material from a steep slope or cliff, through discontinuities of different nature. The detached mass rotates around some pivotal point, below or low in the mass. Only the rock block topple type is analysed in this research.
- 3 Rock block topple: forward rotation and overturning of rock columns or plates (one or many), separated by steeply dipping joints. The rock is relatively massive, and rotation occurs on well-defined basal discontinuities. Movement may begin slowly, but the last stage of failure can be extremely rapid. Occurs at all scales.
- c) Slide: phenomena where a weak mass slides, separating from a more stable underlying material. In this research, the following typologies are detected:
- 4 Clay/silt rotational slide ("soil slump"): Sliding of a mass of (homogeneous and usually cohesive) soil on a rotational rupture surface. Little internal deformation. Prominent main scarp and back-tilted landslide head. Normally slow to rapid but may be extremely rapid in sensitive or collapsible soils.
 - 5 Clay/silt planar slide: Sliding of a block of cohesive soil on an inclined planar rupture surface, formed by a weak layer (often pre-sheared). The head of the slide mass separates from stable soil along a deep tension crack (no active wedge). May be slow or rapid.
 - 6 Gravel/debris slide: Sliding of a mass of granular material on a shallow, planar surface parallel with the ground. Usually, the sliding mass is a veneer of colluvium, weathered soil, or pyroclastic deposits sliding over a stronger

substrate. Many debris slides become flow-like after moving a short distance and transform into extremely rapid debris avalanches.

- d) Spread: phenomena characterised by lateral extension of material along very gentle slopes or flat terrain. The slope failure is linked to the liquefaction of a ductile lithotype underlined a brittle lithotype, which begins to break into blocks. The landslide is so characterized by blocks and plastic/liquefied material spread along the slope. Spread type is not analysed in this research.
- e) Flows: rapid to very rapid movements of a mixture composed of air, water, and sediments of varying sizes. Hungr et al. (2014) distinguish ten different types of flows based on the involved material. In this research, the following are detected:
 - 7 Sand/silt/debris flowslide: very rapid to extremely rapid flow of sorted or unsorted saturated granular material on moderate slopes, involving excess pore-pressure or liquefaction of material originating from the landslide source. The material may range from loose sand to loose debris (fill or mine waste), loess, and silt. Usually originates as a multiple retrogressive failure. May occur subaerially, or underwater.
 - 8 Debris flow: very rapid to extremely rapid surging flow of saturated debris in a steep channel. Strong entrainment of material and water from the flow path.
 - 9 Mud flow: Very rapid to extremely rapid surging flow of saturated plastic soil in a steep channel, involving significantly greater water content relative to the source material. Strong entrainment of material and water from the flow path (Plasticity Index > 5 %).
 - 10 Earthflow: Rapid or slower, intermittent flow-like movement of plastic, clayey soil, facilitated by a combination of sliding along multiple discrete shear surfaces, and internal shear strains. Long periods of relative dormancy alternate with more rapid “surges”.
- f) Slope deformation: large-scale gravitational deformation of steep, high mountain slopes, valleys, or hill slopes. Usually, they are very slow. This type of landslide is not detected in this research.

2.1.2. Feature and geometry of a landslide

The landslides are characterised by specific features. A nomenclature for these features, largely accepted in the literature, is proposed by Cruden & Varnes (1996) and reported

below. Figure 2.1.2.1 shows the original schemes proposed by the authors for the position of these features in an earth slide.

- Crown (1): the non displaced material adjacent to the highest parts of the main scarp;
- main scarp (2): the steep surface on undisturbed ground at the upper edge of the landslide area caused by movement of the displaced material (13) away from the undisturbed ground. It is the visible part of the surface of rupture (10);
- top (3): the highest point of contact between the displaced material (13) and the main scarp (2);
- head (4): the upper parts of a landslide along the contact between the displaced material and the main scarp (2);
- minor scarp (5): the steep surface on the displaced material of a landslide produced by differential movements within the displaced material;
- main body (6): the part of displaced material of a landslide that overlies the surface of rupture between the main scarp (2) and the toe of the surface of rupture (11);
- foot (7): the portion of a landslide that has moved beyond the toe of the surface of rupture (11) and overlies the original ground surface (20);
- tip (8): the point on toe (9) farthest from the top (3) of a landslide;
- toe lower (9): usually curved margin of the displaced material of a landslide, most distant from the main scarp (2);
- surface of rupture (10): the surface which forms (or which has formed) the lower boundary of the displaced material (13) below original ground surface (20);
- toe of surface of rupture (11): the intersection (usually buried) between the lower part of the surface of rupture (10) of the landslide and the original ground surface (20);
- surface of separation (12): the part of the original ground surface (20) now overlain by the foot (7) of a landslide;
- displaced material (13): the material displaced from its original position on the slope by movement in a landslide; forms both the depleted mass (17) and the accumulation (18);
- zone of depletion (14): the area of a landslide within which the displaced material (13) lies below the original ground surface (20);
- zone of accumulation (15): the area of a landslide within which the displaced material lies above the original ground surface (20);

- depletion (16): the volume bounded by the main scarp (2), the depleted mass (17), and the original ground surface (20);
- depleted mass (17): the volume of displaced material that overlies the surface of rupture (10) but underlies the original ground surface (20);
- accumulation (18): the volume of displaced material (13) that lies above the original ground surface (20);
- flank (19): the undisplaced material adjacent to sides of the surface of rupture. Compass directions are preferable in describing the flanks, but if left and right are used, they refer to the flanks as viewed from the crown;
- original ground surface (20): the surface of the slope that existed before a landslide took place.

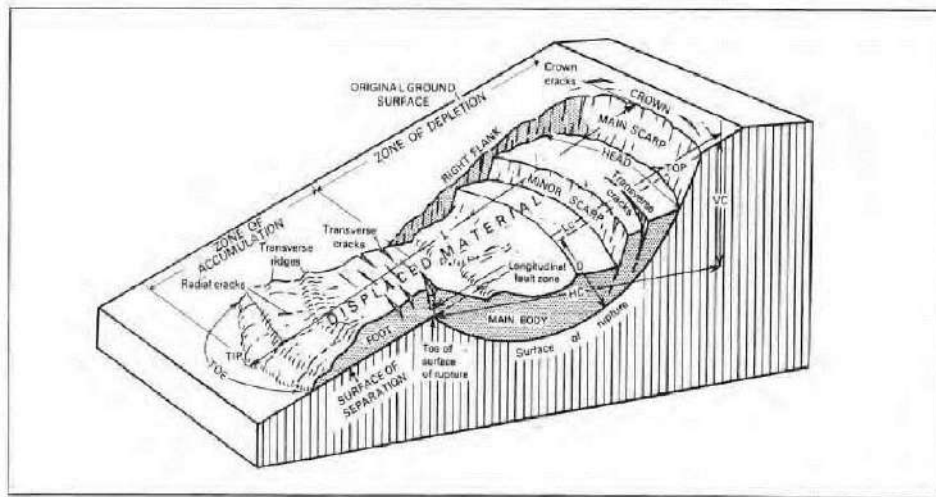


Figure 2.1.2.1: Main element of idealized complex earth slide-earth flow (modified from Cruden and Varnes 1996)

Theoretically, the feature described above is common to all types of landslides. However, it is not simply recognising all the features in all types of slope failures (e.g., falls).

Furthermore, starting from the nomenclature established by the IAEG Commission on Landslides (1990), Cruden and Varnes (1996) update the list of morphometric parameters of a landslide. The original definition of these parameters is reported in Table 2.1.2.1 and shown in Figure 2.1.2.2.

NUMBER	NAME	DEFINITION
1	Width of displaced mass, W_d	Maximum breadth of displaced mass perpendicular to length, L_d
2	Width of surface of rupture, W_t	Maximum width between flanks of landslide perpendicular to length, L_t
3	Length of displaced mass, L_d	Minimum distance from tip to top
4	Length of surface of rupture, L_r	Minimum distance from toe of surface of rupture to crown
5	Depth of displaced mass, D_d	Maximum depth of displaced mass measured perpendicular to plane containing W_d and L_d
6	Depth of surface of rupture, D_r	Maximum depth of surface of rupture below original ground surface measured perpendicular to plane containing W_r and L_r .
7	Total length, L	Minimum distance from tip of landslide to crown
8	Length of center line, L_{cl}	Distance from crown to tip of landslide through points on original ground surface equidistant from lateral margins of surface of rupture and displaced material

Table 2.1.2.1: definition of landslide dimension (modified from Cruden and Varnes 1996)

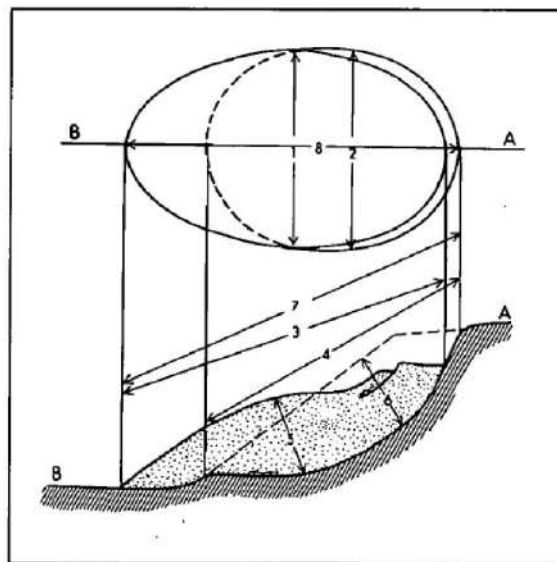


Figure 2.1.2.2: Landslide dimension: upper portion, plan of typical landslide in which dashed line is trace of rupture surface on original ground surface; lower portion, section in which hatching indicates undisturbed ground, stippling shows extent of displaced material, and broken line is original ground surface (modified from Cruden and Varnes 1996)

2.1.3. Landslide activity and evolution

A landslide is a physical system that develops in time through several stages (e.g., Terzaghi 1950; Leroueil et al. 2012). As reviewed by Skempton and Hutchinson (1969), the history of a mass movement comprises pre-failure deformations, failure itself and post-failure displacements. Many landslides exhibit several movement episodes, separated by long or short periods of relative quiescence. The evolution of a landslide can be evaluated considering the following aspects (Cruden and Varnes 1996):

- i. *State of Activity*, which describes what is known about the timing of movements;
- ii. *Distribution of Activity*, which describes broadly where the landslide is moving;
- iii. *Style of Activity*, which indicates the manner in which different movements contribute to the landslide.

The state of activity of a landslide describes, through geomorphological and historical information, the temporal evolution of a slope failure. According to the morphodynamic indications suggested by the recognized feature or by historical documents and data and referring to the time of recognition of the phenomenon, the authors suggest the following terms define a landslide:

- a) *active*: those landslides currently moving;
 1. *new activation*;
 2. *reactivations*
 - i. *reactivated*: landslide that is again active after being inactive;
 - ii. *suspended*: landslides that have moved within the last annual cycle of seasons but that are not moving at present;
- b) *inactive*: landslides which last activity happened more than one annual cycle of seasons ago.
 1. *dormant*: inactive landslide that can be reactivated by the original trigger;
 2. *natural abandoned*: inactive landslide that cannot be reactivated from its original causes;
 3. *stabilised*: if by artificial remedial measures the movement of the landslides have been stopped;
 4. *relict*: landslides that have clearly developed under different geomorphological or climatic conditions, perhaps thousands of years ago, so a reactivation due to the original or other causes is not possible.

It is important to note that if erosion moves the newly acquired equilibrium of a slope failure, landsliding can restart, consequently transforming a dormant/inactive landslide into an active one.

For this reason, in light of the predictational perspective of the topics of this research, all the recognizable landslides were grouped in the same dormant/active undifferentiated class, as they share the same meaning and suitability for calibrating susceptibility models.

The distribution of the activity of a landslide refers to diachronic multi-storied landslides, expressing the past spatial evolution of the slope failure rupture surface. This type of characterization, in the hypothesis of continuity of the movement, can also provide information about the future evolution of the phenomenon. The distribution of the activity of a landslide is distinguished in the following classes (Figure 2.1.3.1):

1. *advancing*: if the surface of rupture is extending in the direction of movement;
2. *retrogressive*: if the surface of rupture is extending in the direction opposite the movement of the displaced material;
3. *widening*: if the surface of rupture is extending at one or both lateral margins;
4. *enlarging*: if the movement can be limited to the displacing material or the surface of rupture;
5. *progressive*: if the surface of rupture of the landslide is enlarging in two or more directions;
6. *confined*: if movements have a scarp but no visible surface of rupture in the foot of the displaced mass;
7. *diminishing*: active landslide in which the volume of material being displaced is decreasing with time seems free of undesired implications;
8. *moving*: a landslide in which displaced materials continue to move but whose surface of rupture shows no visible changes.

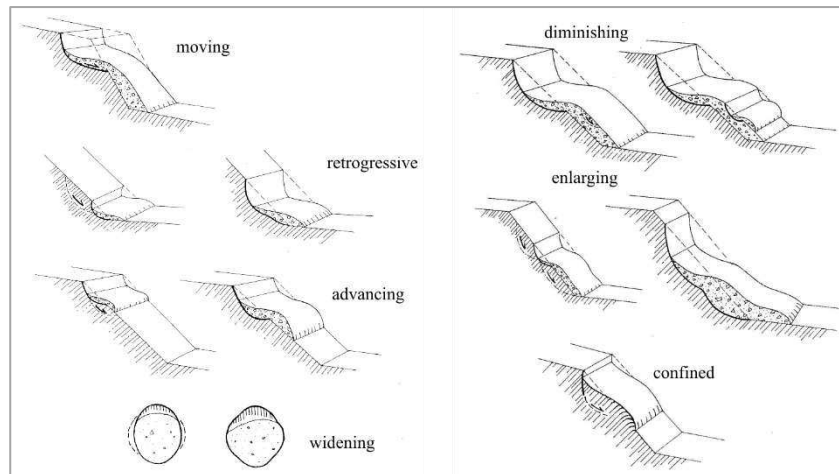


Figure 2.1.3.1: distribution of activity of a landslide (modified from Amanti et al. 2001).

The style of the activity of a landslide (figure 2.1.3.2) describes the way in which different movements contribute to the same single or multi-storied landsliding. The type of style can be:

- a) *single*: when the failure is characterised by a single movement;
- b) *complex*: if the failure is characterised by the combination, in temporal sequence, of two or more types of movement;
- a) *composite*: landslides in which different types of movement occur in different areas of the displaced mass, sometimes simultaneously;
- b) *successive*: when the recognized movement appears as a repetition of a phenomenon of the same type that occurred previously in the same portion of the slope or closely;
- c) *multiple*: landslide shows repeated movements of the same type, often following enlargement of the surface of rupture. The newly displaced masses are in contact with previously displaced masses and often share a surface of rupture with them.

It is important to note that, according to Hungr et al. (2014), in this research, all the landslides detected are reported as single phenomena. In fact, even when complex or composite phenomena are present, more information about a single event is collected.

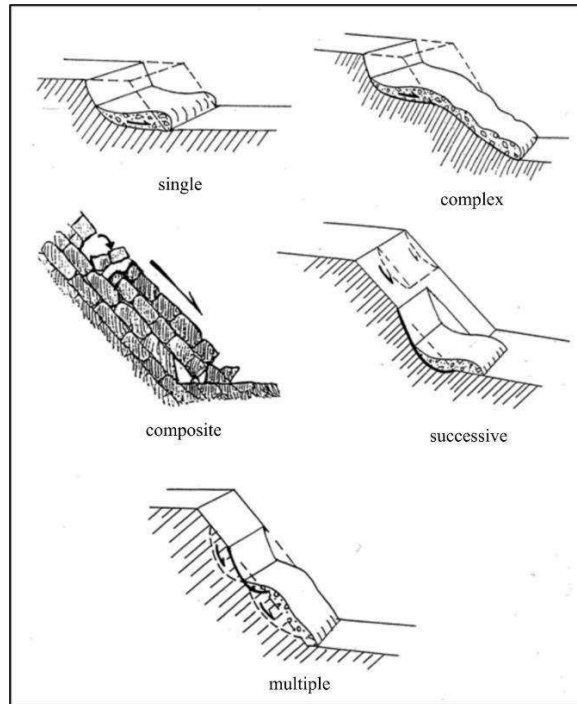


Figure 2.1.3.2: the style of activity of a landslide (modified from Amanti et al. 2001).

2.1.4. Landslides controlling factors

The assessment of landslide susceptibility requires in-depth knowledge of the controlling factors that affect slope stability, which is divided into predisposing and triggering factors. The formers correspond to the geo-environmental conditions which characterise the study area driving the landslide activity and acting constantly over time. The most important predisposing factors for slope stability are lithology and its geomechanical properties, land use, tectonics, slope morphology, and hydrogeology. Just a few of these factors actually are directly involved in the static slope equilibrium, while the majority actually act as a proxy factor.

Triggering factors are considered all impulsive causes that could modify the natural slope equilibrium causing the landslides activation. They can be extreme meteorological events (intense rainfall, and also intense wind for landslides of fall and topple type), fast snow melting, earthquakes, volcanic eruptions, anthropic actions (as alteration of the natural profile of the slope, increasing of pore pressure).

Therefore, the triggering factors cause the landslide activation due to:

- decrease of shear strength due to the variation of pore pressure (for an increase of water content and a relative decrease of cohesion or for dynamic solicitation) or loss in cohesion;

- increase of shear stress for modification of slope geometry and for natural or artificial vibrations.

Among the controlling factors, extreme meteorological events and, more in general, rapid soil saturation, represent the most common landslide triggers. Besides, soil saturation can occur according to different causes and time trends as well as the increase in water content is both predisposing and triggering factor. Indeed, the variation of pore pressures occurs due to infiltration driven by rainfalls, snow melting, changes in the coastline or in the water level of lakes, rivers, and natural or artificial dams, anthropic action. The greater the intensity of causes, the faster the increase in pore pressure and the soil saturation will transform from a predisposing factor to a triggering factor.

Earthquakes are the second most frequent type of trigger. The energy released by these events often causes the loss of cohesion of the pseudo-coherent material for a decrease in shear strength. The dilation of the material also facilitates the rapid infiltration of water and a rapid increase in neutral pressures.

2.2. Landslide Susceptibility

2.2.1. General assumptions

Landslide susceptibility is the likelihood of a landslide occurring in an area depending on local terrain conditions (Brabb 1984), consisting of the prediction of “where” landslides are more likely to occur. Therefore, the temporal probability (or time recurrence) of slope failures and their associated magnitude is not included in a landslide susceptibility evaluation, which only provides the proneness of a slope to be affected by a specific landslide typology (National Research Council 2004). Nevertheless, information about magnitude can be indirectly included by landslide susceptibility assessment if focusing on specific typologies or different-sized landslides (Carrara et al. 1995). In particular, according to their expected movement type, landslides can be subdivided into rapid/normal/slow types, as well as into surficial/shallow/deep (or regolith/substratum/bedrock) slope deformations. In this sense, a landslide susceptibility map for rotational slides, configure large medium velocity diachronic deformations, whilst fall or debris flows typically involve small very rapidly moving movements.

In mathematical language, landslide susceptibility can be defined as the probability of spatial occurrence of slope failures, given a set of geo-environmental conditions (Guzzetti et al.

2005). In common parlance, a landslide susceptibility map conveys in a nontechnical language where landslides are most likely to be a problem in the future (Brabb 1991)

In light of its definition, landslide susceptibility assessment usually inspects regional to basin-scale areas. Not surprisingly, landslide susceptibility studies have increased considerably in the last 30 years, proportionally with the growth of Geographic Information System (GIS) and computational capabilities. In fact, due to the optimization of informatics instruments, collecting, manipulating, and analysing data (predisposing factors but also landslide archives) is simpler than in the past. Also, day by day, the quality and free availability of the required input data increases exponentially so as the resolution of remotely acquired images and associated Digital Terrain Models (DTM).

As a general statement of the issue, landslide susceptibility assessment in a given area requires its partitioning into mapping units (pixels, dtm-derived terrain units, statistical multivariate unique conditions units, etc.), corresponding to homogenous domain sharing the same stability/instability conditions, and the categorical/ordinal/numerical characterization/scoring of each mapping unit through the assignment of a measure of its more or less propensity to “spatially host” a new landslide in the future.

The assessment of landslide susceptibility is based on some theoretical-scientific assumptions widely shared by the researchers. These assumptions can be synthesised in three largely agreed rules (Varnes 1984; Crozier 1986; Hutchinson 1995; Guzzetti et al. 1999, 2006):

- i. landslides leave discernible signs, most of which can be recognized, classified, and mapped in the field or from stereoscopic aerial photographs.
- ii. landslides are controlled by mechanical laws that can be determined empirically, statistically, or in a deterministic way. In light of this, the instability factors linked to slope failures can be analysed to understand which condition could cause the landslides.
- iii. for landslides, the past and present are keys to the future. According to this rephrasing of the actualism principle (Lyell, 1833), slope failures in the future will be more likely to occur under the conditions which led to past and present instability.

In view of the above, a systematic mapping of past and present slope failures can offer the tools for investigating and evaluating the areas which are more prone to landslide occurrence due to their geo-environmental conditions.

However, the success in the mapping of landslide phenomena depends on several conditions that can weaken the correctness and completeness of the derived archives. In fact, if it is true that landslides leave clearly distinguishable shapes on the ground, it is also true that timeliness in recognition is essential: the ease in identifying the typical morphologies of a landslide is considerably reduced with the increase in the time elapsed between the occurrence of the phenomenon and its mapping. This effect is obviously much more important for those types of landslides which involve limited volumes of rocks, leaving on the landscape only surficial easily blurrable signs. Over time, therefore, only an expert observer is able to correctly distinguish the forms of a failure (Petschko et al. 2014), thus also determining a non-univocity in the inventories produced by different observers (Guzzetti 2005). For flow landslides, this difficulty in recognizing phenomena can be more pronounced. In fact, for this type of slope failure, the persistence over time of the signs is considerably reduced, especially in urbanised or cropped areas (Petschko et al. 2014). The surface of rupture is in fact very small and superficial (since, almost always, the deformation affects only the regolith layer) and this implies that in a short time the shape can be cancelled by new processes of runoff water erosion. The landslide body moves along channels and its residues are quickly erased by runoff waters; at the same time, colluvial deposits tend to fill the topographic concavities. Finally, the accumulation fan can undergo different processes, from anthropic to natural actions, which cause its cancellation (Figures 2.2.1.1 and 2.2.1.2). Again, this problem grows in climatic environments that favour rapid plant growth.

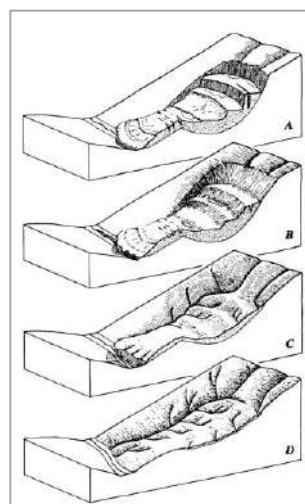


Figure 2.2.1.1: a schematic view of landslide deposits modification (from McCalpin 1984). A) Active landslide; B) Landslide features modified slightly by erosion; C) Landslide features modified extensively by erosion; D) Landslide features so modified by erosion.

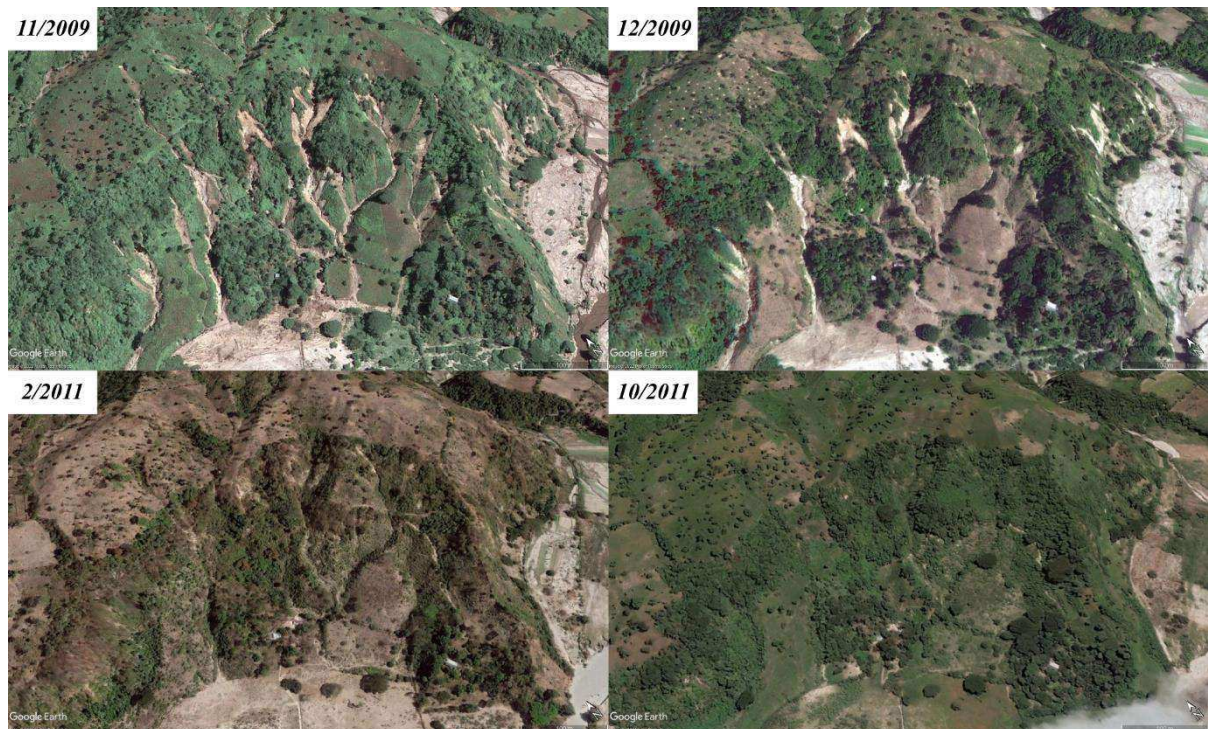


Figure 2.2.1.2: evolution of debris flows shapes in Ilopango Caldera, El Salvador. The sketch shows how shapes are modified in just two years.

The above-recalled limits are obviously of different extent depending on the adopted type of landslide survey. Field mapping generally allows to recognize almost all the forms connected to recent instability phenomena (some of which are not appreciable with a remote mapping on orthophoto) and to capture even small instabilities landforms whose traces could be undermined by vegetation or agricultural actions. On the other hand, field surveys require high efforts in economic and temporal terms. Instead, remote landslide recognition allows landform mapping in a much shorter time, maintaining rather high quality. However, even in this case, some problems must be faced. In fact, in order to have a good quality mapping, the resolution of the images must be high and the acquisition period close to that of slope failures. As regards this point, two main conditions are given: single-extreme-events (SEEs) and multiple-standard-events (MSEs). The first case is configured by image acquisition performed soon after a strong extreme (storm/earthquake) triggering event and actually allows the interpreter to consider all the recognized phenomena as coeval and dated at the time of the triggering event. SEEs are typically the result of post-disaster remote recognition aero-photogrammetric flights. In the second case, which is actually the much more frequent one, unless specific but typically occasional landslide dating, the interpreter has to accept that the landslide scenario is the result of cumulated multiple activations since a far past the time of the recognized image, which could be set if antecedent images are available. This

drives the paradox that actually all the recognized and mapped landslides from the same image could have been triggered by different standard events in different times, potentially spanning through decades. An intermediate very marginal case is the one configured when an aerial image has been taken casually soon after an extreme event. In that case, the interpreter could single out among the whole set of recognized landslides a coeval subset presenting very fresh signs on the field which can be referred to as an extreme event not far in the past from the date of the image itself.

Nowadays, the acquisition of high-quality recurrent satellite images is certainly favoured by the presence of a very dense satellite constellation. In addition, the development of Unmanned Aerial Vehicles (UAV) platforms facilitates the acquisition of high-resolution aerial photos from which algorithms can be applied to obtain point clouds, Digital Elevation Models (DEMs), and orthophotographs (Conoscenti et al. 2021). However, this choice can face criticalities linked to times and the cost of acquisition once again. On the other hand, the use of Google Earth™ (GE) has found wide use in landslide susceptibility studies (e.g., Costanzo et al. 2012a, b; van den Eeckhaut et al. 2012; Borrelli et al. 2015; Regmi and Poudel 2016; Conoscenti et al. 2016; Mandal and Mandal 2017; Vargas-Cuervo et al. 2019) thanks to the direct immediate no-cost access to a very performing remote surveying technology. Nevertheless, the images obtained from the GE system do not always have a coeval, homogeneous and high-resolution coverage for the whole investigated area and, obviously, the acquisition epoch is not necessarily linked with natural events or landsliding, rather depending on satellite recurrence and/or aerial flight plan cover. Therefore, it is often necessary to resort to compromises: reduction of the study area, splitting or even abandonment of the study area, or aerial/satellite cover. In this way, the forced choice of giving up the image of a specific epoch could result in a rather important loss of information and, certainly, the "jump" of a few years is more serious for those areas where coverage is not frequent.

In light of all the above-recalled points, the limits in the reliability of the landslide inventories can strongly affect the quality of the geomorphological analysis: the lack of some phenomena could produce information gaps in the landslide inventory, leading to a significantly misleading gravitational instability scenario of an area. However, this problem can be differently endured by several approaches used for landslide susceptibility.

2.2.2. Methods for landslide susceptibility evaluation: a general view

Several approaches have been adopted for landslide susceptibility, which can be discussed and classified depending on the type of score or class description they produce mainly, quantitative or qualitative, direct or indirect, inventory dependent or independent.

Direct qualitative

Qualitative methods are intrinsically based on the direct "expert" judgment of the interpreter geomorphologist, which has to correctly decipher the morphodynamic evolutive future tendency of the observed slopes, in light of the complete framework of landforms and running processes obtainable by field and/or remote surveys. Thanks to consolidated geomorphological conceptual models, this analytical approach is capable of synthetically capturing the complexity of the morphodynamic directed and crossing relations acting between landslides and their controlling factors. However, for the same reason, the future landslide scenario derived from this analytical approach is characterised by a more or less extended degree of subjectivity, depending on the expertise of the operator, as well as by mapped classes which are qualitatively discriminated into different degrees of susceptibility in terms of near discursive-descriptive terms. The same delimitation of the boundaries of the mapping units is actually dependent on the interpretation of the operator. As a consequence, the effectiveness of this approach is strongly dependent both on the geomorphological expertise of the subject who assesses the landslide susceptibility and of the one who finally reads and uses the obtained map. At the same time, direct analytical methods obviously require the systematic geomorphological recognition of the study areas, resulting in detailed but time/cost-ineffective protocols, unless incautious simplifications are assumed.

Landslide Inventorying

A specific category of direct, analytical, and quantitative susceptibility/hazard assessment methods is exclusively based on the use of landslide inventories. In this approach, the expert-based predictions are limited to interpreting the evolution of landslide areas (those sectors where landforms produced by past phenomena are recognized), which are all considered to the same degree, the only susceptible sectors in the study area. Besides, according to a geomorphologically sound standardised schematic approach, hazard levels are assigned to each landslide area, depending on estimated extension/volume, expected velocity and state of activity, as estimated by landslide recognition. This approach, which is very rigidly linked

to the principle stating that new landslides are more likely to occur under the same conditions which activated the past ones, is widely used by the Administrative users from Basin Authorities, in spite of its evident limits. In fact, although the inventorying approach will never produce a false negative in an area which has been already hit by a landslide, it is hampered by a number of weak features, whose main items are: blind mapping for new activations or re-activations of unknown not-inventoried past landslides; subjectivity in the association of a magnitude or hazard class to a single extension/typology/state of activity condition; an increasing grade of subjectivity in the estimation of extension/volume, movement typology and state of activity, respectively. The hazard/susceptibility maps which are obtained through this kind of method distinguish classes in ordinal terms, with mapping units totally corresponding to the landslide bodies and blind unmapped areas in the outer sectors.

A quantitative using of landslide inventories is configured when past landslides or landslide areas are used to compute their spatial frequency into a regular grid of cells in which the study area is partitioned, assuming the obtained 0-1 score as expressing landslide susceptibility. This approach, which relies on a spatial statistical basis, is however very limited in terms of resolution, being suitable only for regional assessment when the grid-cells as meaningfully larger than a single landslide body.

Deterministic

Deterministic approaches are based on the setting of a physical-mathematical model representing the slopes from which, depending on physical-mechanical parameters (strength and cohesion) and on the geometry of topographic, groundwater and future-hypothesised/past-recognized rupture surface, furnish an estimate of deforming stress and resistant strength resulting in a safety factor, corresponding to a susceptibility score. This approach is obviously cost/effectively applicable only on a single slope or site scale, being totally un-useful for basin-scale analysis. In fact, it requires a large investment for direct and indirect prospecting as well as for geotechnical laboratory tests on samples.

Indirect quantitative

Indirect methods perform the susceptibility assessment by analysing the spatial distribution of a set of controlling factors, selected as expressing the causes of the landslide activity in a given study area. These methods typically produce a quantitative mapping and have become more and more diffused with the development of GIS technology and the production of large

open access webgis database of geo-environmental thematic layers and satellite images. However, two very different categories can be distinguished among the indirect approaches: *heuristically* and *statistically* based.

In the heuristically based approaches, once the set of controlling factors is defined, subjectively expert-based analysis is to be applied for the re-classification of the factors and the assignments of scores to each class, expressing the degree of favourable conditions for slope failure. Finally, a more or less structured general function (typically, weighted sums or products) is defined for integrating all the scores produced into a single mapping unit, depending on its geo-environmental features, and computing multiple composed scores corresponding to a quantitative ordinal estimation of landslide susceptibility. The heuristic approach is very frequently implemented on a pixel partitioned layer of the study area and adopted for large scale assessment offering, although down from a subjective procedure of classification, a solution unconstrained to the availability of a landslide inventory. At the same time, heuristic models can be subjected to a pure validation procedure, as they are calibrated according to expert classification and scoring, resulting totally blind to any known landslides.

Statistically based modelling diverges from the heuristic approach as no re-classification of factors is mandatory and, more important, the scoring of factors and classes is quantitatively and objectively inferred by statistically analysing the spatial relation between the factor layers and at least one available training landslide inventory. A number of statistical techniques are proposed in scientific papers, mainly ascribable to: conditional analysis, Fisherian principal component and discriminant analysis, and generalised linear models (linear and logistic regressions). In particular, conditional analysis is mainly based on the computation of the landslide frequency or density inside each analysed uni- or multi-variate class, searching for a generalised efficiency of the derived predictive function on the representativeness of the calibration inventory. Differently, Generalised Linear Modelling makes hypotheses on the processed calibration inventory (the sample), inferring the parameters for future landslides (the population) by testing for the significance of all the applied parameter estimations.

To briefly summarise what is above described, the approaches used for the landslide susceptibility evaluation can be grouped into five main categories (Guzzetti et al. 1999). However, there is no clear distinction between the different methodologies, and frequently the researchers use more than one type of integrated approach. Table 2.2.2.1 resumes the characteristics of the main approaches.

The final aim of landslide susceptibility evaluation is to formulate ordinances and regulations to direct landslide risks in land management, contributing to adopting policies and taking proactive actions to avoid landslides and their negative consequences (Brabb 1991), and address rescue in case of widespread landslide activation. For this reason, the landslide susceptibility maps must be objective (the result does not change according to who defines the map), quantifiable (which areas are more susceptible than others in an absolute way) and must represent as much as possible the reality. However, landsliding is a complex natural phenomenon, in which different predisposing conditions interact with each other and with a trigger (varying by type and intensity), determining the instability of an area. If detecting the single interactions between the predisposing factors and the occurrence of landslides may be relatively simple, it is much more complex to understand how the variables interact with each other and the presence of failure. Any landslide susceptibility evaluation has to replicate reality through simplifications. However, the degree of adaptation of the model to reality will also be inversely proportional to the degree of simplification applied.

Approaches to landslide susceptibility evaluation		Description – Based on	Type
Analytical	Geomorphological mapping	<i>expert judgment of actual and potential slope failures, including their evolution and possible consequences</i>	direct and qualitative
Landslide inventorying	Landslide activity	<i>past distribution of landslide</i>	indirect and qualitative
	Landslide density/frequency	<i>past distribution of landslide</i>	indirect and quantitative
Deterministic	Physically-based	<i>physical laws controlling the slope stability (geotechnical parameters)</i>	indirect and quantitative
Heuristic	Index-based	<i>classification, ranking, and weighting (by experts) of instability factors according to their assumed or expected importance in causing mass movements</i>	indirect and qualitative
Stochastic	Statistic modelling	<i>functional relationships between instability factors and the distribution of landslides</i>	indirect and quantitative

Table 2.2.2.1: schematic resume of main approaches used for landslide susceptibility evaluation.

As an example, we can say that a mudflow can occur on clays, and it can certainly be said that high slope steepness favours the phenomenon. However, other factors affect the landslide: the exposure of the slope, the concavity of the slope, the presence of water, and others. Not considering the other factors that are involved in the activation of a phenomenon means potentially offering a model that is only partially representative of reality.

With this view, the methods based on the analysis of inventories do not identify the relationships between the predisposing variables and the landslide scenario but simply assign the level of landslide susceptibility of an area based on the density of landslides present in the past for the same area, thus entrusting the prediction skill of the model only to the quality of the archive. In this way, the result will be reliable only if the archive used is systematic and contains all the failures that occurred in the past. However, as seen in the previous chapter, rarely can an archive be defined as systematic and complete, due to uncertainties and errors associated with landslide inventories and to the complexity of landslide phenomena, methods based solely on landslide density may be misleading or incorrect (Guzzetti 2005). At the same time, the geomorphological mapping of susceptibility is not preferable among the different approaches because it is highly subjective. It is true that "subjectivity is not necessarily bad, particularly if it is based on the opinion of an expert" (van Westen et al. 1997) but subjectivity adds to the uncertainty of the model (Guzzetti 2005).

Similarly, heuristic methods are affected by the investigator's judgment on how the individual factors of instability can influence the occurrence of the phenomenon. Once again, therefore, subjectivity is introduced into the evaluation. This method also does not allow for determining how the predisposing factors can interact with each other in the triggering of the phenomenon.

Deterministic methods use geotechnical variables that are generally situ-specific and do not have a large spatial resolution. In fact, they are methods usually adopted for the analysis of instability on a slope scale and normally include specific information about the instability (e.g., surface depth of failure). Although very detailed, they are therefore not suitable for a spatial prediction study of phenomena (and to answer the only question where failure will occur in the future).

Conversely, the indirect methods produce a completely objective landslide susceptibility evaluation. These methods provide for consequential procedures which can be summarised as follows:

- i. recognition and mapping of landslides in the study area (or collecting of available landslide archive) and extraction of diagnostic morphodynamic areas;
- ii. identification of geo-environmental factors directly or indirectly expressing the landslide controlling factors and production of relative layers (e.g., geological map, topographical indices, and so on);
- iii. partitioning of the study area into suitable mapping units and assignments of factor conditions and unstable/stable status to each;
- iv. estimation of the relative contribution of each factor to landsliding and classification of the study area in different susceptibility sectors;
- v. validation of the landslide susceptibility map produced and analysis of model prediction skill.

In light of all the above-described pros and cons associated with the issue, quantitative, indirect, objective statistical methods are the one which more and more are adopted in landslide susceptibility modelling for basin studies to a scale up to 1:10.000.

2.2.3. Statistic modelling

In the last years, statistical methods have been widely applied in landslide susceptibility evaluation (Reichenbach et al. 2018). This approach allows to:

- i) optimise information input;
- ii) achieve objective results (mathematically obtained from data input) and numerically measurable.

The first point is linked to the statistical inference. Statistical inference consists of the use of statistics to draw conclusions about some unknown aspect of a population-based on a random sample from that population (Sinharay 2010). In other words, the goal of statistical inference is to understand by analysing a sample of the population, all the characteristics of the population. In the case of landslides, by investigating the relationships between failures and geo-environmental conditions, the aim is to detect all areas that potentially can be affected by slope failures considering their characteristics.

The second point is another advantage of the statistical approach: if the input data (landslides inventory and predisposing factors) do not change, the results are replicable by any researcher. Furthermore, the results attained for different sectors (catchment area, region) can be compared since susceptibility is numerically expressed.

Several statistical techniques are used in landslide susceptibility evaluation. Below, the main approaches used in this research are described and, in the following paragraph, the single methods used are explicated.

Index-based methods

These techniques measure, directly or in a weighted form, the relative or absolute abundance of landslide area or numbers in different terrain categories. Differently from heuristic methods, the weights are assigned to the terrain categories, according to objective measurement (proportion, percentage, frequency, incidence of landslides).

Bayesian statistical methods

These methods are based on Bayes theory which defines the probability of an event according to the a priori knowledge of the conditions that could be related to the event. This probability is also known as conditional probability and can be written as:

$$P(A | B) = \frac{P(B | A) \times P(A)}{P(B)}$$

where $P(A|B)$ is the probability of event A occurring conditioned by the fact that event B has occurred, $P(B|A)$ is the conditional probability of event B occurring given that event A has occurred, $P(A)$ is the “prior” probability of event A occurring, and $P(B)$ is the “prior” probability of event B occurring.

In landslide susceptibility evaluation, event B corresponds to all the predisposing factors that can condition landsliding and A represents the study (better the mapping units) that are affected by slope failures.

Among approaches based on the analysis of conditional probability, Reichenbach et al. (2018) highlight that the weight of evidence method is the most used in landslide susceptibility evaluation (e.g., Sujatha et al. 2014; Regmi et al. 2014; Wang et al. 2016; Xie et al. 2017; Gupta et al. 2022).

Fisherian statistical methods

These methods are based on the analysis of the probability of frequency, according to which the probability of an event is its frequency over time, that is, its relative frequency of occurrence after repeating a process a large number of times under similar conditions.

Therefore, these methods draw conclusions from sample data by means of emphasising the frequency or proportion of findings in the data. In addition to developing first the idea that statistics could be inferred as a probabilistic frequency, Fisher developed the concept of "significance testing" and the relative "p-value", which indicate the significance of a statistic measure when two hypotheses were compared.

According to Brenning (2005), among frequentist methods, logistic regression and discriminant analysis were the most frequently adopted classification modelling tools. However, a recent review of the literature (Reichenbach et al. 2018) shows that also linear regression analysis was largely used.

2.2.3.1. Statistical methods

As mentioned above, in this paragraph a description of the methods used in the research conducted is reported.

Linear regression

Linear regression is used to detect linear relationships between dependent and independent variables. In linear regression, both the dependent and the independent variables are continuous.

In this way, the relationship is shown by the following equation:

$$Y = \alpha + \beta x + \varepsilon$$

where Y is the dependent variable, x is the covariate, β is the slope of the line, α is the intercept and ε is the error which follows a normal distribution with a mean equal to zero and variance constant across levels of the independent variables.

The values of parameters β and α are randomly assigned for calculating the value of Y for a given x.

The performance of linear regression is evaluated by the mean squared error (MSE - or derived metrics) that calculate the error (residual) between the observed value of y and the calculated value \hat{y} , according to the formula:

$$MSE = \frac{1}{n} \sum_{i=1}^N ((y_i - \hat{y}_i)^2)$$

Binary Logistic regression

In landslide susceptibility evaluation, linear regression is hard to use because predictors can be continuous or discrete, and the output is binary (0 = no landslide or 1= landslide).

For this reason, binary logistic regression is preferred. In fact, logistic regression is used to binary classify elements by calculating the probability of each element belonging to one of the two groups, by using independent variables that can be continuous or discrete (Hosmer and Lemeshow 2000).

Different from linear regression, logistic regression does not assume that the dependent variable is linearly correlated to the covariate. However, first, the binary separation between the cases is determined by detecting the best-fitted line following the linear regression. Then, the predicted values are converted as the probability (scoring between 0 and 1) according to the sigmoid or logistic function, so passing from linear to a curvilinear relationship:

$$\pi(x) = \frac{1}{1 + e^{-(x)}} = \frac{e^x}{1 + e^x}$$

The equation can be rewritten as:

$$\pi(x) = \frac{e^{(\alpha + \beta x)}}{1 + e^{(\alpha + \beta x)}}$$

where $\pi(x)$ represents the conditional mean of Y given x when the logistic distribution is used.

The inverse of logistic function is known as logit function or log-odds and is written as:

$$g(x) = \ln \left[\frac{p(x)}{1 - p(x)} \right] = \alpha + \beta x + \varepsilon$$

The logit transformation has many of the desirable proprieties of a linear regression model. The logit, $g(x)$, is linear in its parameters, may be continuous, and may range from $-\infty$ to $+\infty$, depending on the range of x (Hosmer and Lemeshow, 2000).

Moreover, in the case of a dichotomous outcome variable, the quantity ε may assume one of these values:

- if $y=1$ than $\varepsilon = 1 - \pi(x)$ with probability $\pi(x)$;
- if $y=0$ than $\varepsilon = -\pi(x)$ with probability $1 - \pi(x)$.

The values of parameters β and α are determined by using an iterative procedure aimed to obtain the best fitting between the predicted and the observed Y. Given the dichotomous nature of Y, the maximum likelihood method must be used. This function $l(\beta)$ expresses the probability of the observed data as a function of unknown parameters (Hosmer and Lemeshow, 2000):

$$l(\beta) = \prod_{i=1}^n \pi(x_i)^{y_i} [1 - \pi(x_i)]^{1-y_i}$$

However, generally the log of the likelihood function is used:

$$L(\beta) = \ln l(\beta) = \sum_{i=1}^n \{y_i \ln[\pi(x_i)] + (1 - y_i) \ln[1 - \pi(x_i)]\}$$

The maximum likelihood estimator converges toward those parameters that maximise this function allowing the better consistency with the observed data. To estimate the global fitting of the model the negative log-likelihood (-2LL) is used. The latter estimates the goodness of fit, by comparing the fitting of the model with only the intercept (all the β s are set to 0, so is considered the model without the variable in question) and the full model (the predictor coefficients are non-null, so the variable is included). For evaluating the significance of the regression coefficients, the chi-square test and the pseudo- R^2 statistic can be used.

In this research, the BLR models were implemented through the ‘stats’ package of RStudio software (RStudio Team 2020).

Multivariate Adaptive Regression Splines

The MARS (Multivariate Adaptive Regression Splines - Friedman 1991) method, is a nonparametric technique that allows linear and non-linear adaptation relationships between predictors and independent variables. In practice, MARS divides the range of independent variable X into small intervals by knots and optimizes linear regression function (hinge function) between two consecutive knots. In this way, the result is a piecewise linear function that best fits the relationship between the predictors and outcome, according to

$$y = f(x) = \alpha + \sum_{i=1}^N \beta_i h_i(x)$$

where y is the dependent variable (the outcome) predicted by the function $f(x)$, α is the model intercept, β_i are the coefficients of the h_i basis functions and N is the number of basis functions.

A basis function is structured as a hinge function delimited by knots. More complex basis functions can be defined as the product of one or more hinge functions associated with different covariates. A particular case is the basis function that corresponds to the model

intercept, set to a constant value of 1. The application of the MARS algorithm is based on a two-stage procedure. In the first stage (forward pass), a model is generated by stepwise adding (starting from a constant only model) pairs of terms corresponding to the mirrored hinge functions generated by a knot. At each step, the added pair of terms that result in the regression giving the maximum reduction of the residual sum-of-squares error (RSS) is added. In light of the simple structure and fast computing, the search for the best pair is run systematically (in a “brute force” fashion). This stage can be run up until either a minimum RSS gain is obtained or the whole set of possible basis functions are added. In the second stage (backward pass), MARS stepwise prunes the best fitting but typically overfitted model, by dropping out of the model at each step the single term whose removal results in the lowest generalized cross-validation parameter (GCV; Craven and Wahba 1979). The criterion expressed by the GCV parameter is in fact the best compromise between fitting (low RSS) and model complexity, the latter depending on the number of terms. At each pruning step, the best model subset is then obtained.

In this research, the MARS models were implemented through the ‘earth’ R package (Milborrow 2014) of RStudio software, whose output also includes an estimation of the predictors’ importance.

2.2.4. Validation schemes and tools

2.2.4.1. Main validation schemes

In a landslide susceptibility study implemented through statistical techniques, the validation of the model is a fundamental step. Without a severe and rigorous (objective and quantitative) validation step, the prediction model and image are totally useless and have hardly any scientific significance (Chung and Fabbri 2003). For this reason, efforts have been made in the last years to standardise the required validation indexes that should be produced together with the associated final maps (Guzzetti et al. 1999).

According to Chung and Fabbri (2003), who were the first to define systematic blind tests and validation schemes for landslide susceptibility models, their associated prediction image or susceptibility map must be validated by comparison to a target pattern, which represents the areas affected by landslides. By comparing the cumulative curve obtained in a dispersion graph plotting %study area Vs. %landslides for decreasing score, rate curves whose subtended area corresponds to a standard performance index. However, two very different

types of accuracy performance can be evaluated depending if the target pattern is made of known, the one exploited for training (calibrating) the model, or unknown, a set of new testing (validation). In fact, in the first case the model *goodness-of-fit* is evaluated, whilst in the second case, it is the real *prediction skill* that is assessed. Coherently, Chung and Fabbri (2003) distinguished success and prediction rate curves, for known and unknown landslide pattern, respectively. In this way, to fully validate a susceptibility model, it is necessary to divide the landslide inventory into two subsets: a training (calibration) subset and a test (validation) subset. In the calibration phase, the model "learns" to recognize the relationships between the dependent and the independent variables by using the training dataset and so defining for each mapping unit a predicted status (stable or unstable). As a consequence, a success rate curve represents the maximum performance that a susceptibility model can obtain, as it only relies on the model fitting, in some way configuring the target of performance the prediction rate curve can achieve.

However, this kind of analysis is not a real validation of the model prediction skill but still can be useful to evaluate the maximum performance of the model attesting if the landslides archives and the predictors can have some limits or not. In this sense, an important concept in predictive modelling, the overfitting conditions, arises when the model too strictly adapts itself to the calibration subset so that it then hardly reproduces any unknown target pattern. To proceed for a complete validation calibration and validation subsets are required. Chung and Fabbri (2003) describe the three techniques used to obtain the bipartition of landslides (calibration and validation dataset) and the structure of the related modelling (characteristics of the calibration and the validation phases). In the last years, many applications of such techniques by researchers (e.g., Fabbri and Chung; Conoscenti et al. 2008a, b, 2018; Costanzo et al. 2012a, 2014; Rotigliano et al. 2012; Lombardo et al. 2014; Cama et al. 2015, 2016, 2017) made it possible to refine these methodologies, however proving their validity and robustness.

In this research, all the three strategies have been applied but with a few differences with respect to the original schemes proposed by Chung and Fabbri (2003). In the following, a brief description of the adopted procedures is given.

Chrono-validation scheme

In time partition, for the study area, two or more landslide archives linked to different epochs are required so that temporal separation of the failures be carried out. The calibration phase,

or the first step of modelling, involves the preparation of a model and related prediction image (success-rate curves) through the use of a single-epoch landslide archive. The validation phase, or the second step, consists in comparing the prediction image produced in the first step with the landslide distribution of the different epoch. Two schemes can be applied, forward and backward chrono-validation, depending on the temporal relation between the calibration and the validation dataset (antecedent or subsequent calibration dataset, respectively).

Spatial-validation scheme

In spatial partition, the study area is divided into two (or more) subzones, A and B, thus also developing a spatial subdivision of phenomena. The method assumes that the calibration model is trained with only one area, such as area A, while the prediction image is produced on the remaining part, for example B.

As the literature suggests (Costanzo et al. 2012a; Lombardo et al. 2014), the subzones may also not be adjacent but, to correctly apply the procedure, it is necessary that the landslides are well distributed throughout the investigated area and that the characteristics between the areas are homogeneous.

Random-validation scheme

In random partition, by using specific tools, landslides are randomly split. Generally, the training dataset is composed of 75% of the inventory while the remaining 25% represents the validation dataset. In this way, according to the methods seen before, first, a model is developed trained with the calibration set, then the prediction image is produced for the validation dataset.

2.2.4.2. Main validation tools

Two main validation tools have been adopted for estimating the accuracy of the models prepared in the present research: ROC-plots and confusion matrices. Besides, by applying cross-validation schemes, the robustness of the same models and the derived maps was assessed.

ROC curve

ROC-curves are obtained from graphs very similar to those rate curves (Chung and Fabbri 2003) are drawn from.

A ROC curve (Receiver Operating Curve - Goodenough et al. 1974; Lasko et al. 2005; Fawcett 2006) allows the evaluation of the accuracy of a model by calculating the subtended (Area Under Curve: AUC) in a graph where true versus false positive rates are plotted, by cumulating the assessed mapping units through a decreasing (from 1 to 0) susceptibility score. For any given reference value of score (threshold or cut-off), all the mapping units, depending on the score assumed down to the model calibration step, can be split according to the predicted status into positive (above the threshold) and negative (below the threshold), so that, after comparison to the real observed status, true positive (TP), false positive (FP), true negative (TN) and false negative (FN) are produced. By decreasing the reference threshold, a corresponding vector of TP and TN is obtained and plotted in a dispersion graph. The ROC curve matches the obtained series of dots, with typical monotonically decreasing trend. The AUC is the metric through which the accuracy of the model is determined. According to Hosmer and Lemeshow (2000), the AUC value allows to define the performance of the model as acceptable, excellent and "out of the ordinary" or exceptional for AUC value between 0.7 and 0.8, 0.8 and 0.9 or greater than 0.9 respectively.

ROC curves can be plotted for *goodness-of-fit* and *prediction-skill* assessment, depending on the nature of the landslide inventory adopted for assigning the real observed status to the mapping units.

In light of their construction, ROC curves furnish a general cumulated score-decreasing response for the assessment of its accuracy, averaging the performance along the score axis, with greater emphasis on the more susceptible cases (left side of the plot). Besides, ROC curves also allow to geometrically calculate the optimal cut-off value which, according to Youden (1950), results in the best TP-rate value simultaneously with the lowest value of the FN-rate. In other words, the optimised Youden index cut-off (Figure 2.2.4.2.1) permits to simultaneously increase sensitivity and specificity, being the basis for passing to a binarized approach to the accuracy assessment.

Confusion matrix

A confusion matrix is a simple table that permits directly detecting the success and the error of the binarized prediction image (Table 2.2.4.2.1). In fact, by exploiting a cut-off (in the literature frequently a standard 0.5 value is used but, in this research, only the optimised

Youden index cut-off was applied), the mapping units are divided between stable and unstable predicted cases. By comparison with the observed stable (N) and unstable (P) cases of the validation set, the correct predictions as True Positive (TP - cases predicted as unstable with landslide) and True Negative (TN - cases predicted as stable without a landslide) or the prediction errors as False Positive (FP - cases predicted as unstable without a landslide) and False Negative (FN - cases predicted stable with a landslide) are defined.

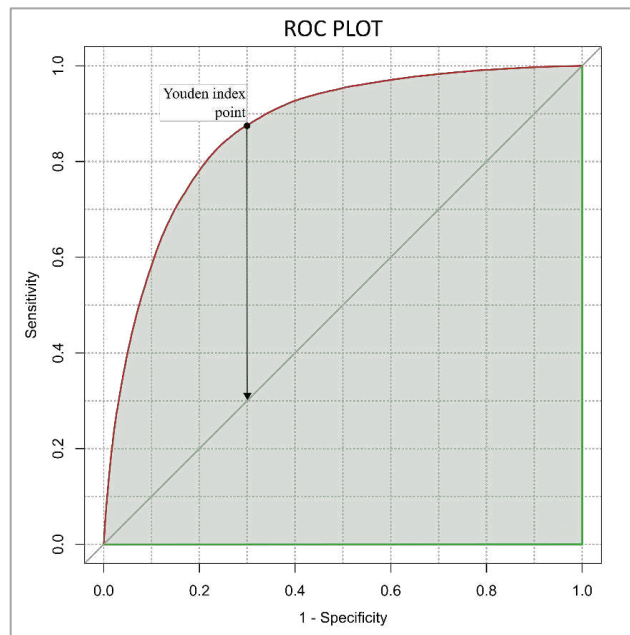


Figure 2.2.4.2.1: example of ROC plot: in red line is the ROC curve, the filled area is the AUC, and the point along the red curve is the best cut-off point calculated according to Youden 1950.

Once the observed and predicted cases are discriminated, the specific indices for prediction skill evaluation can be calculated. In table 2.2.4.2.2 the main indices are reported:

		Observed status	
		Stable (0)	Unstable (1)
Predicted status	Stable (0)	True Negative (TN)	False Negative (FN)
	Unstable (1)	False Positive (FP)	True Positive (TP)

Table 2.2.4.2.1: confusion matrix. The table shows the possible combination of the cases.

Together with the accuracy, Sensitivity and Specificity (the ability to recall real positive and real negative cases, respectively), PPV and NPV (the success in predicting positives and negatives, respectively) directly refer to a binarized (more likely to be stable or unstable) representation whose performance index can diverge in some cases from that marked by cumulated index such the ROC_AUC is.

Index name	Formula
Sensitivity or True Positive Rate (TPR)	$TPR = \frac{TP}{P}$
Specificity or True Negative Rate (TPR)	$TNR = \frac{TN}{N}$
Positive Predictive Value (PPV)	$PPV = \frac{TP}{TP + FP}$
Negative Predictive Value (NPV)	$NPV = \frac{TN}{TN + FN}$
Accuracy (ACC)	$ACC = \frac{TP + TN}{P + N}$

Table 2.2.4.2.2: the main validation indices derived from the confusion matrix.

Whatever the tool adopted for estimating the accuracy of the susceptibility models, it is worth to correctly interpret the two type errors and their nature.

Errors, in general, can be due to any lacking in the basic assumption we pose in the assessment of landslide susceptibility: status/position errors in the landslide inventories, values/boundaries errors in the layers of the controlling factors, missing of some fundamental controlling factor, difference in the triggering event responsible for the calibration and the validation subsets.

At the same time, while false negatives are to be considered as errors (the type II very severe error: a landslide is where it was predicted as safe), false positives actually include two types of cases: errors and future positives. In facts, as we apply a statistical spatial analysis with a temporal predictive perspective, new cases (negatives, at present, but positives in a near/far future) are to be considered as the main goal of the predictive map.

2.2.4.3. Cross-validation for model robustness and error mapping

The estimation of the model robustness aims at estimating, together with the accuracy (the correctness of the predicted cases) of the score/status estimations, their precision (the closeness of each produced score for the same assessed mapping units, both in the calibration

and the validation steps. This type of validation, frequently underestimated by the researchers, is a fundamental tool for the evaluation of the reliability of the model obtained. The robustness assessment basically aims at analysing if the parameters of the model and its derived prediction images change as the input data (calibration cases and modelling steps) change. The strategy for robustness assessment relies on the possibility of building a number (typically, hundreds) of datasets from a single dataframe by randomly extracting the calibrated cases, without replacement (each mapping unit is selected only one time). From each replicate dataset a model is calibrated, and its derived prediction image compared to a specific validation set. In this way, hundreds of estimates both for the model parameters and assessed score or predicted status of each mapping unit are obtained. The random sub-extraction from the study area typically is a presence/absence balanced merging the whole set of positive cases with an equal number of negatives. As negative cases are generally ten to one hundred times more than positives, hundreds of extractions of negatives can be performed, and different datasets obtained.

In this way, the different behaviour in terms of AUC values obtained (standard deviation) and susceptibility scores assigned (which produced the so-called error maps) to each mapping unit can be analysed and the precision and accuracy of the models evaluated.

A low robustness suggests failing of the "Law of missing data" (Rubin 1987), according to which the population of data not used in modelling (25%), in function of the selected extraction principle (not affected by the characteristics of the cases or neither from X nor from Y), can be defined as missing at random (Missing Completely At Random- MCAR). In other words, the training and the validation sample are not a random subsample of the original population. Actually, this means that the main archive is incomplete and, moreover, that the missing is not random. For example, a very frequent case of missing not at random is the landslides for a part of the study area since not accessible for a field investigation or blind by cloud from a satellite detection (e.g., Rotigliano et al. 2019).

2.2.5. Mapping units and diagnostic areas

The landslide susceptibility evaluation required an adequate subdivision of the study area in terrain mapping units (TMU). Mapping units are defined as the portion of terrain where the geo-environmental conditions differ from the adjacent units across distinct boundaries (Carrara et al. 1995; van Westen et al. 1997; Guzzetti et al. 1999, 2006). The TMU are

essential both in predicting performance and output results, playing a very important role to determine the design of landslide susceptibility maps (Martinello et al. 2021).

Based on the concept of a distinct and easily definable unit, different TMU typologies have been proposed (Meijerink 1988; Carrara et al. 1995; Guzzetti et al. 1999):

- i) *grid-cells* subdivide the territory in regular squares of predefined dimensions. Usually, grid-cells are directly derived through a Digital Elevation Model (DEM), so cells correspond to the pixels of dem;
- ii) *slope-units* are defined as the slope sectors limited by drainage and water divide lines. This division results into homogenous hydrological regions. Slope-units can be obtained by using specific GIS tools or by manually identification;
- iii) *terrain units* subdivide the territory according to environmental characteristics or with respect to the materials, forms and processes active in that area. Therefore, these units reflect the geomorphological and geological conditions of the specific sector outlined;
- iv) unique conditional units (UCUs) delimit areas with specific conditions of the control factors. To delineate the UCU, a reclassification in categorical classes of each predictor is necessary. Then, by overlapping the obtained layer, the portions of the territory with homogeneous properties are circumscribe. The number and characteristics (dimensions, geometry, etc.) of these units depend on the criteria used to reclassify control factors;
- v) *geo-hydrological units* derive from a further partitioning of the slope units according to the main outcropping lithologies in the area. This subdivision is considered fundamental for the recognition of zone with different behavior within the same slope;
- vi) *topographic units* derive from a particular division of slope units, based on vectors of tubular flow elements of irregular size and shape. For each tubular element, the morphometric and hydrological variables are calculated, including the cumulative drainage of the area above the unit;
- vii) *political or administrative units* correspond to national, political, administrative or demographic regions and, generally, are used for studies involving very large areas.

As part of this research, a new TMU has been proposed (Martinello et al. 2021, 2022): the Landform Classification Slope Units (LCL_SLU). This type of TMU derived from a

partitioning of classical slope units with the Landform Classification (LCL - Guisan et al. 1999; Wilson and Gallant 2000) map. This particular subdivision aims to detect sectors with a different geomorphological characteristic in a single slope unit. The details of this procedure and the research aimed at obtaining these cartographic units are described in the chapter 5, sections 5.4 and 5.5.

Martinello et al. (2022) reports that the choice of a specific mapping unit arises from several factors: i) the analysis target; ii) study scale; iii) resolution of both the input (required data) and output (depicted maps); and iv) suitability of the final results and derived maps for risk managers and land use planners.

Each type of mapping unit is characterised by pros and cons that can affect the results of the geomorphological analysis. However, grid cells, the slope units and UCUs are largely preferred due to their particularly useful in association with statistical methods (Clerici et al.; Rotigliano et al. 2011; Poiraud 2014; Reichenbach et al. 2018).

Once the mapping unit has been chosen, a status relative to landsliding needs to be assessed. It means determining if a specific mapping unit is stable or unstable. The identification of the landslide phenomenon in space takes place through the delineation of the diagnostic area. The diagnostic area represents the sector of the territory characterised by the presence of an instability and, as such, identifies the areas in which the set of triggering factors and the predisposing factors have caused the activation of the phenomenon itself.

Therefore, the diagnostic area becomes the fundamental element in landslide susceptibility studies, identifying the place where the model must "learn" to identify the conditions that caused the landslide occurrence. This means that, once the mechanisms causing landsliding in the past is detected, the model will be able to predict the status of mapping units based on the distribution and characteristics of the control factors.

The correct identification of the diagnostic areas becomes fundamental to obtain good results of the landslide susceptibility evaluation.

In the literature, three main typologies of diagnostic area are applied (Figure 2.2.5.1):

- i) *landslide Identification Point* (LIP), which corresponds to the highest point along the crown of the landslide area;
- ii) *landslide body*, that outline the surface directly affected by the slope failure;

iii) *geometries*, generally circular, which identify a portion of the surface influenced by the event. These geometries can include both the phenomenon itself and the portions of surface not directly affected by the landslide but very close to it or only the latter.

The first type of diagnostic area produces a points inventory of landslides; the last two of polygonal type. Since each typology identifies different portions of the surface, the results obtained are strongly influenced by the methodology used (Rotigliano et al. 2011). Rotigliano et al. (2011) proves that the choice of the diagnostic area is strictly linked to the landslide type. According to the authors, for debris flow susceptibility assessment, by using LIPs best performances arise; for the evaluation of rotational slide susceptibility, the choice is linked to the elements that better defining the instability factors on the crown of slope failure (LIP or geometries that delineate the surface more closely to the landslide crown without the landslide body namely Buffered-LIP).

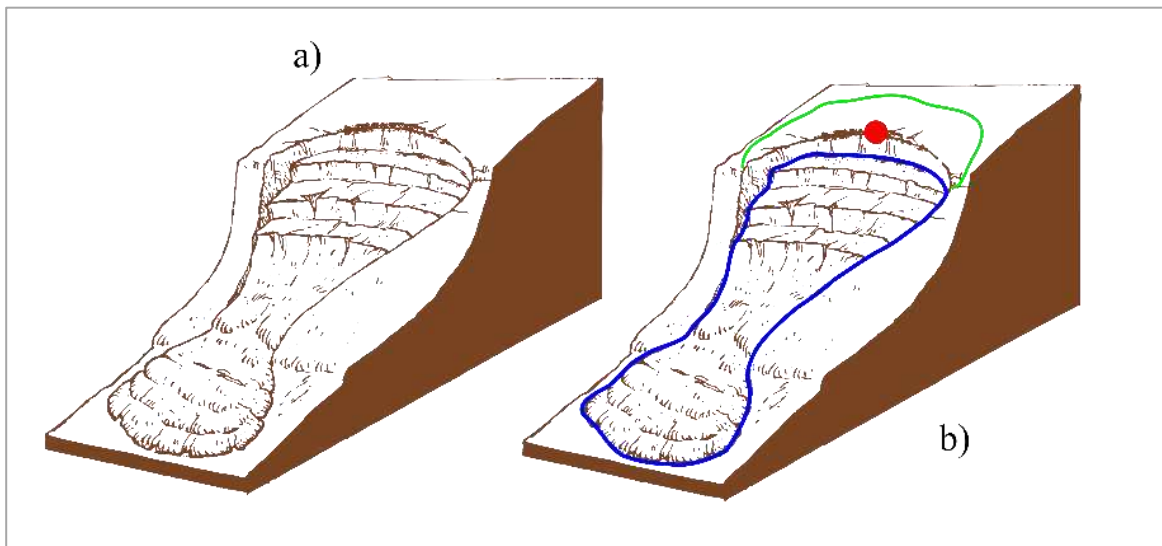


Figure 2.2.5.1: a) scheme of a slope failure (earth slide), b) an example of the main diagnostic area types: the red point is the LIP, the blue line is the landslide body, the green line is a Buffered LIP.

2.3. Landslide predisposing factors

Generally, in landslide susceptibility evaluation, the predictors selected as predisposing causes of landslides are really proxy variables.

A proxy variable is a factor used instead of an unobservable or immeasurable variable of interest. Although a proxy variable is not a direct measure of the desired variable, it is strongly related to the latter so that it can somehow represent its characteristics. In fact, a

good proxy must have a close correlation (positive or negative), not necessarily linear, with the variable of interest.

In this research, the choice of the geo-environmental predictors was defined both on the basis of an expected direct or proxied role in the physics of slide-type slope failures and in light of the availability of good source layers.

According to the literature (e.g., Conoscenti et al. 2008a; Rotigliano et al. 2011; Costanzo et al. 2012a, 2014; Cama et al. 2015, 2016, 2017; Lombardo et al. 2015; Vargas-Cuervo et al. 2019), terrain analysis was employed to derive topographic predictors as primary and secondary attributes of elevation. Below is a list of basic topographic predictors generally exploited in this research. Open-source Geographical Information System software (GIS; Quantum GIS(QGIS.org 2022), GRASS GIS (GRASS Development Team 2022) and SAGAGIS (Conrad et al. 2015)) were used for processing the thematic (geology and soil use) spatial data and a Digital Terrain Model (DTM).

1) *Elevation*

The elevation expresses the altitude above sea level. Generally, it is correspondent to the Digital Elevation Model. Actually, a DEM represents the bare-earth surface, without any natural or artificial features. On the other hand, DTM or Digital Terrain Model represents the earth's surface but natural features (e.g., rivers) are here included. By using GIS software, DTM may be interpolated to generate a DEM, but not vice versa.

To obtain a DEM (but also for cleaning DTM from built/artificial features), accurate classification techniques focused on the selection of undesired ground points are applied. In this way, starting from a more complex point cloud (e.g., which of LIDAR), it is possible to target and isolate undesired ground points from the remaining dataset. Then, by using one of several interpolation algorithms to create a mesh jointed fabric, an accurate image of the real-world ground model is obtained.

The DEM is one of the main factors in landslide susceptibility evaluation. In fact, elevation could be a proxy for differentiating the mapping units in terms of the mean annual rainfall, which typically reflects the altitude. On the other hand, from DEM are derived the topographic predictors generally used for the landslide susceptibility evaluation.

2) *Steepness*

The steepness, the first derivative of elevation, is obtained by measuring the rate of altitude variation, in the same direction in which the slope steepness decreases. Among the predisposing factors of landslides, the slope inclination plays a key role since it determines the direction and the speed of the water both superficial (of runoff) and underground (sub-superficial movement or epidermal and underground). The steepness is also considered a proxy for the inclination of potential underlying rupture surfaces (Martinello et al. 2022). In the literature, several algorithms are reported that can be used for the study of steepness but the most used is the method of Neighborhood (Burrough and McDonnell 1998) or the "neighborhood analysis". The method analyses the maximum variation of the slope with respect to a central point, implementing a window of 3x3 cells to study the trend of the neighbor cells. The steepness can be reported in degrees, radians, or as a percentage of inclination.

3) *Aspect*

The slope aspect corresponds to the direction in which the slope degrades more rapidly (slope direction). Aspect controls insolation, evapotranspiration, weathering, physicochemical erosion operated by temperature and vegetation, distribution and abundance of flora. All these elements determine seasonal wet/dry cycles of soils (Auslander et al. 2003) so that the aspect (also linked to the elevation) can be considered as a good proxy of this variable.

The aspect is calculated from the elevation by using an algorithm (Wilson and Gallant 2000a) that exploits a moving 3x3 cell window to derive the local surface direction of the central cell by comparison with the neighbouring cells. The results are expressed in degrees, in a range from 0 (minimum value indicating north) to 360 (maximum value coinciding again with the north), while the value -1 marks the flat areas for which it is not possible to define exposure.

Usually, the obtained results are reclassified according to Table 2.3.1 or transformed into continuous values by applying cosine and sine to the slope aspect (northernness and easternness).

Degree range	Classes
0 - 22.5 and 337.5 - 360	North
22.5 - 67.5	NorthEast
67.5 - 112.5	East
112.5 - 157.5	SouthEast
157.5 - 202.5	South
202.5 - 247.5	SouthWest
247.5 - 292.5	West
292.5 - 337.5	NorthWest

Table 2.3.1: the classes used for reclassified the aspect.

4) *Landform classification*

Landform classification (LCL - Guisan et al. 1999; Wilson and Gallant 2000) is a factor that allows automatically identifying the morphologies of the slope from a DEM. The landform classification is actually based on a further factor, the Topographic Position Index (TPI). The TPI compares the elevation of each DEM cell with the average elevation of the nearest cells. In this way, by exploiting a specific inner/outer radius (e.g., 100/1000, 100/2000 meters), the valleys (depressed areas with respect to surrounding areas), the slopes (elevated areas with respect to the surrounding areas), and flat areas or constantly inclined (which present with respect to the areas surrounding a gradient of elevation near zero) are detected. In particular, the classes detected by the algorithm are streams, midslope drainages, upland drainages, valleys, plains, open slopes, upper slopes, local ridges, midslope ridges, and high ridges.

In light of this, landform classification directly differentiates the morphological setting of the mapping units, which is assumed to play a central role in controlling and expressing their morphodynamic behavior.

5) *Topographic curvature*

The topographic curvature is a factor that allows discriminating of the areas of convergence and those of divergence of flows (both runoff waters and landslides).

Generally, two types of study of topographic curvature are carried out: the profile curvature and the plan curvature (Zevenbergen and Thorne 1987).

The *profile curvature* studies the geometry of the slope surface in the direction of the maximum steepness of the slope. This variable is a proxy of the direction of flow. Positive values indicate concavity facing upwards; negative values indicate that the surface has a convexity facing upwards; values equal to zero indicate flat areas (Figure 2.3.1).

The *plan curvature* studies the geometry of the slope surface perpendicular to the direction of the maximum steepness of the slope. In this case, the results can be used to identify areas of activation and propagation of landslides (Ohlmacher 2007).

Positive values indicate that the surface has a facing concavity upward; negative values indicate that the surface has a convexity facing upwards; values equal to zero indicate flat areas (Figure 2.3.2).

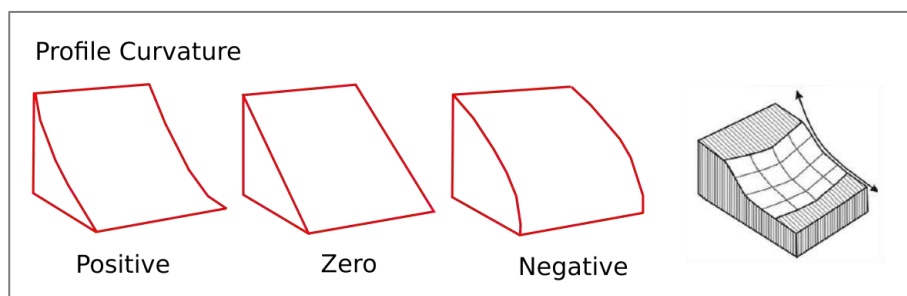


Figure 2.3.1: sketch of the possible geometries of profile curvature.

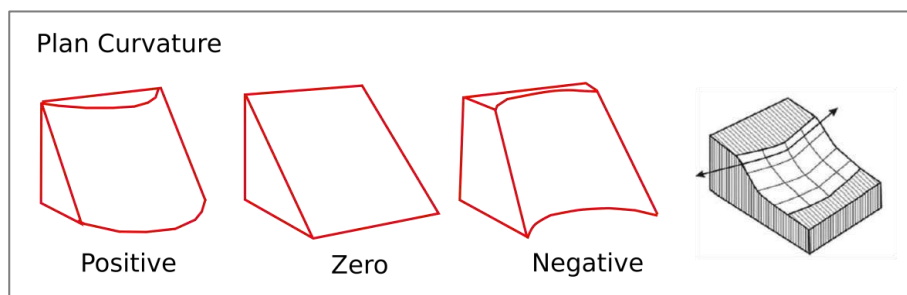


Figure 2.3.2: sketch of the possible geometries of profile curvature.

6) Topographic Wetness Index

According to (Beven and Kirkby 1979), the Topographic Wetness Index, computed on each cell, is the natural logarithm of upslope drained cells divided by the local slope.

The algorithm identifies the number of cells that feed the supply of water that arrives in each pixel. In other words, this parameter identifies the amount of water that reaches each cell by runoff. In this way, the topographic wetness index is a good proxy for estimating the potential infiltration or saturated soil thickness ((Rotigliano et al. 2011; Martinello et al. 2022).

In order to calculate this factor, GIS software requires flow tracing or analysis of the path of the water threads with respect to the reference basin (catchment area). The simplest GIS tools used to calculate this factor assign a weight of 1 to each cell so that, in the output raster, each cell will be characterized by a value that derives from the sum of the pixels that "flow" into the cell. Therefore, cells characterized by high values indicate areas heavily affected by runoff: this method can therefore be used to identify the gullies and rivers.

The parameter is also closely related to the characteristics of the soil (percentage of organic matter, regolith depth, etc.).

7) *Stream Power Index*

The stream power index is calculated as the natural logarithm of the catchment area multiplied the tangent of the slope gradient (Florinsky 2012).

The index can be used to describe potential flow erosion or the energy of the flowing water on the bed and banks of channels. As catchment area and slope gradient increase, the amount of water contributed by upslope areas and the velocity of water flow increase, hence stream power index and erosion risk increase (Florinsky 2012). For this reason, the stream power index can be considered a proxy of intensity of surface water erosion (Martinello et al. 2022).

8) *Topographic Ruggedness Index*

The Terrain Ruggedness Index is used to express the local morphology of earth's surface. Developed by Riley et al. (1999), the method exploits a 3x3 cell window to calculate the difference of elevation of the central cell with respect to each of the 8 neighbouring ones.

The algorithm automatically squares each of the eight-elevation difference values, sums them, and takes the square root values to obtain positive results.

The terrain Ruggedness index is assumed to express the convergence, divergence, and variability of both runoff and shallow mechanical stresses (Ohlmacher 2007; Costanzo et al. 2012, Martinello et al. 2022).

9) *Lithology*

The mechanical behavior of landslides is determined by the geotechnical properties of the involved material. However, no layers of geomechanical properties of terrain are generally available spatially distributed at basin scale. On the other hand, geomechanical properties are intrinsically linked to the lithology. For this reason, the outcropping lithology is assumed to be a good proxy for the physical-mechanical properties of rocks (Martinello et al. 2022).

The outcropping lithology maps can be always available since they can be directly derived from geological maps, by unified formations characterized by similar geomechanical properties.

For each study area, in the following section, a detailed analysis of outcropping lithology is reported.

10) *Soil use*

Soil use potentially expresses the role of potential anthropogenic hydrological and/or surface hydric erosion/wash-load/creep/solifluction-induced disturbances (Martinello et al. 2022).

Vegetation directly influences runoff and infiltration and the presence of surficial underground water: the foliage captures rainwater, allows to diminish the impact of water drops to the ground (sheet erosion), and promotes slow infiltration. In addition, through the root system, the water of aeration zone (the upper part of the ground level) is gradually absorbed. However, roots accelerate the mechanical degradation of lithotypes. In general, the effects of water erosion are much more intense in abandoned and vegetation-free areas. The urbanization, through the waterproofing of the surfaces, favours the runoff of the waters which, if not properly conveyed, can flow into restricted areas, thus causing intense phenomena of local erosion and rising of the water level for that area (increasing of pore pressure). The areas subject to agricultural actions are frequently involved by works that gradually causes soil erosion. Such operations often also cause the deletion of path of concentrated water runoff (such as grooves) thus favouring the long surface runoff on the slope. Among

the agricultural operations, the watering of plants (if it is not well managed) favours the water accumulation in the aeration zone.

For each study area, in the specific section, a detailed analysis of soil use is reported.

3. Introduction to the applications

During the three years of activity, applications were carried out aimed to investigate the main methodological topics that were theoretically explained in the first part of the thesis.

The nature of the topics is shown below. For each section, the reference to the application carried out is also reported, which will then be further explored in Chapter 5.

Table 3.1 shows the main applications developed during the three years of activity and the relative topics faced, which have been the subject of published/submitted papers in international journals.

		TOPICS			
		Trigger	Modelling and Validation strategies	Mapping Units and Susceptibility mapping	Inventories
5.1	Predicting the landslides triggered by the 2009 96E/Ida tropical storms in the Ilopango caldera area (El Salvador, CA): optimizing MARS-based model building and validation strategies. <i>Environmental Earth Sciences</i> , 2019, 78(6), 210	X	x		X
5.2	Evaluation of debris flow susceptibility in El Salvador (CA): a comparison between Multivariate Adaptive Regression Splines (MARS) and Binary Logistic Regression (BLR). <i>Hungarian Geographical Bulletin</i> , 2018, 67(4), pp. 361–373		X		
5.3	Investigating limits in exploiting assembled landslide inventories for calibrating regional susceptibility models: a test in volcanic areas of El Salvador. <i>Submitted: Applied Sciences</i>		X		X
5.4	Optimal slope units partitioning in landslide susceptibility mapping. <i>Journal of Maps</i> , 2021, 17(3), pp. 152–162		X	X	
5.5	Landform classification: a high-performing mapping unit partitioning tool for landslide susceptibility assessment—a test in the Imera River basin (northern Sicily, Italy). <i>Landslides</i> , 2022, 19(3), pp. 539–553		X	X	

Table 3.1: main applications developed during the three years of activity and the relative topics faced.

3.1. Triggers

A very basic key element potentially hampering the whole real effectiveness of landslide susceptibility models and derived maps are connected to the type and strength of the trigger responsible for the calibration inventory. In fact, together with basin long term analysis, which is based on inventories typically cumulated in the time span of decades, event inventories can be obtained only if mapping the landslides produced by a single specific extreme event (frequently activated in the time span of one or few hours). This is the case of seismically induced or intense storm triggered landslide. Under these conditions, it is possible to verify if and how landslide susceptibility changes depend on the type and magnitude of the related reference triggering event, highlighting limits and related solutions to a weaker holding of the “the past is the key to the future” basic brick.

In the last decade, several studies have examined landslide susceptibility with respect to a meteoric trigger both "normal" (e.g., Costanzo et al. 2012a; Conoscenti et al. 2016;

Persichillo et al. 2017; Bordoni et al. 2020a, b), that is, with rainfall values coherent with the average rainfall trend of the areas under study, and extreme (e.g., Lombardo et al. 2014, 2015; Cama et al. 2015; Vargas-Cuervo et al. 2019), while rare are the cases in which the two typologies are investigated at the same time. However, these researches do not define the predictive capacity of the models when the intensity of the trigger varies, thus limiting the application of the results obtained to an expected trigger event of magnitude equal to the meteoric phenomenon in which the models were calibrated with.

Thus, some questions arise on the issue to which the scientific community must inevitably answer in order to be able to consider the results obtained from this type of study suitable for applications. What is the actual predictive capacity of stochastic models to identify the instability triggered by a trigger of a different intensity than the calibration one? Is there a linear correlation between the amount of rainfall and the number of activated phenomena? Are new regression laws established between the control variables and the stability/instability of the area in the event of extreme rainfall?

Solving these scientific problems appears to be a priority given the current severity of the hydrogeological instability and the high importance of prevention with respect to this issue. In fact, the definition of valid landslide susceptibility maps even in the case of an extreme trigger means minimizing the risk to the population and damage to material assets, maximizing the effectiveness of the precautions taken, and developing management of the territory consistent with the environmental particularities of urbanization that respects the landscape.

This research has attempted to answer the scientific questions raised above, investigating areas particularly affected by this type of phenomenon and developing specific methodologies.

In fact, the study area examined is characterized by some peculiarities that make it an ideal application field for achieving the objective of the investigation. The Caldera Ilopango (El Salvador) is a territory that, due to its geographical position, is subject almost annually to intense meteoric phenomena (cyclones and hurricanes) responsible for the multiple activations of disasters that often cause death and destruction (MARN 2004, 2010a, b, 2011; CEPAL 2010, 2011; NGI 2013; Marineros-Orantes and García-González 2021).

The geomorphological setting as well as the temperate-humid climatic regime that characterizes the area make the latter subject to instability even during the rainy season or in the event of a normal trigger.

The cyclical nature of extreme perturbations and the significant number of landslides triggered during the rainy period allow us to have a large archive of information, essential for robust and complete modelling.

Please refer to section 4.1 for deep information regarding the study areas and to section 5.1 for the specific application.

3.2. Modelling and validation strategies

Efforts in the research activity have been posed also to a deep comparative analysis in terms of pros and cons, driven by both statistical and geomorphological approaches.

In the literature developed in recent years, studies of landslide susceptibility assessment applied several statistical methods (e.g., Multivariate Adaptive Regression Splines – MARS, Binary Logistic Regression – BLR, Support Vector Machine – SVM, Random Forest – RF, Maximum Entropy – MaxEnt).

Studies in which several methods are used at the same time (e.g., Youssef et al. 2016; Pourghasemi and Rossi 2017; Huang et al. 2020; Panahi et al. 2020; Sajadi et al. 2022) are getting more and more frequent in literature. However, these studies often result in a simple application of the different methods, without any solid comparative evaluation capable of highlighting the different geomorphological adequacy of the methods. More generally, it is often missing a clear discussion of the relations between susceptibility and controlling factors in discussing the results in terms of geomorphological adequacy. On the other hand, the quality of the results is often evaluated on a surficial and simple ROC analysis.

In the research developed in these three years, according to the literature (Chung and Fabbri 2003), a robust calibration and validation scheme is proposed, (see all model building and validation strategies of the applications in Chapter 5). At the same time, new strategies focused on preparing and validating models and deeply check their performance, suggesting protocols for validation to be adopted for going behind the simple ROC analysis are proposed (in particular, see the application in section 5.3).

A detailed analysis of the importance of the variables is reported in all the applications. Moreover, in the application 4.5, a deep analysis of the link between the chosen mapping

unit and the resolution of the predictors in the same and the performance of the models is proposed.

Finally, application 4.4 is aimed at showing the difference in terms of the predictive performance of two statistical methods (i.e., BLR and MARS), by using two robust validation schemes.

3.3. Mapping units and susceptibility mapping

In landslide susceptibility modelling, the type of mapping unit adopted plays a very important role in determining the quality, resolution, and suitability of the output results (Guzzetti et al. 1999; Carrara et al. 2008; Martinello et al., 2022). Mapping units are in fact assumed to be diagnostically suitable to train a predictive model to discriminate between potentially stable/unstable geomorphological settings or conditions. At the same time, the type of adopted mapping unit defines the spatial resolution of the model and controls the spatial pattern and geomorphological adequacy of its final prediction images (i.e., the susceptibility map). In the literature, the proposed mapping units can differ in terms of the following: (i) the analysis target; (ii) study scale; (iii) resolution of both the input (required data) and output (depicted maps); and (iv) suitability of the final results and derived maps for risk managers and land-use planners.

Indeed, due to their geomorphological relevance, grid cells and slope units (SLUs) are the most used mapping units (Reichenbach et al. 2018); however, in both cases, their application involves pros and cons that must be evaluated in light of the end users' needs.

A number of papers (Costanzo et al 2012; Costanzo et al 2014; Cama et al 2015; Conoscenti et al 2015; Lombardo et al 2015; Cama et al 2016; Cama et al 2017; Chen et al 2017; Persichillo et al 2017; Lay et al 2019; Zhang et al 2019; Nhu et al 2020; Pourghasemi et al 2020; Bordoni et al 2020) found that grid cells, directly obtained through the rasterization of the study area, offer a very high modelling performance, especially when the initiation points of flow, like landslides or gullies, is to be predicted. Nevertheless, due to their very local significance, without any constraints of spatial coherence or connectivity between the adjacent pixels in a slope, the final maps could be misleading and/or hard to read for the final users. This limit is very evident in the case of shallow to deep landslides (rotational/translational slides) as their slope instability conditions are not so strictly dependent on local (pixel) properties. Conversely, slope units are potentially very suitable for capturing within a whole slope, those clusters of the connected pixel which are actually involved in the slope-failure mechanics (Rotigliano et al 2012). However, the employment

of SLUs entails some difficulties in defining criteria for i) SLU partitioning, which is crucial to finding the best performing model and more adequate coupling between real 3D failure mechanisms and surface landforms, and ii) proxy variable zonation, which determines the adequate and correct definition of the SLU setting. Actually, there is no univocal approach in the choice of optimal criteria (Rotigliano et al. 2012; Alvioli et al. 2016, 2020; Camilo et al. 2017; Cheng and Zhou 2018; Amato et al. 2019; Hua et al. 2020; Sun et al. 2020; Martinello et al. 2021).

In this research, innovative solutions to the topic of setting the more appropriate mapping units both for modelling (Modelling Mapping Units, MMUs) and depicting (Cartographic Mapping Units, CMUs) landslide susceptibility have been tested and compared both to the typical adopted ones and to some new types which have been proposed by other researchers. The emphasis which has been posed on this topic has become stronger and stronger and has attracted some other international research groups (e.g. Van Den Eeckhaut et al 2009; Erenner and Düzgün 2012; Zêzere et al 2017; Ba et al 2018; Qin et al 2019; Jacobs et al 2020). At the same time, the direct strict connection between the research project, including all its methodological scientific components, and the requirements exposed by relevant stakeholders such as the Basin Authority in the framework of the project SUFRA, has given further input and solicitations to the development of suitable solutions for the cartographic representation of landslide susceptibility.

In this research, several approaches to obtain a suitable landslide susceptibility map were tested by exploiting the most used mapping units by the researchers (grid cells and SLU) and by testing a new mapping unit: the Landform-CLassification Slope Units (LCL_SLU). This research was performed in the Imera Settentrionale river basin (northern Sicily, Italy) and has resulted in two main publications (sections 5.4 and 5.5).

3.4. Inventories

The need of optimizing landslide assessment methods with respect also to the stakeholders' requirements finds its main key point in implementing modelling strategies resulting robust to the typical incompleteness or typological misclassification affecting available public inventories. Indeed, civil protection urgently asks for regional-scale landslide susceptibility scenarios attempting to define statistically-based national maps, eventually exploiting even limited but available landslide inventories for their calibration. To this aim, grouping multiple clustered available datasets is frequently adopted as a solution to obtain landslides inventories large enough to train the statistical models. However, such landslide datasets can

result in heterogeneous either in terms of spatial distribution, expertise of the operators, classification and mapping criteria, survey recognition methods and resolution (field, remote, reports), epoch and related triggering events, etc. It is worth to note that these limits could hamper the resolution and precision of the predictive models without giving clear effects down from standard validation procedures.

To cope with this need, approaches have been tested for proposing indexes, suitable for warning the users about the real reliability of the derived susceptibility maps.

By exploiting landslide inventories from five volcanic areas of El Salvador, for which rainfall triggered debris flow archives were available, a multiscale validation strategy was applied to verify the actual predictive skill of the regional susceptibility model. Tools and strategies for detecting negative effects produced by inaccurate/incomplete landslide inventories are applied and proposed. For more information about the study areas, please see the section 4.1, while for the application please see the section 4.5.

4. Study areas

In this chapter, the main characteristics of the study areas are described. For each area, a paragraph of regional setting is displayed and then a subparagraph with the specific geomorphological condition of each study sector is reported.

4.1. El Salvador

4.1.1. Regional setting

The Salvadorian territory stretches SE–NW along the Central American Volcanic Front for about 250 km on the Pacific side of Central America, near 150 km inboard of the Middle American Trench, where the Cocos plate is subducted beneath the Caribbean plate (Jibson et al. 2004a; Agostini et al. 2006; Lexa et al. 2011).

The Caribbean plate is a lithospheric element composed of a slightly deformed crust of the oceanic plateau of the basins of Colombia and Venezuela and that of the continental block Chortis of the Paleozoic-Mesozoic age, both surrounded by deformed margins, the result of the interaction with the adjacent Nazca, Cocos, North and South America Plates, from Mesozoic to Present. The thickness of the Caribbean plate is very variable, going from 3-5 km in the Venezuela Basin, up to 20 km in the southern belts (Diebold and Driscoll 1999). The northeast subduction of the Cocos plate and the Nazca plate below the Isthmus causes an intense deformation of the deep soils and the rise of magmas that stay or cross the crust and come out to form the Mesoamerican Volcanic Arc.

Small-scale fault systems (such as the Polochic-Motagua fault, Santa Elena-Hess system fault) are associated with large-scale faults through which lateral sliding, lowering, and lifting they have produced are carried out in the current morphotectonic structure of Central America (Figure 4.1.1.1)

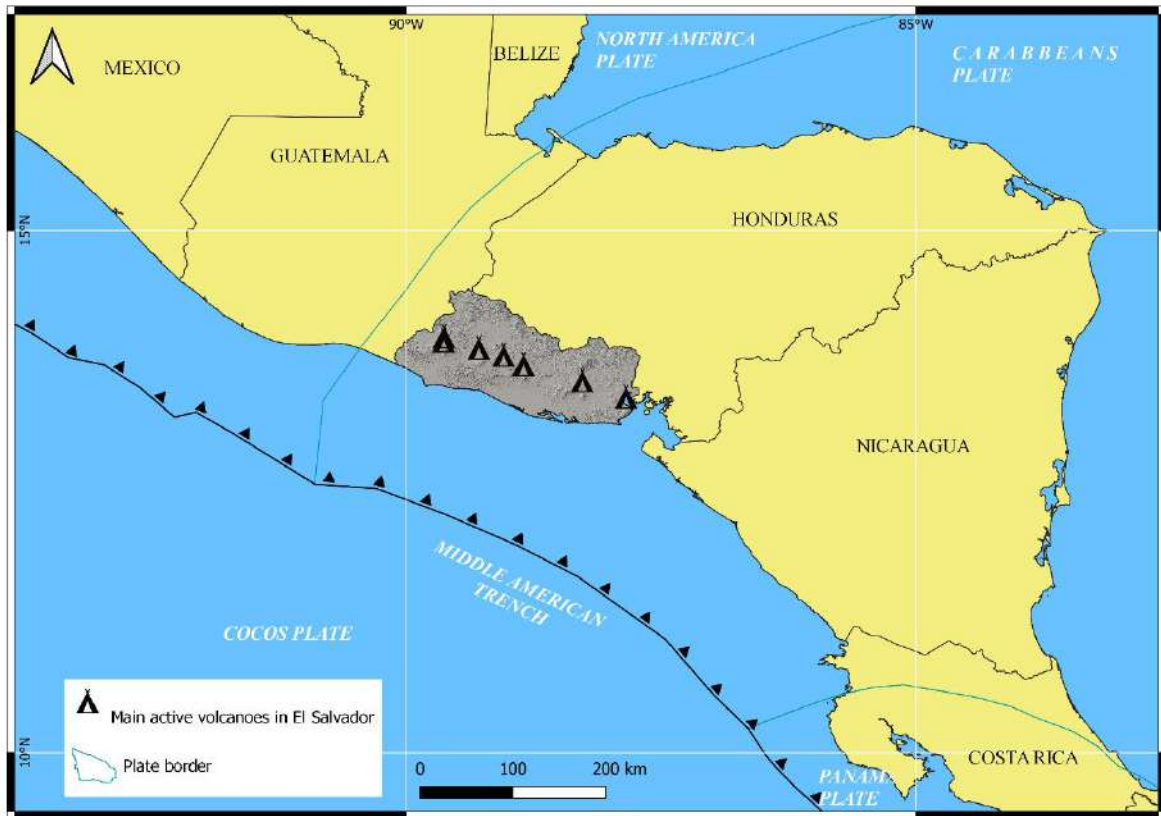


Figure 4.1.1.1: regional setting of Central America (modified from Corti et al. 2005, Lücke et al. 2015, and Major et al. 2003).

The interactions between the plates constantly accumulate stress along the edges, originating an intense seismic activity that makes Central America one of the most active seismic regions in the world (Corti et al. 2005; Lücke et al. 2015). Most of the seismicity is concentrated along the plate edges with earthquakes of high magnitude and with epicentres located on the structures tectonic. In addition, the obduction of the Caribbean plate causes horizontal and vertical movements of the weak crust which is dissected into small parts through a set of faults, many of them such as seismogenic.

As a result of the regional collisional tectonic setup and in accordance with the characteristics of the Central American Isthmus, the Salvadorean territory is characterized by the presence of the Mesoamerican Volcanic Arc which extends from north-northwest to south-southeast near the Pacific coast. In El Salvador, the Mesoamerican Volcanic Arc consists of an alignment of 22 volcanoes. Among these, the San Salvador, San Vicente, San Miguel, Ilopango Caldera, Santa Ana, Izalco and Conchaguita are considered active, so it is considered one of the most active volcanic regions of the world (Major et al. 2003).

A second volcanic range is located northeast along the border with Honduras: it is the Sierra Madre de Chiapas Mountain range, and it crosses the region from north-northwest to south-southeast.

Frequently, the crater of the volcanoes, some of which are still active, is occupied by lakes. Among these, Ilopango is the largest in the country (72 km²), followed by Olomeca (24.2 km²), Coatepeque (24 km²) and Güija (45 km²) in common with Guatemala.

The Salvadorian territory is almost completely composed of volcanic soils derived from the intense Plinian eruptions of the Tertiary period (Schiaidt-Thomé 1975) In particular, the outcropping lithologies of the central part of the region derived from the recent eruption of the Ilopango Caldera. At least four exceptional eruptions in the last 100kys, the last of which was nearly 2500 years ago, produced tephra layers and ignimbrites deposits which covered wide sectors of the central part of the country (Stoiber and Carr 1973).

In this way, often the steep slopes of the region are characterized by pseudo-coherent materials particularly prone to soil erosion and landsliding (Crone et al. 2001; García-Rodríguez et al. 2008; García-Rodríguez and Malpica 2010), especially in the region of the Cordillera El Bálsamo, the Ilopango caldera and the flanks of San Vicente, Usulután, El Picacho, San Salvador, and Chalatenango volcanoes (Jibson and Crone 2001). Landslides can be activated by both seismic and climatic triggers as well as by eruption.

Several earthquakes caused landslides: during the 1965's earthquake (M 6.3) 125 people died, mostly near the Caldera Ilopango, where landslides, liquefaction and diffusion phenomena also occurred affecting pumice slopes; in the 1986 earthquake (M 5.5), devastation linked both to the earthquake and also to the numerous landslides triggered along the roads between San Salvador and Lake Ilopango, caused 1500 dead and 100000 homeless; many failures activated by the sadly known 2001 earthquakes (M 7.7 and M 6.6), especially along the Cordillera El Bálsamo where two debris flows at Las Colinas (Figure 4.1.1.2) and Las Barrioleas, caused nearly 1000 deaths (Jibson et al. 2004b).



Figure 4.1.1.2: the January 2001 earthquake-induced slide that demolished much of the Las Colinas neighbourhood of Santa Tecla, a suburb of San Salvador (from United States Geological Survey)

Rainfall triggered landslides are linked both to the normal rainy season and to climatic extreme events. In fact, El Salvador, as well as the Central American area, falls within the zone of humid tropical: the average annual temperatures are between 19 and 31 °C, while average annual rainfall values are often higher than 1800 mm (The World Bank Group 2021). The rainy season is between May and October and frequently precipitations occur in the form of thunderstorms. During this period, El Salvador and, in general, the Central America area, can be affected by tropical cyclones.

A tropical cyclone is a storm system characterized by a closed circulation around a low-pressure centre, in association with strong winds and a high amount of rainfall. Tropical cyclones develop almost exclusively in tropical regions of the planet, due to the collision of hot air masses originating on large marine surfaces. If the climatic conditions are favourable, the cyclone continues to acquire energy and increases its size; at this point, it will begin to dissipate only when the contact ceases with the ocean (direct source of supply for the storm) and after a long path on the ground, during which it will download the energy possessed through intense precipitation and strong winds.

The phenomena often turn out to be of low or medium power (respectively called tropical depressions and tropical storms) and only rarely reach energy levels high (in this case we will speak of a hurricane).

Another very important climatic phenomenon, exclusive to the tropical Pacific, is ENSO – El Niño Southern Oscillation. ENSO is a phenomenon characterized by the combination of an oceanic component, namely El Niño or la Niña, and an atmospheric component, called Southern Oscillation, the latter characterized by pressure changes in the West-central Pacific.

El Niño consists of a warming of the waters of the central-southern and the eastern Pacific Ocean, for values equal to or greater than 0.5 °C and duration over 5 months; la Niña, on the other hand, consists of an analogous cooling having equal duration. On average, the maximum observed intensity of the temperature oscillation is of the order of 3-4 °C.

The two components, the oceanic and the atmospheric one, are mutually involved: when El Niño is underway, the Western Pacific pressure is high, while when it is in the course of La Niña, the pressure in the western Pacific is low (Figure 4.1.1.3).

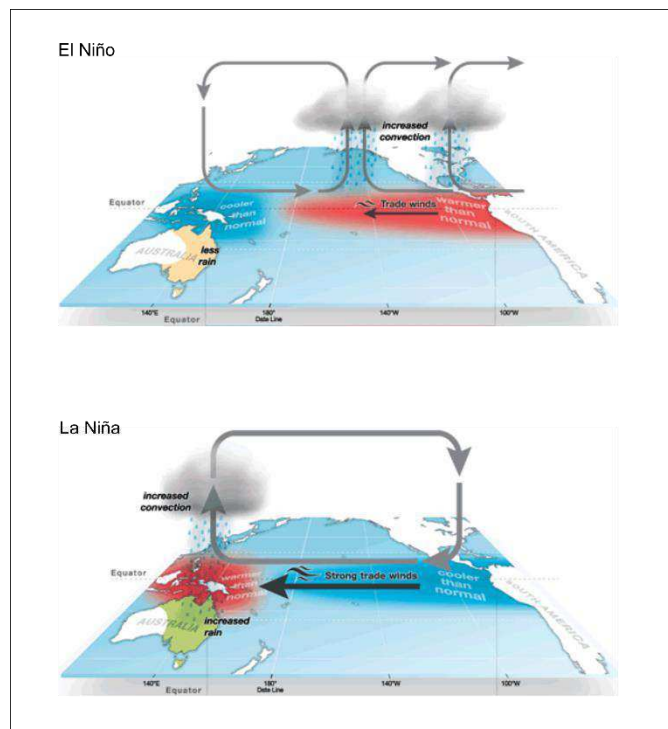


Figure 4.1.1.3: El Niño and La Niña conditions in the equatorial Pacific, modified from the Australian Bureau of Meteorology (<http://www.bom.gov.au/climate/ens0/history/ln-2010-12/three-phases-of-ENSO.shtml>).

The causes of these fluctuations are still being studied. The return time of the ENSO is not easily definable, being placed in an interval that goes from 2 to 7 years. Generally, El Niño occurs between December and January, while La Niña occurs between August and October. The mechanisms that govern ENSO generate ideal conditions for the development of cyclones so much so that many of the phenomena that occurred in the tropical Pacific belt

can be related to that cause. The perturbations generated by ENSO are characterized by intense rainfall in the areas directly affected by the cyclone, while the more distal areas from the low-pressure vortex are affected by drought.

Therefore, whether it is tropical cyclones s.s. or cyclones generated by ENSO, the tropical regions are periodically hit by severe disturbances, often with tragic consequences.

In this research, landslide phenomena linked to two extreme events are detected: the hurricane IDA (2009) and the tropical depression Twelve-E (2011). Below, is a short summary of the main characteristics of these events.

The hurricane IDA

The Hurricane Ida developed on 4th November as a tropical depression in the south-western sector of the Caribbean Sea, increasing its strength up to tropical storm grade on 7th November, when it crossed the shoreline of Nicaragua, and to a second level hurricane at the midday on the 8th (Avila and Cangialosi 2010). The hurricane then moved northward crossing the Caribbean Sea and the Mexico Gulf, weakening back to a tropical storm and to depression on the 9th and completely dissipating on the 12th. During these same days, the low-pressure system 96E moved from the eastern Pacific Ocean causing intense rainfall between November 7th and 8th (CEPAL 2010, 2011). In these two days, Ida and 96E simultaneously struck an area of around 400 km² centred between Ilopango Lake and San Vicente Volcano, producing more than 300 mm/24 h at the Ilopango and San Vicente villages (Figure 4.1.1.4). In this area, large damages were recorded caused by floods and landslides with around 200 deaths and a quarter of a billion dollars of economic losses (MARN 2010a). The larger part of this was in the north-western flank of San Vicente Volcano, where huge debris flow phenomena severely struck the villages of Verapaz and Guadalupe. At the same time, in the Ilopango Caldera area, hundreds of landslides triggered by steep slopes caused damage to cropland, rural houses and roads, as well as strongly affected and modified the connected fluvial system.

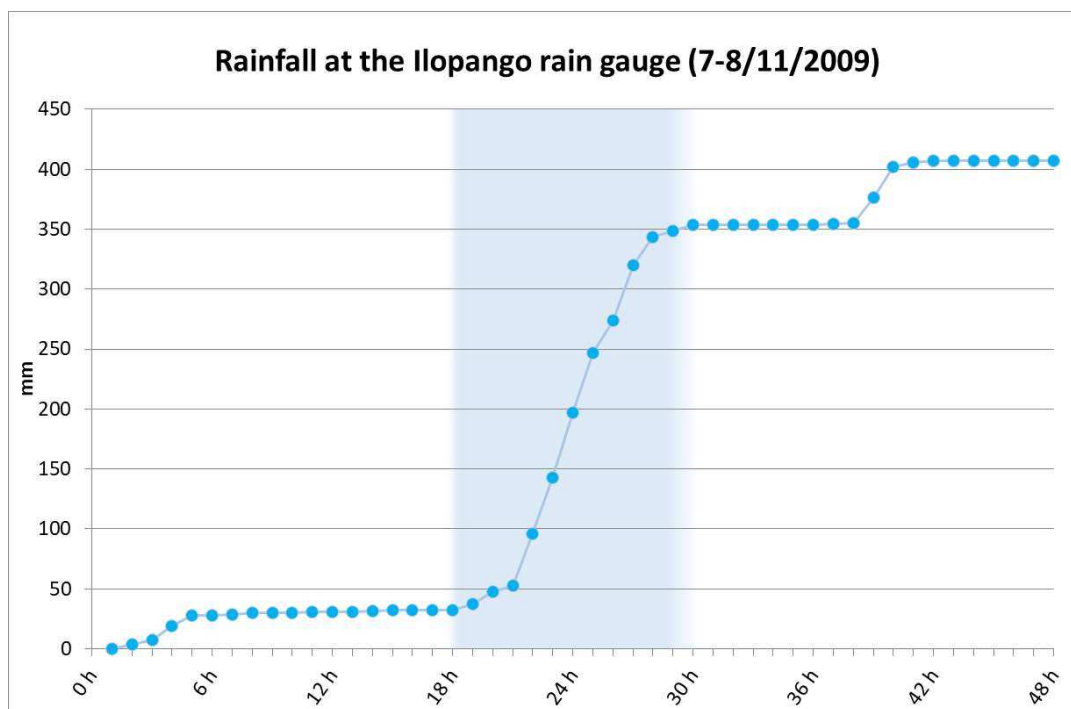


Figure 4.1.1.4: cumulative rainfall recorded by the Ilopango rain gauge during the Ida Hurricane event.

The Tropical Depression 12E

Starting on October 6 as low pressure from the Gulf of Tehuantepec, several hundred miles south of the Mexican coast, the disturbance quickly developed and became a tropical depression just six days after (Brennan 2011). After hitting the southern Mexican territory among the state of Oaxaca and the municipality of Arriga, 24 hours after its formation, the Tropical Depression 12E dissipated its energy. However, by joining forces with a monsoon system, the Tropical Depression 12E continued to blow with its winds the Central American territory, causing also heavy rains for about 10 days.

Tropical Depression 12E affected El Salvador during the period from 10th to 20th October. With a cumulative maximum of 1513 mm, equivalent to 42% of the mean annual rainfall of the period 1971-2000 (CEPAL 2011), the tropical depression 12E was defined by the minister of MARN Herman Rosa Chávez as “the most severe meteorological event recorded in the region”. Also in this case, with 10% of the national territory affected especially along the coastal plains and the volcanic mountains, El Salvador was heavily hit by the related floods and landslides, reporting 35 victims and an economic loss of more than nine hundred million dollars (CEPAL 2011; MARN 2011).

4.1.2. Main characteristics of the studies sectors

The choice of the study areas was determined by the availability of landslide archives or by the quality of the input layer necessary for the landslide susceptibility evaluation. In particular, the first and the second applications (see section 5.1 and 5.2) were conducted in a small catchment of the Ilopango Caldera for which a pre- and post-hurricane IDA high-resolution satellite image for the remote landslides mapping was detected. For the third application, a set of volcanoes/calderas areas where debris flows recurrently activate and where landslides archives were already mapped, was selected. This set was composed of (Figure 4.1.2.1): i) the Coatepeque area, which extends for about 82 km², east of the homonymous caldera lake; ii) the San Salvador area, surrounding for about 144 km² the homonymous volcano; iii) the watershed inner basins of the Ilopango caldera, for a total area of about 121 km²; iv) the San Vicente area, which include the whole homonymous volcano, extending for about 287 km²; v) the tip sector of the San Miguel volcano, for a total area of about 11 km².

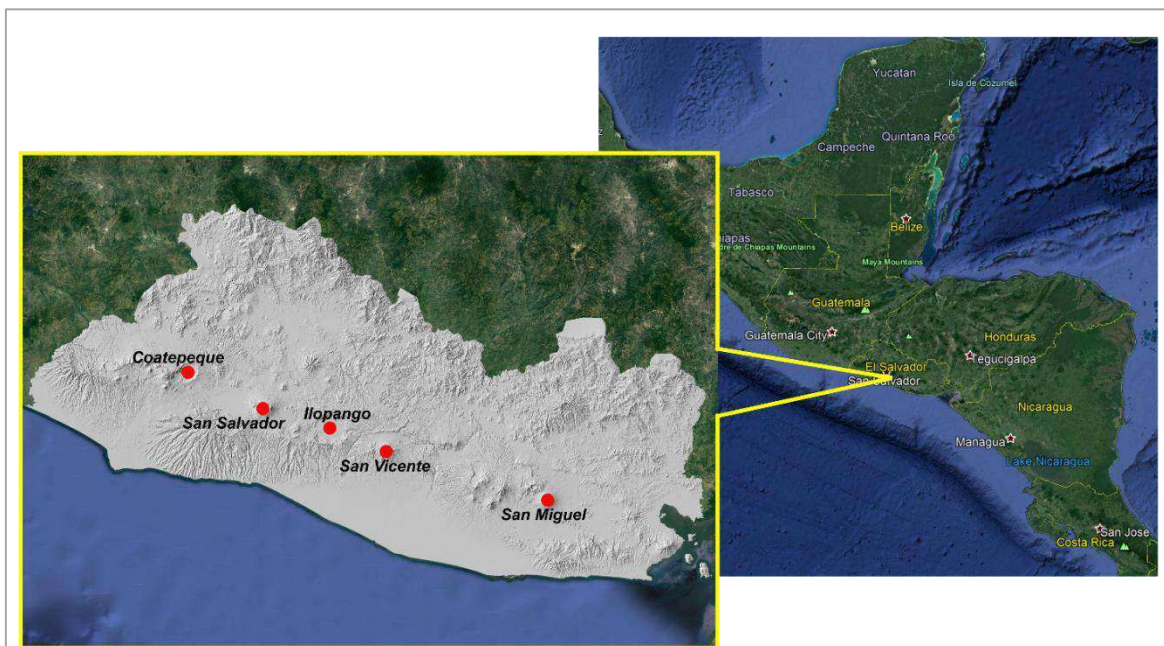


Figure 4.1.2.1: location of the study areas

These areas are characterized by different elevations (Figure 4.1.2.2). There is a good overlap in terms of altitude between the areas of Coatepeque and Ilopango, with a range between ~ 500 m and ~ 1200 m a.s.l.. The territory of San Vicente, which includes the entire volcano and also the foothills, has altitudes starting from ~ 100 meters and reaching peaks of ~ 2200, but even in this case most of the territory is between ~ 500 m and ~ 1200 m a.s.l.

The areas of San Miguel and San Salvador cover the summit areas of the volcanoes, with altitudes between 820 and 2120 m for the first, and 500 and 1820 m for the second.

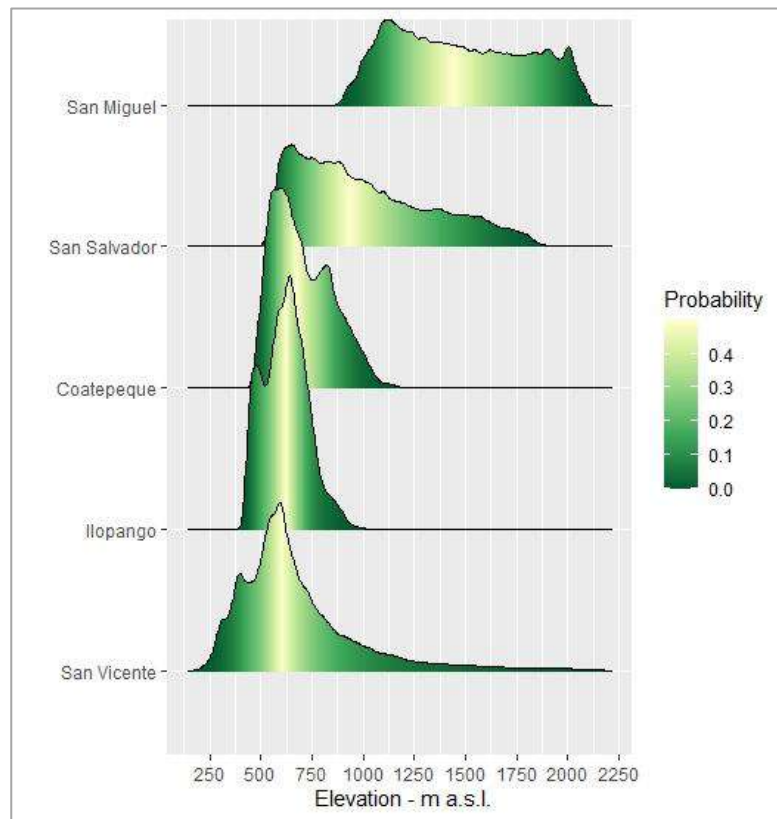


Figure 4.1.2.2: distribution of the elevation in the five study sectors.

With regard to the slope aspect, Figure 4.1.2.3 shows that all directions are represented in each of the study areas. However, it is possible to detect dominant exposures for some areas: for the San Miguel a prevalent exposure from W to S is identified while for the Coatepeque area the prevalence is towards the directions between NE and S. On the other hand, the San Salvador area has several areas exposed to the N and NW.

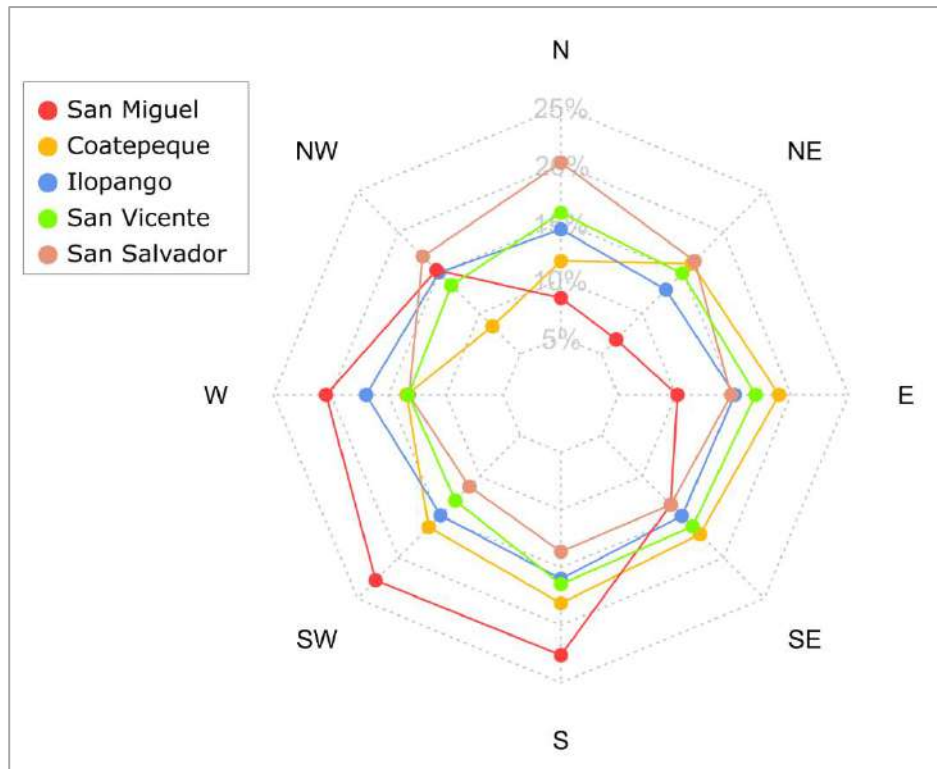


Figure 4.1.2.3: distribution of the exposure of the slopes in the five study sectors.

The analysis of the Landform Classification (LCL) classes distribution in the five areas (Figure 4.1.2.4) shows that the open slopes class, albeit in a variable percentage but always higher than 35%, is the most present class of LCL. On the other hand, the upland drainages and local ridges classes have very low frequencies in all areas. In the Coatepeque area, the other most important classes are Midslope drainages and midslopes ridges, thus characterizing a predominantly mountainous/hilly area. For the San Vicente area, in addition to the classes that represent the high sloping areas (slopes ridges and upper slopes), the plains and valleys classes are also represented and identify the foothills of the volcano. For the Ilopango area, all the classes are present, witnessing a territory that, starting from slopes with different inclinations, gently degrades into valleys and flat areas. The San Salvador area also has a similar trend to that of the Ilopango area, although here the open slopes clearly prevail, with a percentage that almost touches 60%. Finally, the San Miguel area is instead characterized mainly by slopes with different inclinations, with the total absence of flat areas.

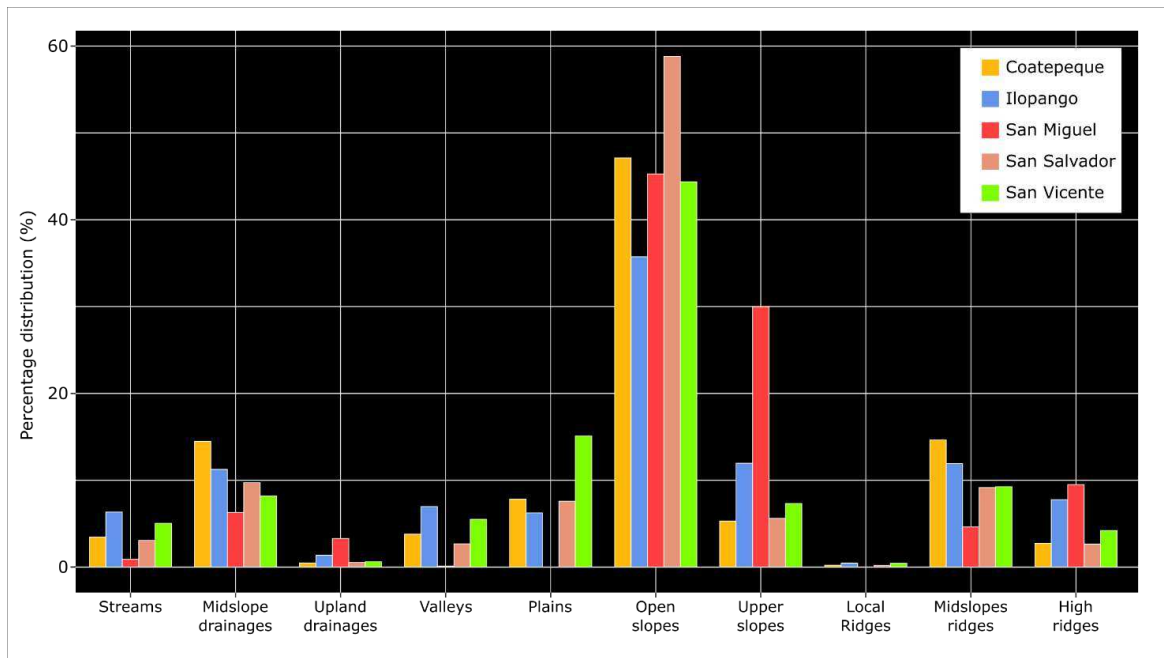


Figure 4.1.2.4: distribution of the landform classification classes in the five study sectors.

With regard to land use (Figure 4.1.2.5), cultivated areas prevail in the five territories, both with permanent and annual crops. Mixed crops are also very present in all territories except in the San Miguel area. In the latter, in fact, probably because of its position on the top of the volcano, more than 80% of the territory has shrub vegetation and it should be emphasized that no type of urbanization is present. In general, about 10% of the territory of each sector has urbanized areas.

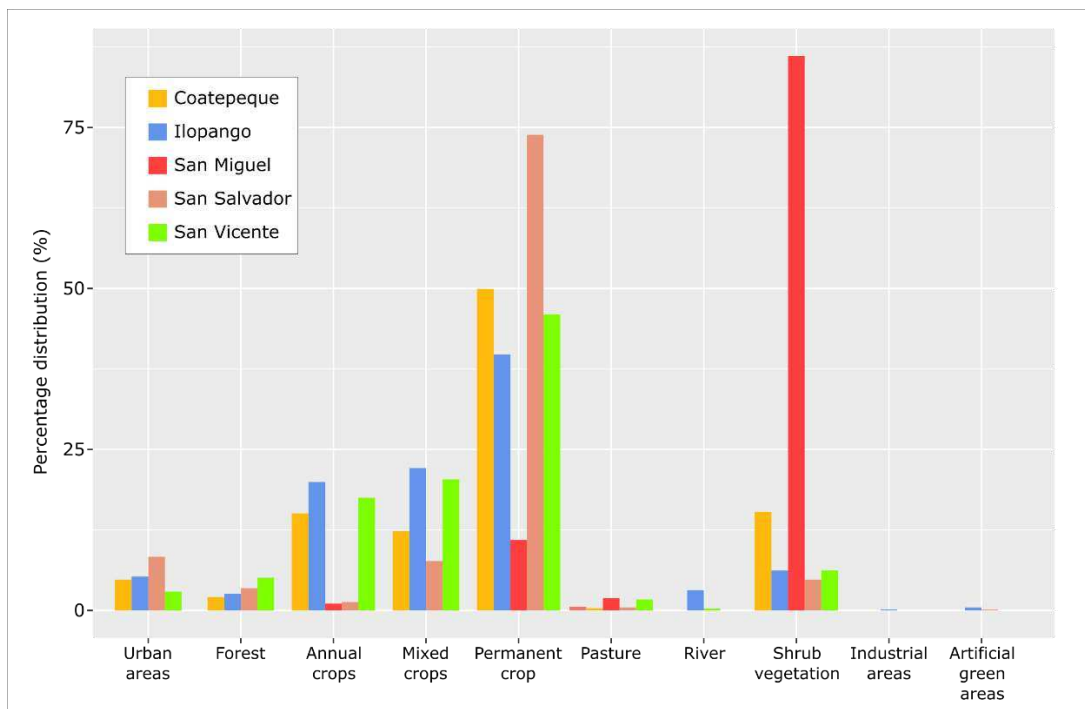


Figure 4.1.2.5: distribution of the land use classes in the five study sectors.

Finally, Table 4.1.2.1 shows the distribution of the outcropping lithologies in the study sectors. The outcropping lithologies, consisting of primary volcanic deposits and remodelled material, are grouped into three main formations (Schmidt-Thomé 1975).

	Formation	Lithology	Epoch	Code	Outcropping area
Coatepeque	Bálsamo	Basic-intermediate pyroclastics and epiclastic breccias and lavas	Miocene	b1	0.25%
	Bálsamo	Basic-intermediate effusive rocks, pyroclastics and epiclastic breccias and lavas	Miocene-Pliocene	b2	6.51%
	Bálsamo	Basic-intermediate effusive rocks	Pliocene	b3	4.04%
	Cuscatlán	Acid effusive	Pleistocene	c2	0.21%
	San Salvador	Quaternary sedimentary deposits	Holocene	Qf	2.51%
	San Salvador	Acid pyroclastics, epiclastic breccias and lavas and basic-intermediate effusive	Pleistocene	s1	3.46%
	San Salvador	Basic-intermediate effusive rocks	Pleistocene	s2	1.87%
	San Salvador	Acid pyroclastics, epiclastic breccias and lavas ("Tobas color café")	Holocene	s3a	77.45%
	San Salvador	Accumulation cones	Holocene	s5c	3.70%
Ilopango	Bálsamo	Basic-intermediate pyroclastics and epiclastic breccias and lavas	Miocene	b1	6.37%
	Bálsamo	Basic-intermediate effusive rocks	Pliocene	b3	6.53%
	Cuscatlán	Piroclastitas ácidas, epiclastitas volcánicas	Plio- quaternary	c1	25.12%
	Cuscatlán	Acid effusive	Pleistocene	c2	9.58%
	Cuscatlán	Efusivas-básicas-intermedias	Pleistocene	c3	0.67%
	San Salvador	Quaternary sedimentary deposits	Holocene	Qf	6.09%
	San Salvador	Efusivas ácidas	Holocene	s3b	0.40%
	San Salvador	Acid pyroclastics ("Tierra Blanca")	Holocene	s4	44.90%
	San Salvador	Accumulation cones	Holocene	s5b	0.34%
San Miguel	San Salvador	Basic-intermediate effusive rocks	Pleistocene	s2	26.58%
	San Salvador	Accumulation cones	Holocene	s5b	72.39%
	San Salvador	Quaternary sedimentary deposits	Holocene	Qf	1.03%
San Salvador	San Salvador	Quaternary sedimentary deposits	Holocene	Qf	0.71%
	San Salvador	Basic-intermediate effusive rocks	Pleistocene	s2	54.67%
	San Salvador	Acid pyroclastics, epiclastic breccias and lavas ("Tobas color café")	Holocene	s3a	11.98%
	San Salvador	Acid pyroclastics ("Tierra Blanca")	Holocene	s4	9.00%
	San Salvador	Efusivas básicas intermedias	Holocene	s5a	5.42%
	San Salvador	Accumulation cones	Holocene	s5b	3.82%
	San Salvador	Tuffs and dusty deposits	Holocene	s5c	14.40%
	San Salvador	Quaternary sedimentary deposits	Holocene	Qf	1.03%
San Vicente	Bálsamo	Basic-intermediate pyroclastics and epiclastic breccias and lavas	Miocene	b1	6.94%
	Bálsamo	Basic-intermediate effusive rocks	Pliocene	b3	17.02%
	Cuscatlán	Piroclastitas ácidas, epiclastitas volcánicas	Plio- quaternary	c1	30.14%
	Cuscatlán	Acid effusive	Pleistocene	c2	0.81%
	Cuscatlán	Efusivas-básicas-intermedias	Pleistocene	c3	3.57%
	San Salvador	Quaternary sedimentary deposits	Holocene	Qf	1.03%
	San Salvador	Basic-intermediate effusive rocks	Pleistocene	s2	22.84%
	San Salvador	Acid pyroclastics, epiclastic breccias and lavas ("Tobas color café")	Holocene	s3a	0.34%
	San Salvador	Acid pyroclastics ("Tierra Blanca")	Holocene	s4	17.31%

Table 4.1.2.1: geological classes of each study area with description of lithology, epoch, code, and the relative outcropping area.

Bálsamo Formation (Pliocene)

Andesitic lava flows (~ 10 m thick) interspersed with epiclastic and pyroclastic sequences. In the sequence, levels of variable thickness between 0.5 and 1.5 m of reddish paleosol are also found. Once exposed, the pyroclastic rocks (b1) break into irregular blocks as the epiclastic rocks (b2) shatter into medium-fine sized plates. The matrix of pyroclastic rocks is formed by tuffaceous material, greyish or brown, classified and of medium-fine size, with angular blocks of andesitic lava of dimensions varying between 5 and 30 cm. Epiclastic rocks have similar compositions but are more classified. Effusive rocks (b3) have a massive structure and are only possible locally appreciate levels of fine-grained crystals (phenocrysts). On the roof and in the bed of these rocks it is possible to find slag levels. The rocks have a high resistance to weathering.

Cuscatlán Formation (Plio-Pleistocene)

Pyroclastic rocks (ignimbrites – c1), effusive acidic rocks (c2), epiclastic rocks (c3) and levels of reddish-brown paleosol about 0.5 m thick. Pyroclastic rocks are formed from fine-grained yellowish pumice, volcanic tuff, and locally dark grey volcanic ash levels. They are rarely found xenoliths with different chemists with a maximum size of 20 cm. Acid effusive rocks are massive and only locally exhibit levels of phenocrysts, generally isoriated, in places with a glassy matrix.

The ignimbrites, due to the weathering and the discontinuities present, often form the columnar-polygonal bodies with a maximum diameter of 3 m. Where the discontinuities of pyroclastic rocks are more pronounced and irregular due to weathering how epiclastics are shattered into blocks of size and shape irregular.

San Salvador Formation (Late Pleistocene-Holocene)

The formation can be divided into four main members:

- level of effusive rocks. It forms the basal level of the San Salvador formation only near the Boquerón volcano. It is a level of basaltic andesites often from 5 to 10 m, generated by medium-fine-grained lava flows. Due to the scarce outcrops present, it is not clear whether the effusive rocks are interspersed with the member of the Tobas color café. However, the hypothesis seems reasonable enough since the processes that produced the two different members took turns very quickly. The member turns out to be particularly resistant to weathering processes.

- Tobas color café (s3a). Basal member consists of medium-grained or fine acid pyroclasticites, tobacco and yellowish coloured, with different degrees of consolidation and intercalated to black slag. The thickness of this member is maximum near the Boqueron volcano (2 m) and decreases considerably with the distance from it. A horizon of about 1.5 m of brown soil is found above, resulting from the degradation of the underlying rocks. The degree of consolidation of this level is remarkably variable and, often, during the heaviest rains, the material is subject to strong weathering processes.
- Tierra Blanca (s4 - TB). Represents the youngest member of the San Salvador formation. It is formed by white acid pyroclasticites and epiclastic rocks formed on the occasion of the various eruptions of Ilopango. The thickness is greater than 50 m near the caldera and decreases considerably with the distance from it. It consists of fine-grained dacitic pumice (also powder) of a white-greyish colour, interspersed with levels of angular pumice blocks of different sizes and acid xenoliths. Hart and Steen-McIntyre (1983) divide the Tierra Blanca member into 4 levels, each separated from the others by a level of a few meters of reddish-brown paleosol. These levels are informally called TB4, TB3, TB2 and TBJ (Tierra Blanca Joven), respectively from the oldest to the youngest. Rose et al. (1999) date the earliest level to ~ 60,000 years ago while the youngest level is dated to ~ 430 years BC. (Dull et al. 2001). The paleosols testify to an elaboration of the topographical surface of ~ 10,000 years. Levels of andesitic volcanic dust from surrounding volcanoes are often found between the dacitic and rhyolitic levels of the Tierra Blanca. The TBJ level is considered to be the most dangerous material in the area Salvadoran (Rolo et al. 2004). It is, in fact, characterized by the presence of different levels with different degrees of consolidation and permeability. A sequence typical of the TBJ presents at the base a centimeter or decimeter level of lapilli e fall blocks of the Plinian column; a basal sequence of pyroclastic flows with intercalations of falling material (variable thickness up to 10 meters); a permeable layer sequence (medium grain graded pumice) and layers waterproof (volcanic ash); a higher sequence of pyroclastic flows rich in volcanic ash (Figure 4.1.2.6). Due to the different mechanical properties of the different levels, the latter plays a key role in the triggering of landslides (Rolo et al. 2004).
- Juvenile river deposits (Qf). They result from the degradation of the volcanic material described above.



Figure 4.1.2.6: a geological natural cross section of Terra Blanca Joven (TBJ). Photo by Giuseppina Kysar, 1999 (Smithsonian Institution).

Focusing on the five study areas, the lithologic units of the San Salvador formation are the most frequently outcropping rocks: “Tobas color café”, in the Coatepeque area (77%), “Tierra Blanca”, in the Ilopango area (45%) and to a lesser extent in the San Salvador area. Accumulation cones dominate the San Miguel area (72%), while Pleistocene effusive rocks prevail in the San Salvador area (57%) largely outcropping also in the San Vicente area. Besides, acid pyroclastites of the Cuscatlán formation are widely diffused both in the Ilopango and the San Vicente areas. Finally, with very limited outcropping areas, the pyroclastic and effusive rocks of the Bálsamo formation are observed in the Coatepeque, Ilopango and San Vicente areas.

For some of the applications, the above-mentioned outcropping lithologies were grouped based of the geomechanical expected response, as soft, medium, hard rocks; very soft, soft, medium, hard soils (Table 4.1.2.2). Figure 4.1.2.7 shows the distribution of the geomechanical units among the study areas.

It is possible to note that the distribution of the geomechanical units is not uniform, with a clear predominance of medium soil in the Coatepeque and San Miguel areas, while in the San Salvador area soft rock prevails. In the Ilopango area, very soft soil and hard soil together represent approximately 80% of the territory. On the other hand, for the San Vicente area hard soil, soft soil, hard soil and very soft soil classes are present with a variable percentage between 15 and 30%.

Geomechanical classification	Geological units
Hard soil	c1
Soft soil	Qf
Very soft soil	s4
Hard rock	c3, b3
Soft rock	b2, s2
Medium soil	b1, s5a, s1, s5c, s3a
Medium rock	s3b, s5b, c2

Table 4.1.2.2: the geomechanical classes with their corresponding geological unit.

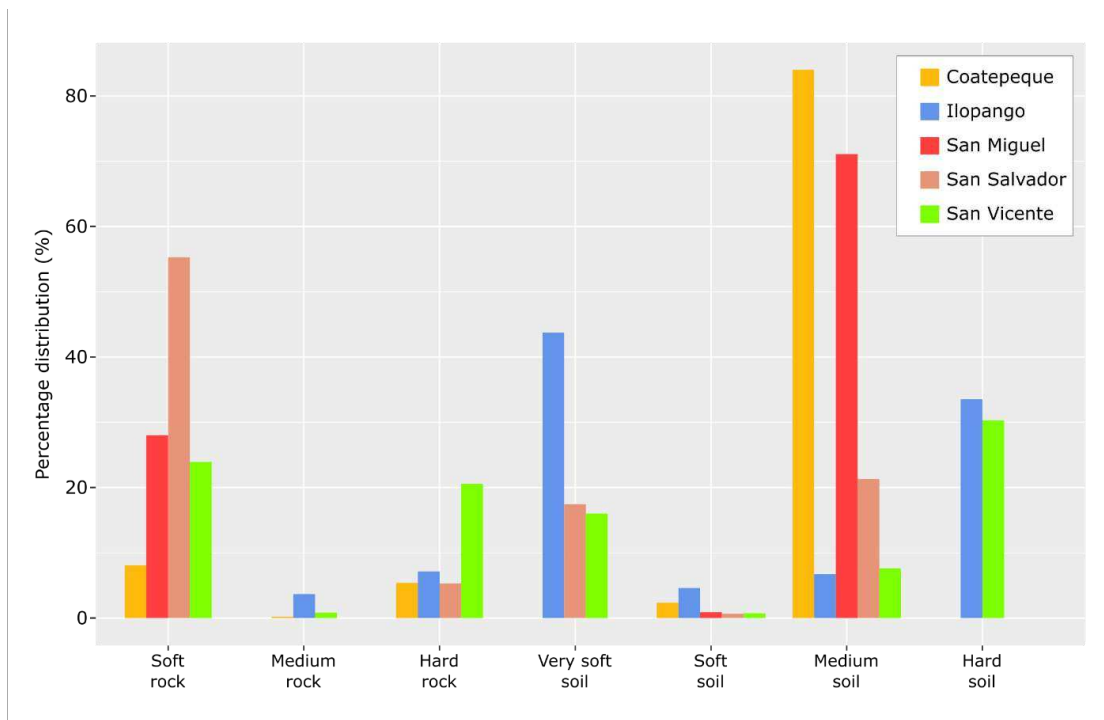


Figure 4.1.2.7: distribution of the geomechanical units in the five study sectors.

4.2. Sicily

4.2.1. Regional setting

Sicily is located in the western central part of the Mediterranean Sea. The region stretches along the African-European plate boundary and is configured as the result of post-collisional convergence between Africa and the European crusts and the roll-back of the subduction hinge of the Ionian lithosphere (Doglioni et al. 1999; Faccenna et al. 2004; Chiarabba et al. 2005). In this way, the Sicilian Fold-and-Thrust Belt (SFTB) is a Neogene-Quaternary southeast-verging sector of Apennine-Maghrebian orogen (Catalano et al. 1996; Avellone et al. 2010; Accaino et al. 2011; Gugliotta et al. 2013).

The chain and its submerged western and northern extensions are partly located between the Sardinia block and the Pelagian-Ionian sector, and partly beneath the central southern Tyrrhenian Sea (Figure 4.2.1.1). The collisional complex of Sicily and adjacent offshore areas is characterized by (Basilone 2012):

- the Pelagian-Iblean foreland with its African crust. The sedimentary succession is 7/8 km thick and includes Triassic and Jurassic carbonates indicative of shelf and a slope-to-basin environment; late Jurassic and Cretaceous-to-Miocene pelagic carbonates, followed upwards by clastic open platform deposits;
- a Late Pliocene-Quaternary narrow foredeep, onlapping the frontal sector of the thrust belt in southern Sicily and units offshore in the Sicily Channel. The sediments are late Miocene-to-Pleistocene in age and include the Gessoso-Solfifera formation of the Messinian age and the overlying Trubi and Monte Narbone formation. The Gela nappe was displaced in the early Pleistocene;
- a complex, south to southeast-vergent fold and thrust belt, locally more than 15 km thick, consisting of a “European” element (Peloritani Units with a metamorphic basement), a “Tethyan” element (Sicilide Units) and an African element (Maghrebian-Apenninic Units). The tectonic units derived primarily from the deformation of some original paleogeographic domains (carbonate basinal and platform succession) that developed during the Meso-Cenozoic interval in the Sicilian sector of the African continental margin.

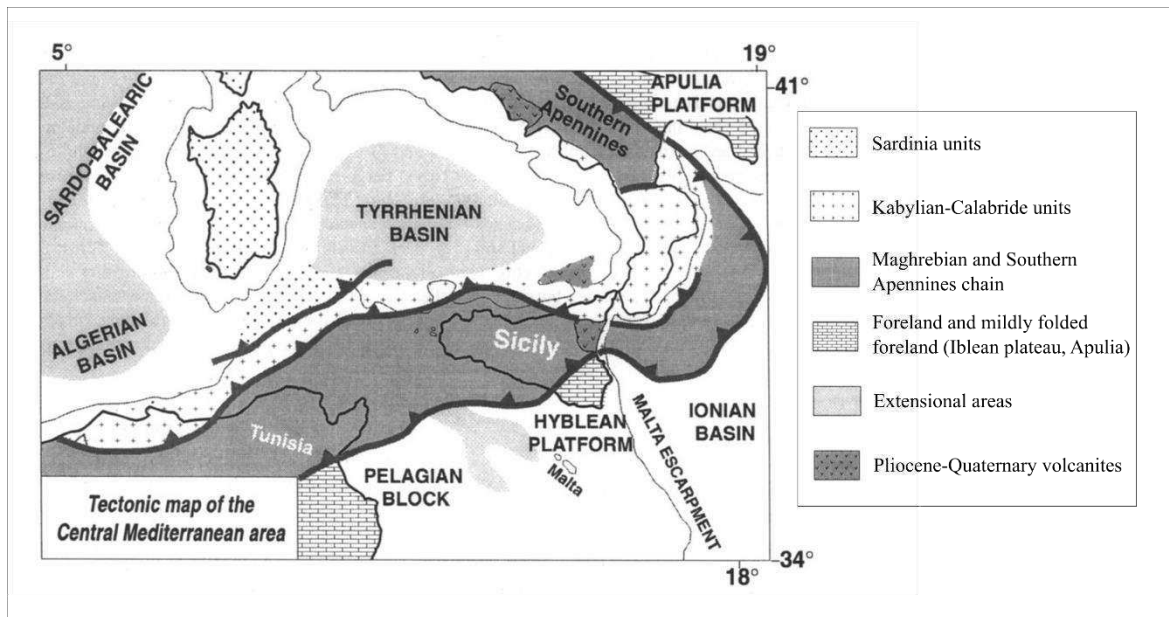


Figure 4.2.1.1: structural map of Sicily (modified from Catalano et al. 1996).

Two main tectonic events produced the current orogenic belt (Catalano et al. 1996; Gugliotta et al. 2013):

- the first step (Event I), developed in the middle Miocene, was characterized by shallow-seated thrusts (present-day SW-verging) and associated folds (at present showing NW SE-trend) which involved relatively thin deep-water carbonate rock successions;
- the second step (Event II), developed since the latest Tortonian, involved the lowermost carbonate platform units by the development of S-verging, deep-seated thrusts and back-thrusts often showing kinematic features of transpressional ramps.

The deep-seated thrusting transferred part of the deformation into the overlying thrust pile and sedimentary cover inducing passive-imbrication, shortening and development of several late Miocene to Pliocene syntectonic basins (Gugliotta et al. 2013).

4.2.2. Main characteristics of the study sector

The Imera river catchment (Figure 4.2.2.1) is one of the largest watersheds of Sicily (southern Italy): the main channel and its tributaries drain an area extending about 343 km² from the northern sector of the Madonie Mountains to the Tyrrhenian Sea, ranging from 1866 m a.s.l. down to sea level (Figure 4.2.2.2).



Figure 4.2.2.1: location of study area.

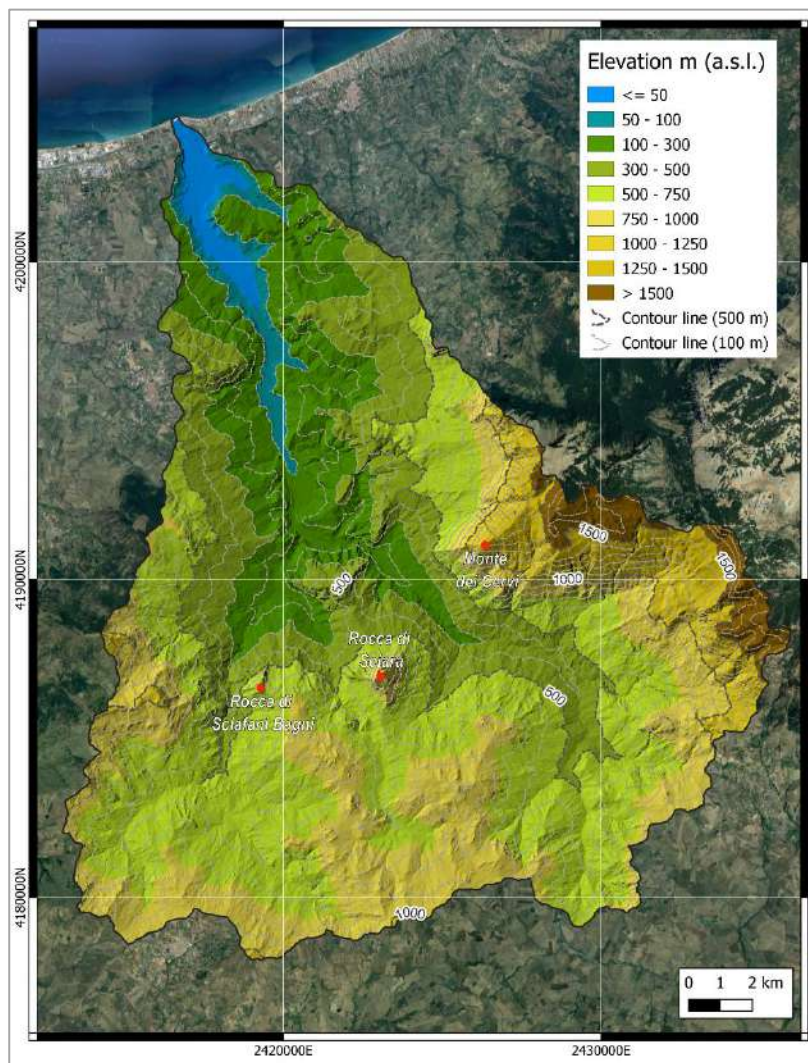


Figure 4.2.2.2: structural map of Sicily (modified from Catalano et al. 1996).

The geomorphological setting of the area is strictly linked to the outcropping lithologies, resulting from intense compressive tectonic activity starting in the Oligocene (Morticelli et al 2015), followed by a syntectonic relaxing phase during which the thrust sheets' basins were filled with terrigenous deposits (Gugliotta et al 2013).

In the area, 3 main sectors can be distinguished (Agnesi et al. 2000):

- on the right bank upstream, the sector of the mountain group of the Western Madonie, dominated by the presence of Monte dei Cervi (1792 m a.s.l.), with more rugged and uneven shapes due to the presence of carbonatic-dolomitic outcrops with fragile behaviour alternating with lithotypes clayey and clayey-marly with ductile behaviour;
- on the left bank upstream, the western sector, in which plastic outcrops prevail, giving rise to gentle and not very steep shapes. The carbonate reliefs of Rocca di Sciara (1080 m) and Sclafani Bagni (755 m) stand out in an isolated position;
- the valley sector, corresponding to the Imera Settentrionale Valley, is mainly characterized by gentle slopes in clayey lithotypes and slopes with higher inclination on clayey-marly lithotypes, with isolated carbonate elements.

Figure 4.2.2.3 shows the outcropping lithology map of the Imera river basin (modified from Abate et al. 1982, 1988; Catalano et al. 2011). Below, is a brief description of the geological units outcropping in the area. Please, see the main text below for the acronym in the legend of the map.

Sicilide Domain Succession

- *Lower varicoloured shales (AVF)*
Varicoloured shales and marls in greenish-grey, red wine, brick red, ochre yellow or whitish-grey tones, often tectonized, jaspers, micaceous and quartzitic sandstones, greenish calcilutites. Cretaceous (Albian-Turonian)-Paleocene.
- *Polizzi formation (POZ)*
Grey to whitish marls in decametric-centimetric strata and greyish-violaceous, marly-clayey thin beds, laminated whitish calcisiltitis, sometimes with lists and nodules of silex, white marls with intercalations and lenses of biocalcarenites, biocalcirudites with macro-foraminifera (nummulitids, alveolinids, discocyclinids). Middle-upper Eocene.

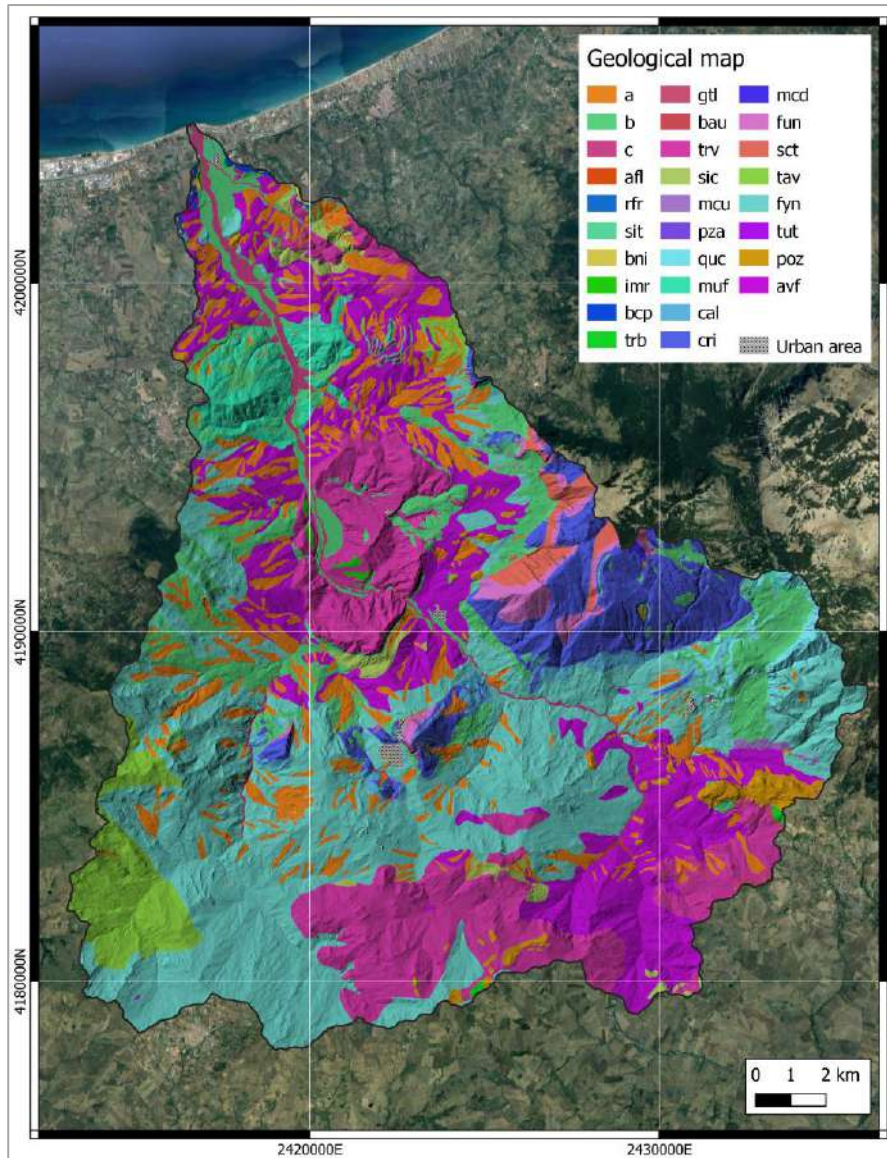


Figure 4.2.2.3: geological map of the Imera river basin (modified from Abate et al. 1982, 1988; Catalano et al. 2011).

- *Tufiti di Tusa (TUT)*

Marls, grey-blackish soapy marly limestones, greenish volcano-clastic sandstones and grey yellowish quartzitic feldspathic sandstones. In the area the marly member of the lithofacies mainly outcrops. Oligocene.

Numidian Flysch Basin Succession

- *Flysch Numidico (FYN)*

Clayey pelites and pelites with thin biocalcarenic arenaceous levels and megabreccias with carbonate elements, tobacco-coloured silty clays with intercalation of arenaceous levels, quartzarenites and microconglomerates. In the area, the quartzarenitic and ruditic facies mainly outcrop. Chattian-Burdigalian.

- *Tavernola formation (TAV)*
Greenish grey pelites, brown-greyish sandy and clayey marls, greyish clays interspersed with centimetre arenaceous levels that alternate with banks of fine yellow or greenish quartz. Upper Burdigalian to Langhian.

Imerese Basin Succession

- *Scillato formation (SCT)*
Grey calcilutites (mudstone and wackestone) laminated with nodules in thin layers, alternating with marly levels, passing through crystalline calcilutites, graded calcarenites and calcirudites and laminated in large banks and upwards, to dolomitic limestones. Upper Carnian and the Rhaetian.
- *Fanusi formation (FUN)*
Dolomite and dolomitic breccias organized in cyclical alternations of graded and laminated dolomites and dolarenites, grey dolomitic limestone and dolomitic breccias. Sometimes they appear as whitish floury, massive, or poorly stratified dolomites, passing upwards to well-stratified grey dolomitic limestones. Lower Liassic.
- *Crinoidal limestones and Altofonte Breccias (MCD)*
Alternation of reddish and yellowish marls and highly recrystallized calcarenites. Middle-upper Liassic.
- *Crisanti formation (CRI)*
The Crisanti formation consists of four main members: the radiolarian member, with laminated radiolarites and polychromatic siliceous argillites; the ellipsactinia breccias member, with calcareous breccias and massive calcareous conglomerates with ellipsactinia alternating with greenish marl; the marly spongolitic member composed of argillites, siliceous marl and marly limestone; the rudist breccias member, composed of limestone breccias, calcirudites, grey resedimented biocalcarenes. Upper Liassic – upper Cretaceous.
- *Caltavuturo formation (CAL)*
Calcilutites and calcisiltites with reddish or variously coloured lists and nodules of chert, marly limestone, and red marls, with intercalations of calcarenites and calcirudites and graded and laminated calcirudites, bioclastic calcirudites. Eocene - Lower Oligocene.

Panormide Domain Succession

- *Mufara formation (MUF)*
Calcareous marl, black calcilutites sometimes laminated and grey marly limestone.
Middle-upper Carnian.
- *Monte Quacella formation (QUC)*
Grey dolostones and dolomitic breccias in massive or indistinct stratified strata, vacuolar, with lenses of calcareous sandstones and calcirudites. Upper Triassic - lower Jurassic.
- *Pizzo Carbonara limestones and dolostones (PZA)*
Dolostones, stromatolitic and loferitic limestones with intraclasts and bioclasts, dolomitic limestones and calcarenites. Upper Triassic - lower Jurassic.
- *Castelbuono marls (MCU)*
Grey marly and micaceous quartzosiltites in thin layers, with frequent interbedded yellowish to light grey marly megastrata. Lower Miocene.

Miocene-Pliocene foredeep deposits

- *Castellana Sicula formation (SIC)*
Sandstones and quartzitic sands, laminated clays, grey-greenish pelites and sandy pelites, sometimes well cemented. Upper Serravallian to the Lower Tortonian.
- *Terravecchia formation (TRV)*
The formation consists of three heteropic members: the conglomeratic member, composed of greyish and yellowish polymittic ortho and paraconglomerates, with alternations of coarse pebbly yellowish sands; the sandy member, composed of yellowish to grey sands and arenites, with cross-bedded lamination, alternating with pelites and sandy pelites and thin conglomeratic layers; pelitic-clayey member, composed of sandy clays and bluish pelites with local arenite intercalations, grey marls, grey-greenish or bluish clays. Upper Tortonian – lower Messinian.
- *Baucina formation (BAU)*
Biocalcarenes and calcirudites, calcareous-marly arenites, massive biocalcarenes.
Lower Messinian.

- *Cattolica formation (GTL)*
The basal calcareous member outcrops in the area. Yellowish-grey crystalline limestones, vacuolar or brecciated dolomitic limestones and dolomites, with thin layer of laminated grey calcilutites. Upper Messinian.
- *Trubi (TRB)*
Marls and white marly limestones, with sandy intercalation, passing to grey-green or whitish sandy and clayey marl, sandy-marly calcarenites. Lower Pliocene (Zanclean).

Quaternary deposits

- *Buonfornello Campofelice synthem (BCP)*
Marine deposits, formed in different sedimentary cycles preceding the Tyrrhenian hot phase, which cover abrasion surfaces. In the area, the deposits of the sub-synthem of Ganci di Cenere outcrops, consisting of deposits of pebbles in a sandy-silty matrix. Middle Pleistocene.
- *Imera Settentrionale river Synthem (IMR)*
It includes fluvial deposits (conglomerates, gravels, sands and silts) of the Imera Settentrionale river. The deposits of Piano Lungo sub-synthem outcrops, with gravels in silty-sandy matrix alternating with fine silty sands. Middle Pleistocene – Tyrrhenian(?)
- *Benincasa Synthem (BNI)*
Polygenic conglomerates, quartzitic sands and reddish or red-brownish silts are associated with colluviums.
- *Barcarello Synthem (SIT)*
Brownish sands and silty sands, conglomerates and siliceous calcarenites. Middle-Upper Pleistocene.
- *Baffo Rosso synthem (RFR)*
Bedded talus deposits with rough and coarse carbonate-dolomitic elements.
- *Capo Plaia synthem (AFL)*
Colluvial and landslide deposits (a), terraced (b) and recent (c) valley floor fluvial and talus deposits, debris flows and accumulation of eolian stuff with variable thickness. Upper Pleistocene.

According to the literature (e.g., Conoscenti et al. 2008a; Rotigliano et al. 2011; Costanzo et al. 2012a; Cama et al. 2017), the above-mentioned outcropping geologic units were grouped based on the geomechanical expected response. The derived units are (1) Anthropogenic deposits; (2) Alluvial deposits; (3) Alluvial fan and talus deposits; (4) Colluvium and old landslide deposits; (5) Evaporitic rocks; (6) Sandstones; (7) Flysch Numidico pelites; (8) Flysch Numidico sandstones/conglomerates; (9) ‘Terravecchia’ pelites; (10) ‘Terravecchia’ sandstones/conglomerates; (11) Varicolours clays; (12) Calcareous and clayey marls; (13) Lithoid units. The lithological map and the relative distribution are shown in Figures 4.2.2.4 and 4.2.2.5.

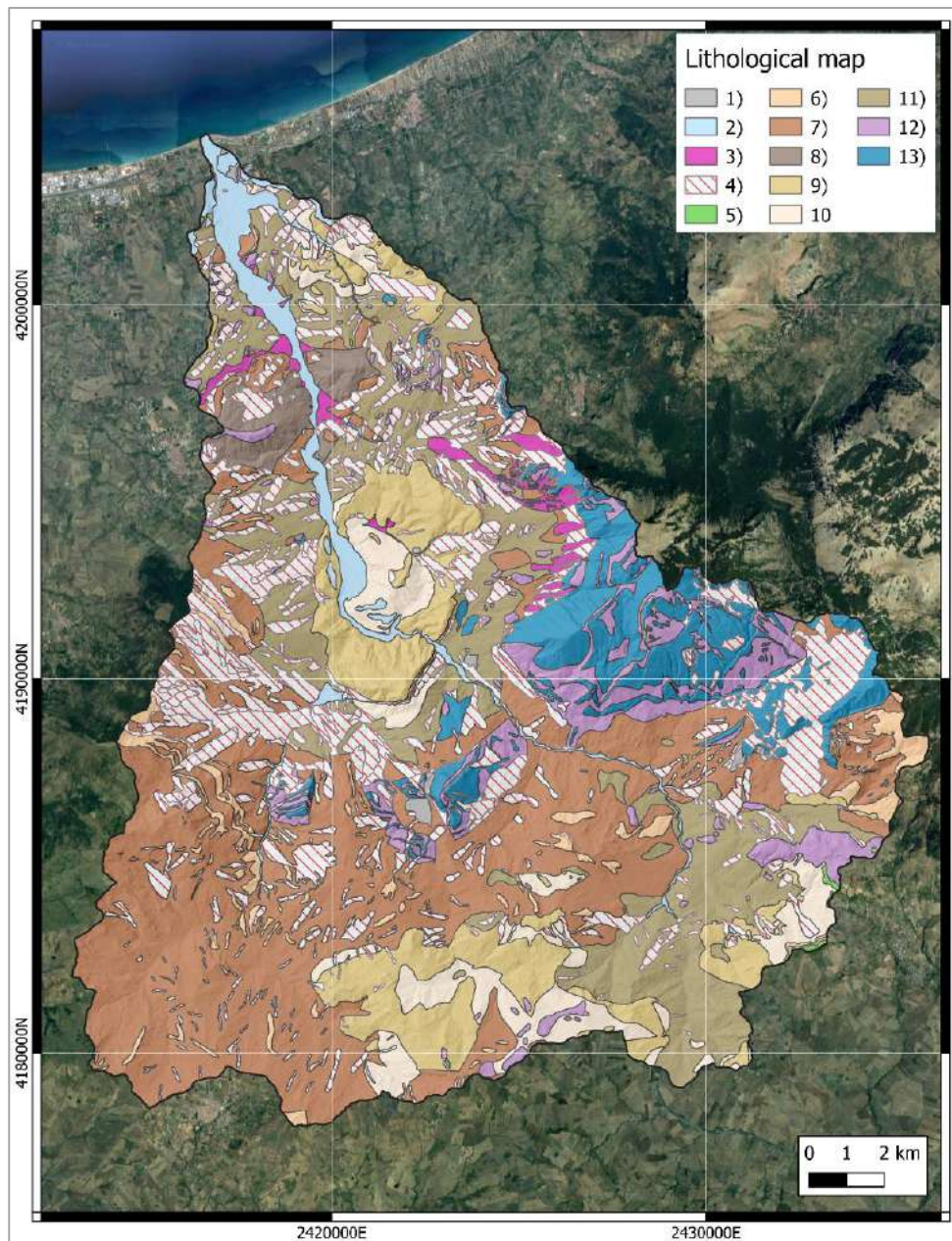


Figure 4.2.2.4: Outcropping lithologies in the study areas (modified from Martinello et al. 2020).

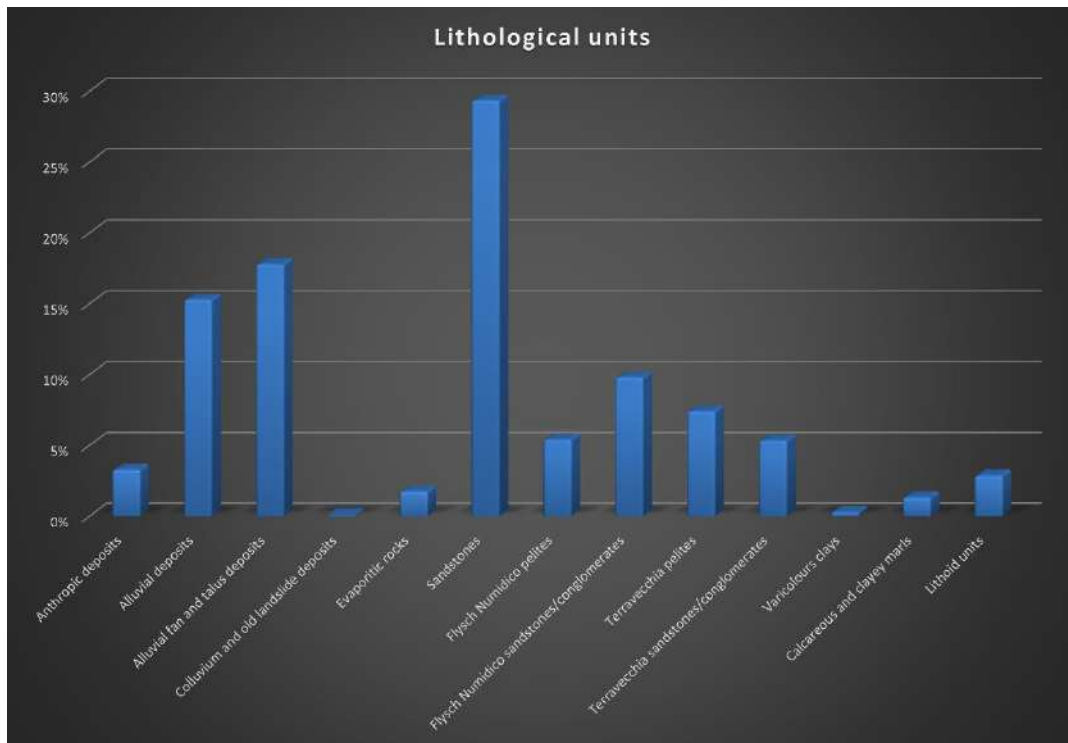


Figure 4.2.2.5: distribution of the lithological classes in study sectors.

In the area, carbonate, siliceous-carbonate and siliciclastic successions alternating with more ductile pelitic flysch sediments, alluvial clastic sediments and marine pelites characterize the slopes where water erosion landforms (rills, gullies, pipes), badlands systems (Cappadonia et al 2011; Buccolini et al 2012; Pulice et al 2012; Cappadonia et al 2016; Brandolini et al 2018) and landslides (mainly of the flow, slide and fall type) shape the landscape (Agnesi and Macaluso 1997; Agnesi et al. 1997, 2005). On the whole, clayey lithologic units largely form (63%) the long to short slopes whose heads are characterized by the outcropping of either thin metric arenitic/marly (9%) or hundreds-of-meters-thick carbonate (7%) caps in the hilly and mountain sectors, respectively. Landslide bodies, debris talus/cones and present alluvial deposits account for 20% of the outcropping units.

For the study areas, all aspect classes are represented but a general major exposure to sectors from SW to NE arises (Figure 4.2.2.6).

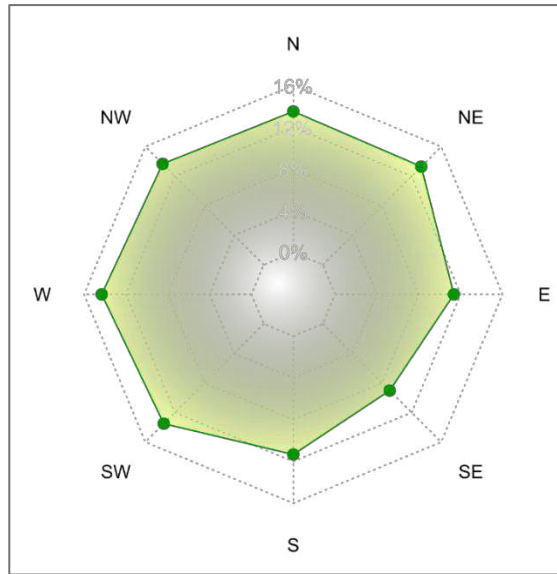


Figure 4.2.2.6: distribution of the exposure of the slopes in the study area.

Based on the more recent Corine (2018) coverage, the soil use recognized in the area (Figure 4.2.2.7) is mainly characterized by arable land (40%), sclerophyllous vegetation (14%), agricultural areas (13%), olive groves (9%), forest (6%) and bare (14%).

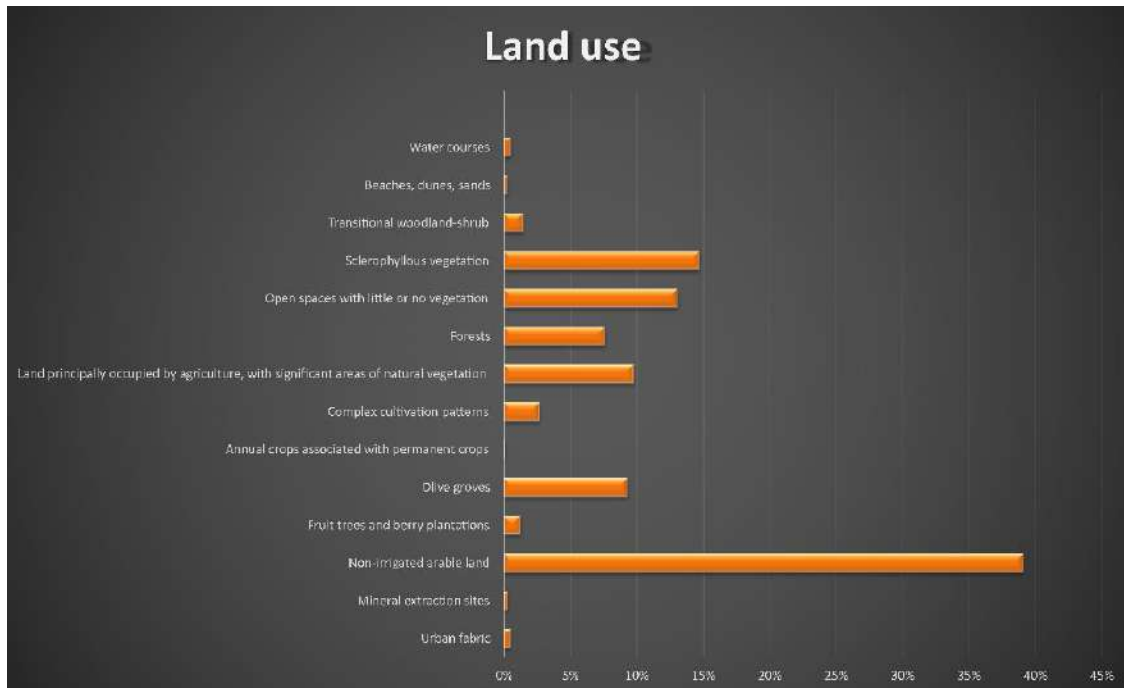


Figure 4.2.2.7: distribution of the land use classes in the study area.

The analysis of the Landform Classification (LCL) classes distribution for the study area (Figure 4.2.2.8) shows that the open slopes class is the most present class of LCL. On the other hand, the valleys, streams, midslope drainages and midslope ridges classes are present with similar abundance (~7%).

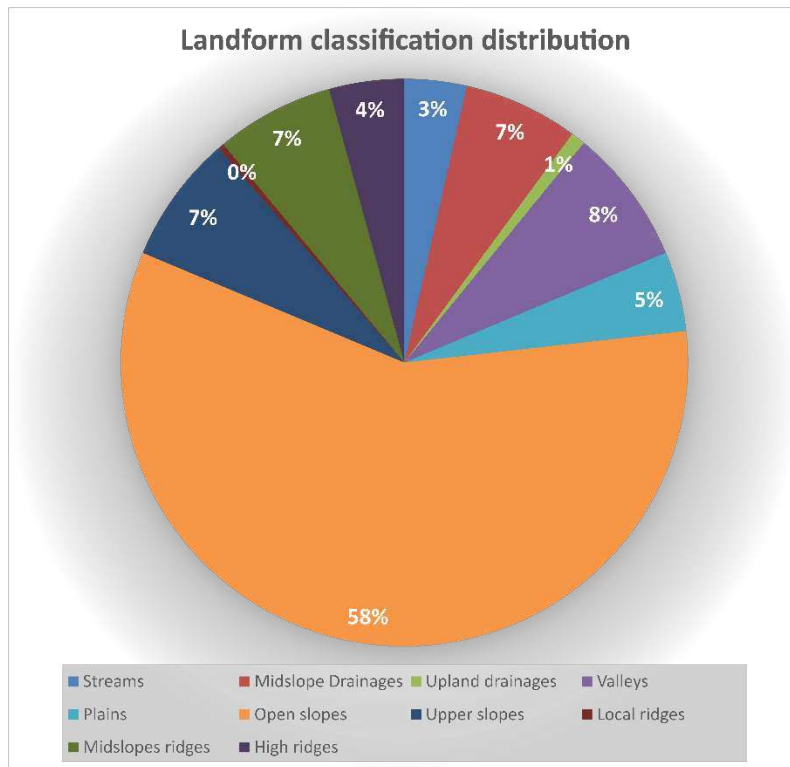


Figure 4.2.2.8: distribution of the landform classification classes in study area.

5. Applications

5.1. Predicting the landslides triggered by the 2009 96E/Ida tropical storms in the Ilopango caldera area (El Salvador, CA): optimizing MARS-based model building and validation strategies

Published on: Environmental Earth Sciences (2019), 78:210, DOI: 10.1007/s12665-019-8214-3

The main topic of this research was to evaluate the effect on the performance of stochastic landslide susceptibility models, produced by differences between the triggering events of the calibration and validation datasets. In the Caldera Ilopango area (El Salvador), MARS (multivariate adaptive regression splines)-based susceptibility modelling was applied using a set of physical–environmental predictors and two remotely recognized landslide inventories: one dated at 2003 (1503 landslides), which was the result of a normal rainfall season, and one which was produced by the combined effect of the Ida hurricane and the 96E tropical depression in 2009 (2237 landslides). Both the event inventories included shallow debris flow or slide landslides, which involved the weathered mantle of the pyroclastic rocks that largely outcrop in the study area. To this aim, different model building, and validation strategies were applied (self-validation, forward and backward chronovalidations), and their performances were evaluated both through cutoff-dependent and -independent metrics. All of the tested models produced largely acceptable AUC (area under the curve) values, albeit a loss in the predictive performance from self-validation to chronovalidations was observed. Besides, in terms of positive/negative predictions, some critical differences arose: using the 2009 extreme landslide inventory for calibration resulted in higher sensitivity but lower specificity; conversely, using the 2003 normal trigger landslide calibration inventory led to higher specificity but lower sensitivity, with a relevant increase in type-II errors. These results suggest the need for investigating the extent of such effects, taking multi-trigger intensities inventories as a standard procedure for susceptibility assessment in areas where extreme events potentially occur.

a) Landslide inventories

In this research, two landslide inventories, ante- and post- the passage of Hurricane Ida into the Ilopango Caldera were detected. A remote recognition was carried out through a systematic GE-based analysis, which was performed on two different epochs: one dated 9/10/2003 (DigitalGlobe Catalog ID: 1010010002459C02) and the other dated 11/21/2009

(DigitalGlobe Catalog ID: 101001000AA5D801), the latter being taken just 2 weeks after the Ida/96E combined event. Unfortunately, the 2003 GE images were affected by partial cloud coverage, so the study area had to be subdivided into a 2003 cloud-free (CF) and a cloudy blind (CB) sector.

In comparing 2003 with 2009 rainfall data, it is clearly evident (Figure 5.1.1) that 2003 can be considered a “normal” rainfall year, during which the maximum 24 h, 48 h, and 72 h rainfall were far below the Ida/96E records. As a consequence, the 2003 and the 2009 landslide inventories were considered a “normal” and an “extreme” one, respectively. It is worth mentioning that, in the time span of some years, a large part of the 2009 landslide areas were almost completely covered by vegetation and hardly recognizable on the field. At the time of our field survey (May 2015), the study area was generally affected by dormant and active landslides, which were mainly classifiable as debris slides or debris flows. The warm humid climate is, in fact, responsible for the fast growth of vegetation so that with the exception of a few cases of very recent landslides, a large part of the study area showed only smoothed forms of the previous slope failures (Figure 5.1.2).

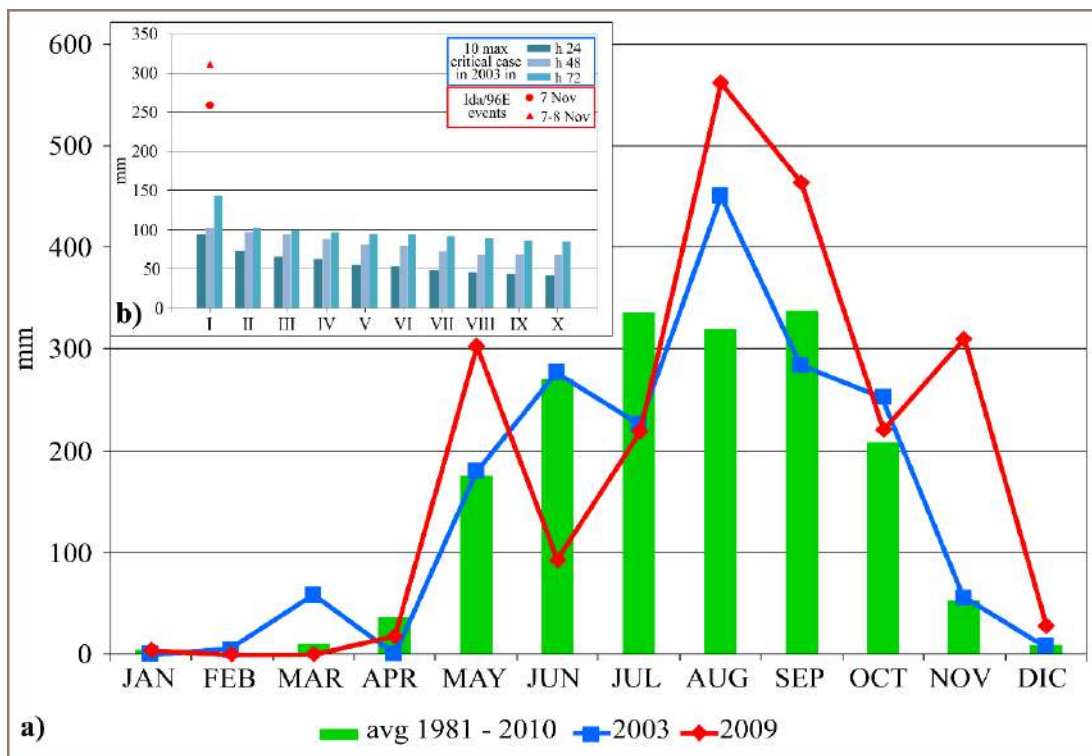


Figure 5.1.1: a) Average, 2009 and 2003 monthly rain at the meteorological station Ilopango. b) Comparison between the Ida/96E rainfall records and 2003 maximum ten critical cases for 24 h, 48 h, and 72 h durations

Each landslide area was mapped as a polygon and represented by means of a landslide identification point (LIP; Costanzo et al. 2014), which was positioned on the highest point

along the crown line. In light of the type of slope movement, LIPs were assumed to be potentially suitable for detecting the site conditions responsible for the previous failures that, as such, can be used as diagnostic landforms (Rotigliano et al. 2011; Lombardo et al. 2014; Cama et al. 2015) for calibrating the predictive models. It is worth noting that, as a consequence, using a LIP inventory for calibrating the susceptibility models obviously led to estimating the probability for a pixel to be an initiating area, to be then integrated with propagation and/or runout stages modelling.

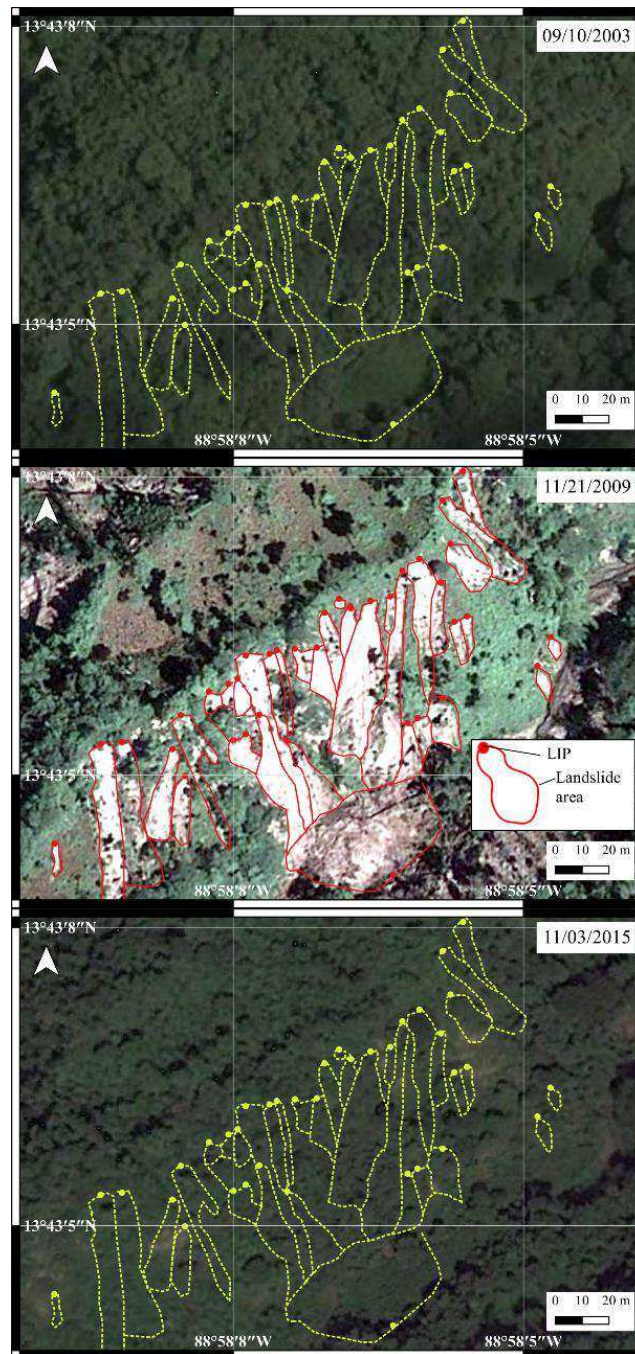


Figure 5.1.2: Comparison between 2003 (a), 2009 (soon after the Ida/96E event; b) and 2015 (c) slope conditions on a representative sector of the study area (LIP: landslide identification point).

The two landslide inventories (Figures 5.1.3 and 5.1.4) included 1503 and 2237 landslides, for 2003 and 2009, respectively. It is worth noting that 253 2009 cases corresponded to the reactivation of the 2003 landslides.

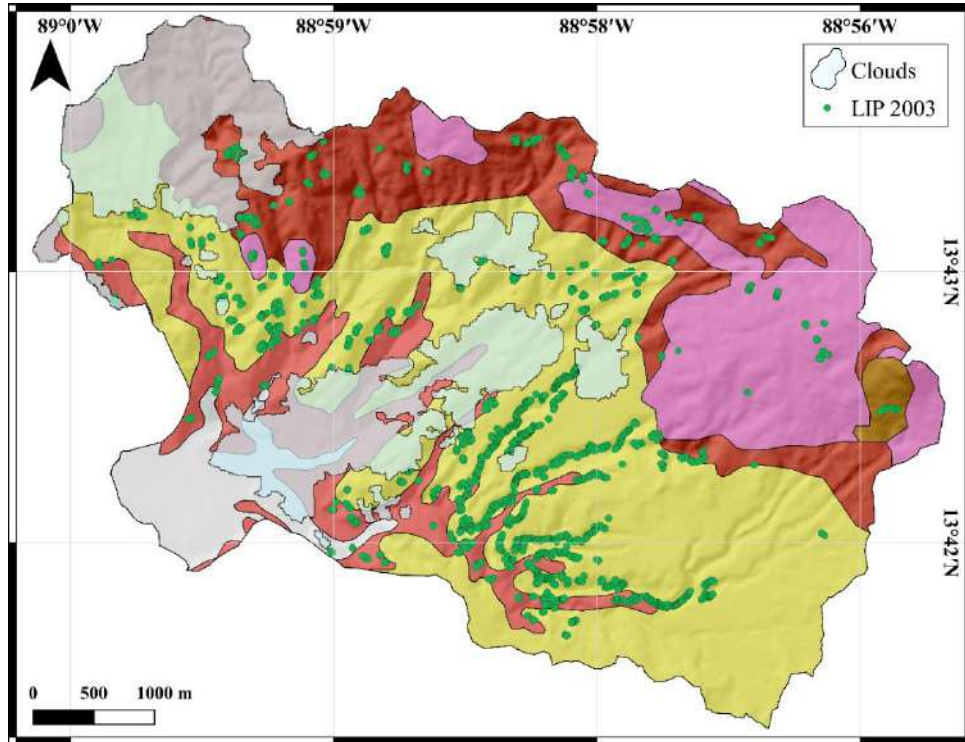


Figure 5.1.3: 2003 landslide inventory map.

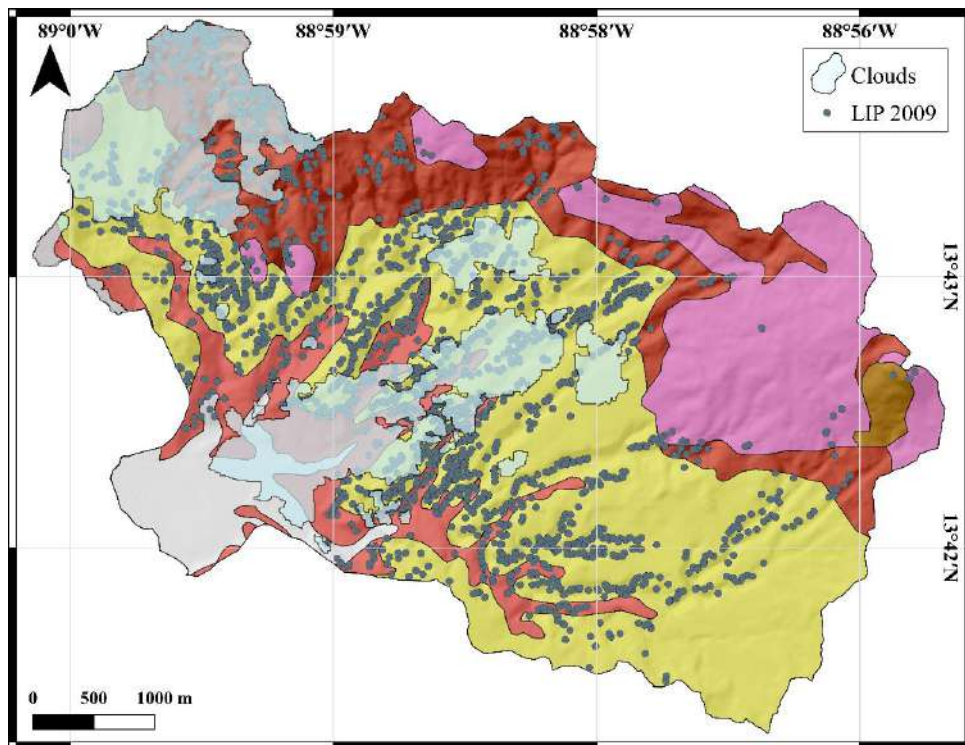


Figure 5.1.4: 2009 landslide inventory map.

b) *Predictors*

The following covariates were assumed at the initial stage as potential predictors for slope failures in the study area: outcropping lithology (LIT), land use (USE), landform classification (LCL), elevation (ELE), steepness (STP), aspect (ASP), plan (PLN) and profile (PRF) curvatures, topographic wetness index (TWI) and terrain ruggedness index (TRI).

The 10 m pixel structure of the source DEM was adopted for partitioning the study area into mapping units (Cama et al. 2016). The classes for each of the categorical predictors (for aspect see the section of predictors 2.3) are listed in Table 5.1.1.

Factor	Source layer	Classes of the variable
LCL	Landform classification	LCL_1 (streams)
		LCL_2 (midslope drainages)
		LCL_3 (upland drainages)
		LCL_4 (valleys)
		LCL_5 (plains)
		LCL_6 (open slopes)
		LCL_7 (upper slopes)
		LCL_8 (local ridges)
		LCL_9 (midslope ridges)
		LCL_10 (high ridges)
LIT	Lithology	LIT_Qf (Quaternary sedimentary deposits)
		LIT_s4 (pyroclastics of “Tierra Blanca”)
		LIT_s5b (accumulation cones)
		LIT_c1 (acid pyroclastics)
		LIT_c2 (acid effusive)
		LIT_b3 (basic-intermediate effusive rocks)
USE	Land use	USE_1 (wood)
		USE_2 (crop cultivation)
		USE_3 (vegetable cultivation)
		USE_4 (crop cultivation and pasture)
		USE_5 (pasture cultivation)
		USE_6 (pasture)
		USE_7 (river)
		USE_8 (continuous urban fabric)
		USE_9 (discontinuous urban fabric)
		USE_10 (precarious urban fabric)
		USE_11 (growing urban fabric)
		USE_12 (low shrubs)
		USE_13 (mine areas)
		USE_14 (uncultivated areas)

Table 5.1.1: list of the categorical predictors.

c) *Model building and validation strategy*

MARS (Multivariate Adaptive Regression Splines) modelling was exploited to regress the predictor variables to each landslide susceptibility archive.

According to the adopted research design, two validation schemes were applied: chrono-validation, based on the 2003/2009-time partition, and self-validation, based on the spatial random partition of each of the two inventories (Chung and Fabbri 2003; Guzzetti et al. 2006; Cama et al. 2015, 2017; Lombardo et al. 2015). In particular, the forward chrono-validation scheme was applied, by calibrating with 2003 and validating in 2009, whilst the opposite scheme was applied for backward chrono-validation. Moreover, due to the presence of the cloudy area in the 2003 GE coverage, chrono-validation schemes were adopted for predicting either the whole 2009 landslide inventory (2009ALL) or the CF (2009CF) subset. For the same reason, the backward chrono-validation procedure was performed only in the CF sector, by calibrating with 2009 landslides and validating in predicting the 2003s. By applying time and random partition schemes, starting from the three available calibration datasets (2003CF, 2009CF, and 2009ALL), the six models of Table 5.1.2 were obtained. Each model building scheme was replicated 100 times.

Model	Validation scheme	Calibration	Validation	Dataset
A	<i>SELF</i> _{2003CF}	<i>2003</i> _{CF_RND(90%)}	<i>SELF</i> _{2003CF_RND(10%)}	10-fold cross-validation
B	^{FRW} CHRONO _{CF-CF}	<i>2003</i> _{CF_(100%)}	<i>2009</i> _{CF_(100%)}	100 (CAL X VAL)
C	^{FRW} CHRONO _{CF-ALL}	<i>2003</i> _{CF_(100%)}	<i>2009</i> _{ALL}	100 (CAL X VAL)
D	^{BCK} CHRONO _{CF-CF}	<i>2009</i> _{CF_(100%)}	<i>2003</i> _{CF_(100%)}	100 (CAL X VAL)
E	<i>SELF</i> _{2009CF}	<i>2009</i> _{CF_RND(90%)}	<i>2009</i> _{CF_RND(10%)}	10-fold cross-validation
F	<i>SELF</i> _{2009ALL}	<i>2009</i> _{ALL_RND(90%)}	<i>2009</i> _{ALL_RND(10%)}	10-fold cross-validation

Table 5.1.2: Characteristics of the validation schemes adopted for the six susceptibility models.

Comparison of model A with model D, or model B with model E, allows investigating the role of the calibration inventory in the prediction skill of the derived susceptibility models. In fact, in both the cases, the landslide scenarios (i.e., 2003 and 2009) were predicted by calibrating the susceptibility models either on samples of landslides caused by the same event or extracted from the other scenario. The different model performances were then more clearly highlighted by directly comparing model B with model D. At the same time, to have reference levels for evaluating the performance of the temporal (chrono-validated) predictions, the 2003CF, 2009ALL, and 2009CF datasets were also submitted to random splitting-based self-validation.

To estimate the potential role of the blind area in hampering the research strategy, B to C and E to F models were also compared.

Each dataset was balanced by adding to the positives (i.e., pixels hosting a LIP) an equal number of randomly selected negatives, corresponding to LIP-free pixels (Conoscenti et al. 2016). For temporal partition-based validations, 100 replicates were obtained by randomly multi-extracting a different subset of negatives both in the calibration and validation datasets.

Self-validations were based on tenfold with ten repetition cross-validation schemes, obtaining one hundred estimates of model parameters and performance metrics (Table 5.1.2).

The performances of the models were evaluated by adopting both cutoff-dependent and -independent metrics. In particular, the prediction skill of the model was evaluated by computing the *AUC* (area under the curve) in the ROC (receiver operating characteristics) sensitivity vs. fallout (1-specificity) plots, as well as from confusion matrixes by distinguishing the true/false positive/negative cases (i.e., TP, TN, FP, and FN, respectively), obtained from Youden index optimized cutoff (Youden 1950).

For each of the validation procedures, the 100 replicates allowed to obtain the mean and variance of all the metrics enabling the estimation of the model performances in terms of precision and reliability.

d) *Results*

To explore the structure of the models in terms of selected variables, the n-subsets criterion was adopted (Conoscenti et al. 2016), by counting the number of model subsets including each selected variable throughout the pruning pass, which is assumed as expressing the variable importance.

Table 5.2.3 summarizes the results for the three calibrated models. With a threshold of variable importance of 1 or more, only 27 variables were extracted at least for 1 model, out of the 44 included at the first step of the modelling procedures, with a larger set of variables included in the 2009CF and 2009ALL models.

Based on the comparison between the results of the three models, five main groups of variables can be defined: I, variables selected for all the three models; II, variables selected only for the 2009CF and 2009ALL models; III, variables selected only for the models calibrated in the CF area; IV, variables selected for the 2003CF and 2009ALL models; V, variables selected only for one single model. TRI and ELE are the most important variables,

with very similar and high mean values. The Ia subgroup is completed by quite important and homogeneous variables. The high importance of the north-eastern aspect observed for the 2003CF model was not exhibited by E and F models. The Ic subgroup includes variables that are very important for the two 2009 models, whilst a lowering of one order of magnitude is observed for 2003CF. The II group includes a large set of variables that are important for the two 2009 models (ASP_South and ASP_SouthEast, in particular), but not extracted throughout the pruning pass in the 2003CF calibration. SLO is selected as a quite important variable only for models calibrated in the CF sector, whilst group IV variables were extracted with varying importance, only for 2003CF and 2009ALL models. Finally, group V variables were extracted only for one of the calibrated models.

<i>Variables</i>	<i>ModA (2003CF)</i>	<i>ModE (2009CF)</i>	<i>ModF (2009ALL)</i>	<i>Type</i>	
LCL_2	6	5	9	I	a
TRI	17	19	21		a
ELE	16	18	20		a
ASP_W	2	3	6		a
ASP_E	7	3	6		a
ASP_NE	12	4	2		b
USE_2	2	12	13		c
TWI	3	10	17		c
USE_4	4	17	19		c
LTL_s5b	NS	2	2	II	
PLC	NS	3	2		
PRC	NS	3	2		
ASP_NW	NS	1	2		
LIT_b3	NS	7	5		
USE_9	NS	2	4		
LCL_6	NS	1	4		
ASP_SE	NS	15	17		
ASP_S	NS	13	17		
ASP_SW	NS	6	12		
SLO	5	3	NS	III	
USE_6	9	NS	8	IV	
LIT_s4	1	NS	6		
LIT_c1	NS	NS	7	V	
LIT_c2	NS	NS	4		
LCL_4	7	NS	NS		
USE_14	3	NS	NS		

Table 5.1.3: Summary of the variable importance index for the three calibrated models

As regards the predictive performances, Figure 5.1.5 shows the average ROC curves that were obtained for the six models through their replicates, while, to ease the comparison of the global accuracy, a box plot displaying each of the corresponding mean *AUC*s was prepared (Figure 5.1.6).

The whisker symbols along the ROC curves (Figure 5.1.5) attest for highly stable results through the replicates, with higher dispersion gradually shifting from true to false positives in the direction of the lower scores. For the calibrated subsets, the frequency distribution of the scores shows a different shape in the intermediate range (0.7–0.3), with a clear bimodal trend for the 2003 model (Figure 5.1.5a-c), resulting in a flat zone, where a wide range of scores is equally represented in terms of mapped pixels.

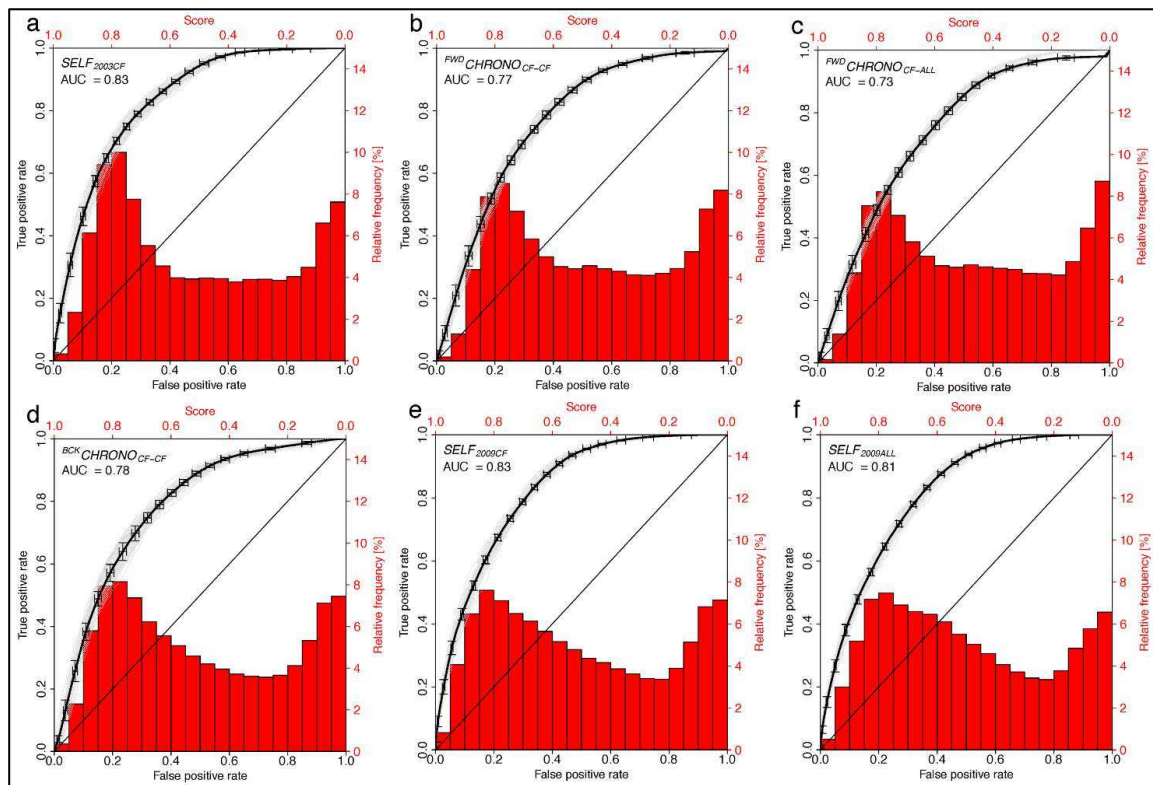


Figure 5.1.5: ROC plots for the six models

As regards the *AUC*s (Figure 5.1.6), the 2003CF, 2009CF, and 2009ALL self-validated models obtained similar excellent performances, with *AUC* values above the 0.8 threshold (Hosmer and Lemeshow 2000). At the same time, in the CF sector, the forward and the backward chrono-validations produced almost the same results in terms of *AUC*s, with largely acceptable values of 0.76 and 0.78, respectively.

For the forward chrono-validations, only a slight performance decrease was observed from the CF sector to the whole catchment ($AUC = 0.74$); the same small difference was observed for the 2009 self-calibrated model, from 2009CF ($AUC = 0.83$) to 2009ALL ($AUC = 0.81$). If cutoff-dependent performance metrics are taken into consideration (Table 5.1.4), it is evident that the loss in prediction skill from 2003 to 2009 self-validation (model A and model E) to forward and backward chrono-validation (model B and model D), respectively, depends on a sensitivity decrease, which is more marked for the 2003 model, with no coupled loss of specificity. Furthermore, by directly comparing the backward (model E) to the forward (model B) chrono-validated models in the CF sector, in spite of the similar AUC performance (0.71 and 0.70, respectively), a marked higher sensitivity and lower specificity of the former arises. In both cases, the specificity does not change from self- to chrono-validation. It is worth noting that the two opposite behaviours of specificity and sensitivity compensated for each other so that the two models resulted in similar accuracy.

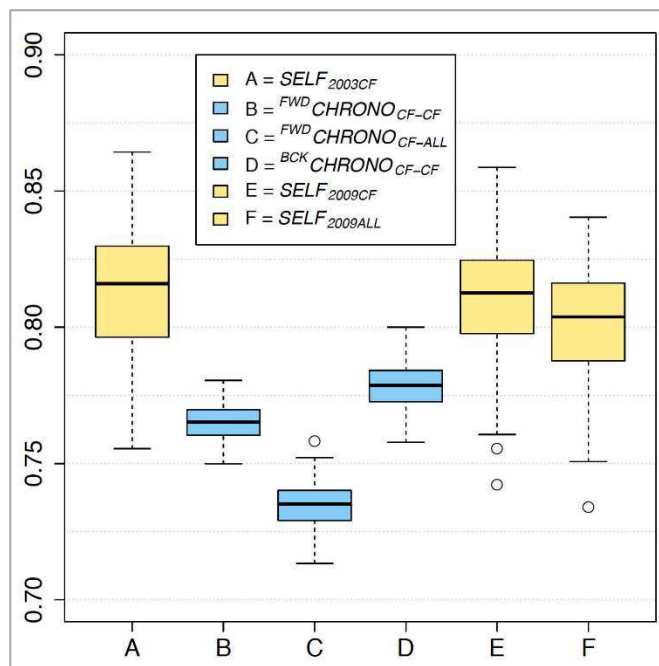


Figure 5.1.6: AUC boxplots for the six models

Figure 5.1.7a, b shows the two susceptibility maps prepared by calibrating the models in the CF sector exploiting the 2003 and 2009 landslide inventory, respectively. The maps were obtained by averaging, for each pixel, 100 estimates of probability values. A map of the residuals is also shown (Figure 5.1.7c), where the difference in the estimated score of the two models (score2003-score2009) is depicted. In spite of the similar general spatial pattern of the two prediction images, the 2009 model produced higher scores on average, whilst

positive and negative residuals stretch along the north-westward and south-eastward slopes of the main SW–NE running pyroclastic ranges, respectively.

However, in terms of positive and negative predictions, applying Youden Index cut-offs, few pixels were differently classified in the two maps (Figure 5.1.8): less than 5% of the pixels with scores diverging for more than one susceptibility class; a larger percentage (13%) of pixels classified with a one-class shift and crossing the cut-off score value.

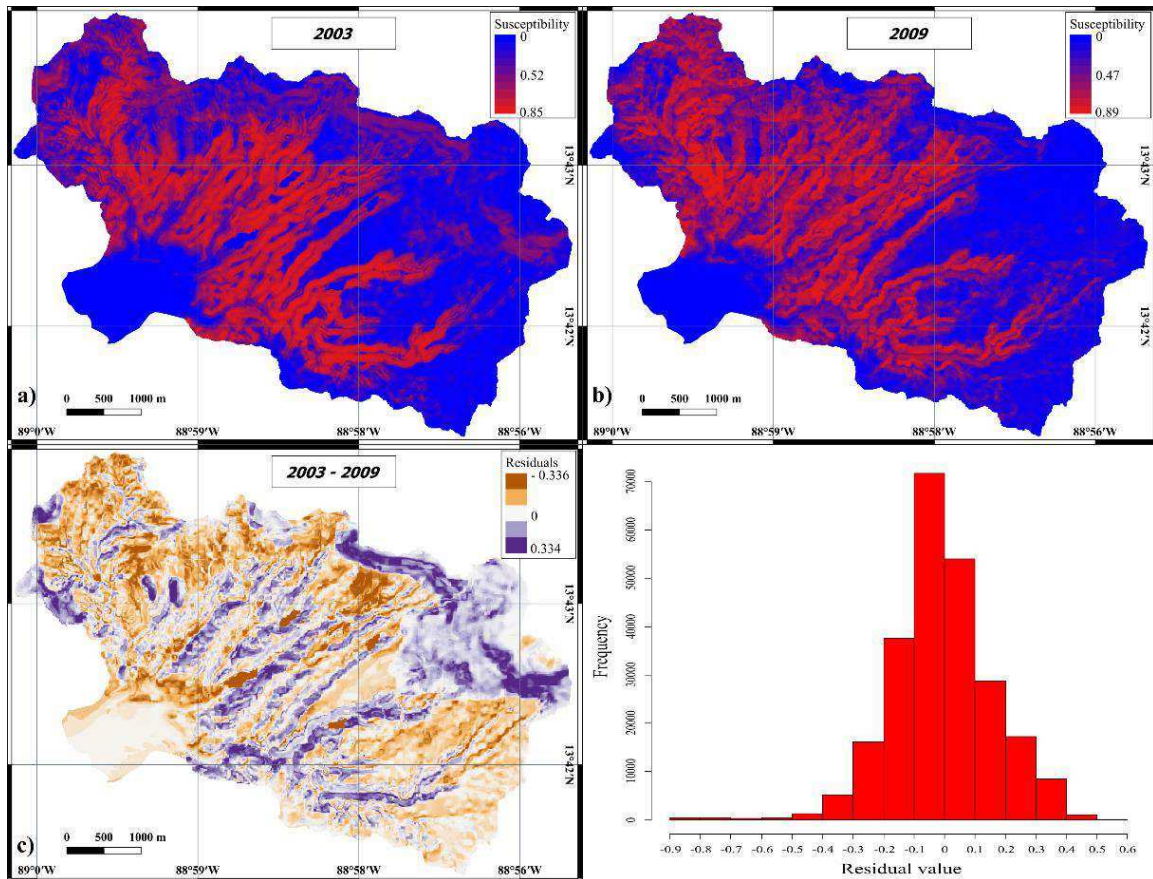


Figure 5.1.6: 2003 (a) and (b) 2009 landslide susceptibility maps. Map (c) and (d) frequency distribution of the residuals.

e) Discussion

The analysis of the variable importance of the three calibrated models highlights that more variables are involved in the definition of susceptibility for the extreme event datasets. At the same time, some variables play a role in the predictive models, no matter the intensity of the trigger, with two topographic factors showing the maximum importance: elevation (ELE) and topographic ruggedness index (TRI). On the other hand, some variables (topographic wetness index, pasture, and crop cultivation soil use) were more important (one order of magnitude) under the extreme scenario, as in the case of south and south-east aspect, which are among the most important variables for the two 2009 models but never extracted

for 2003CF. Conversely, the north-eastern aspect has an importance index of more than 10 only for normal event condition. The SLO variable was selected only for the models calibrated in the CF sector, probably due to the geomorphologic conditions.

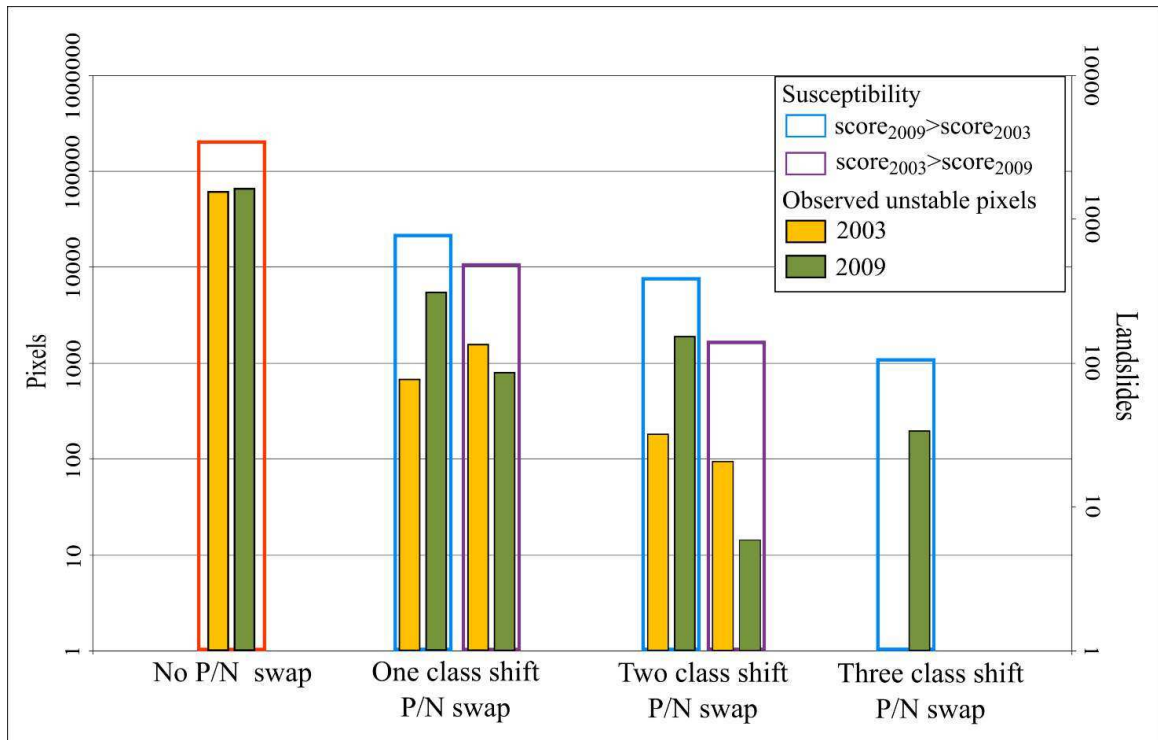


Table 5.1.8: differences in positive (P)/negative (N) predictions between the two models.

Figure 5.1.9 puts the main results of the validation tests inside the framework of the investigation strategy adopted in this research. The results attested that the 2003 landslide inventory allowed to calibrate a predictive model, whose *AUC* performance was estimated as very high and reliable, after a self-validation procedure was applied (model A); that was the only test we could have performed in 2003, before the 2009 Ida/96E event. However, if trying to predict the sites where then debris flow and debris slide phenomena are triggered (model B), a small *AUC* decreases (from above to below the 0.8 threshold), but coupled with a relevant number of false negative occurrences (low sensitivity), arose: relying on a map prepared on 2003 would have resulted in 32% of missing positives (against the 22% expected on the basis of the 2003 self-validation test).

An analogous *AUC* decrease resulted for the backward chrono-validation (model D) with respect to the 2009CF self-validated model (model E) but was caused by a moderate false negative prediction (miss rate) increasing, with only 21% of missing positives (against the 17% obtained from self-validation). It is worth highlighting that the model E showed the same accuracy as the self-validated model B in predicting the 2003 positives, suggesting the model calibrated with an extreme event landslide scenario of a different epoch (2009) as

being able to reach the same performance in recognizing the sites of activation for a normal season landslide scenario of a self-validated one. Conversely, the model calibrated with this lower trigger landslide scenario resulted in a markedly lower sensitivity than the one calibrated under the extreme event (sensitivity = 0.68, against 0.83). In particular, the 2009-calibrated model resulted capable to detect as nearly as 80% of the 2003 landslides, but expecting a higher number of positives, actually corresponding to 2003 stable sites (type-I errors), with low specificity and a high number of false positives. The same model calibrated in 2003 recognized the negative locations in the 2009 landslide scenario with a higher performance than 2009 self-validated itself (specificity = 0.72, against 0.63).

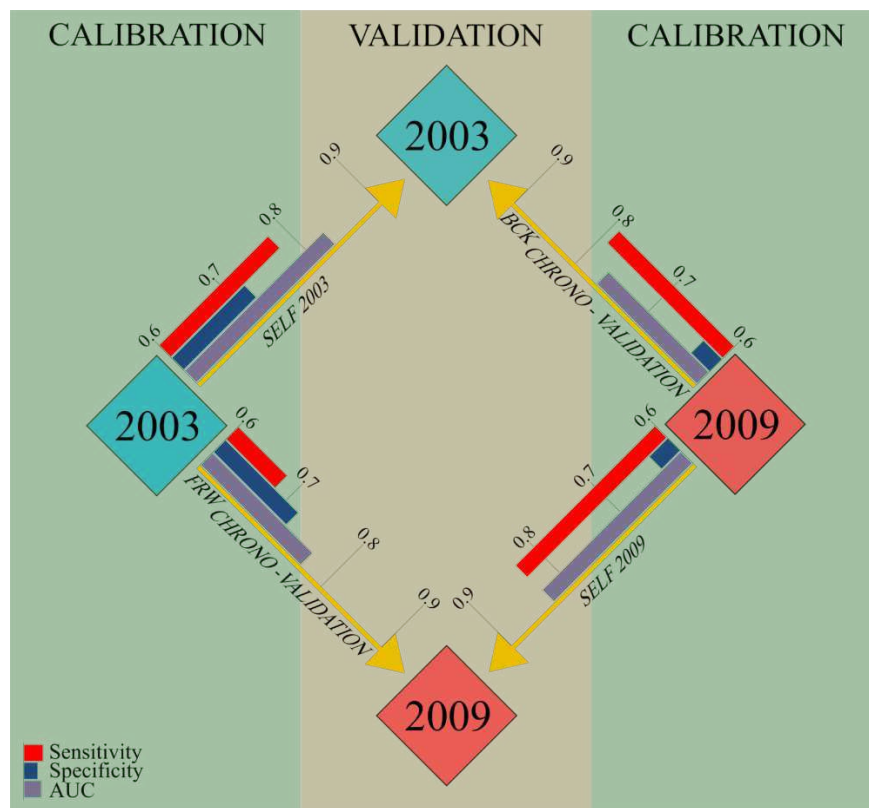


Figure 5.1.9: Graphical summary scheme of the adopted validation strategies and main performance metrics.

The results of this research confirm non-linear stochastic relationships between predictors and outcome under different driving conditions, as the crossing with a more severe landslide scenario does not only correspond to a false-to-true conversion of the predicted positives (actually, a small decrease of PPV is recorded for the 2003 forward chrono-validation), but also to positive occurrences for a number of predicted negatives. However, a similar but slighter effect is observed when models are calibrated with the extreme landslide scenario, which means the larger scenario does not fully include the smaller one.

In terms of the geomorphological model, a more intense triggering of the slopes is responsible for the activation of a large part of those site conditions which typically activate under normal triggering but together with other regions of the multivariate parameter hyperspace, have stable status under normal triggering, as attested by the 2009 models, which are controlled by more variables. This means that, if we focus on the applicative relevance of the prediction, exploiting landslide scenarios caused by more intense triggering events allows us to fit a large part of the normal-trigger caused landslides as well as the same extreme-trigger ones.

At the same time, a source of errors in terms of successful positive predictions is introduced by extreme events, so that a moderate lowering of the sensitivity is to be expected.

This could be due to the activation on 2009 of a secondary triggering mechanisms, caused by landslide coupling, which add a non-stochastic component to the spatial relationships between predictors and outcome, being rather controlled by morphodynamic slope connectivity. In fact, in a relevant number of cases, landslides in that extreme event scenario were triggered by the impact or the erosion (either laterally or at the foot of the slopes) of the moving mass detached from the primary slope failures. In figure 5.1.10 a field example is given, highlighting a number of coupled landslides, in the 2009 landslide scenario. The same setting can be observed in figure 5.1.4.

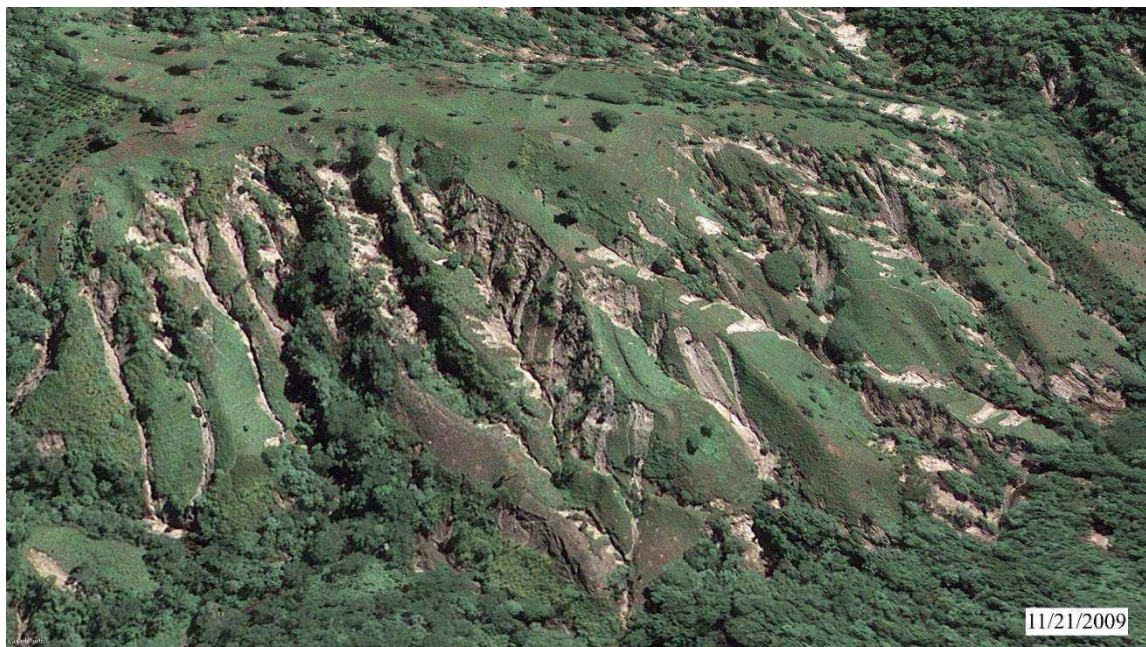


Figure 5.1.10: field example of coupled multiple landslides in 2009.

As regards the susceptibility maps, under an applicative perspective the 2009-calibrated models were confirmed to be much more accurate in predicting positives, avoiding false-

negative predictions. Among the pixels predicted as negatives in 2003, but as positive in 2009, 227 out of 580 (39%) resulted in unstable in the 2009 landslide scenario (Figure 5.1.8); conversely, very few (0.5%) of the negative predicted pixels at 2009, but as positive at 2003, actually resulted unstable in 2003. Again, if considering the potential severity of a false negative prediction, the 2009 model was confirmed to produce a more realistic and prudential prediction image in terms of potential damages.

Differences in temporal validations between models trained under normal or extreme event triggered landslide scenarios have been investigated in other papers (Lombardo et al. 2014; Cama et al. 2015 and references therein).

However, in this research, deepening the analysis to cut-off dependent performance metrics highlighted that, together with the confirmation of an *AUC* decreasing from self- to the other model being the same, a clear difference arises in terms of the type of predictive errors.

f) *Conclusions*

Predicting storm-triggered landslides always poses the problem of the morphodynamic coherence between calibration and validation datasets. In fact, the prediction skill of a model can be hampered by a large difference between the trigger intensity of the event responsible for the calibration and one for the validation landslide dataset.

In the present research, a test was carried out in the Caldera Ilopango, which is a representative area of Central America, where recurrent extreme events occur striking landslide-prone pyroclastic slopes. Two different landslide inventories were exploited: one produced by normal rainfall, the other being the result of a very intense triggering storm (the Ida/96E 2009 event). The results confirmed the relevant role played by the triggering conditions both in the importance of the variable included in the susceptibility models and in their predictive performance. As regards the predictors, it is worth noting that some variables were selected for both the two triggering scenarios, whilst some others were only for the extreme event one, demonstrating that the slope failures occur under different mechanisms depending on the rainfall intensity. At the same time, in terms of predictive performances, the specificity of the predictive models resulted as not conditioned by the type of validation (Chrono or self-validation), nevertheless being higher for the model calibrated under normal event. Conversely, the sensitivity changes from self- to chrono-validation, with the models calibrated with a landslide inventory associated with normal trigger less capable to predict the sites of landslide activation under intense triggering and resulting in very critical type-II errors (high miss rate). On the contrary, models calibrated with extreme

landslide scenarios resulted in very efficient in self-predicting the positives as well as less critically limited in predicting the normal event-triggered landslides. It is worth noting that focusing only on an AUC estimation for assessing the quality of a susceptibility model could be misleading in terms of the applicative exploitation of the susceptibility maps, whose quality is critically dependent on the correctness of binary positive/negative discriminations. This research demonstrated that validating on an extreme event landslide inventory a susceptibility map calibrated with a normal landslide dataset does not result in a simple conversion from false to true positives (i.e., the turning of negatives but susceptible cases into positive), but that new susceptible conditions arise under intense triggering, which cannot be predicted if a normal event inventory is used for calibration. Conversely, extreme landslide inventories allow for calibrated susceptibility maps which are very effective in predicting the landslides produced by normal events but with limits in discriminating stable conditions.

Summarizing what above discussed, models calibrated with a normal landslide scenario result in higher specificity (less Type-I error) but lower sensitivity (more Type-II error). To explain these differences, two main hypotheses are here suggested: the non-linear behaviour in the trigger intensity dimension of regressed relationships that link predictors and outcome; the role of a non-stochastic (morphodynamic), related to the multiple coupled triggering between different landslides under extreme events.

This point is obviously of great importance in terms of applicative consequences. In fact, it means that landslide susceptibility stochastic modelling requires multitemporal calibration inventories, to detect and estimate the effects of differences in the intensity of the trigger, optimizing positive and negative predictions. Strategies for integrating low and high trigger landslide inventories are to be issued and constitute the logical conclusive perspective of this research.

5.2. Evaluation of debris flow susceptibility in El Salvador (CA): a comparison between Multivariate Adaptive Regression Splines (MARS) and Binary Logistic Regression (BLR)

Published on: Hungarian Geographical Bulletin (2021),67(4), 361-373, DOI: 10.15201/hungoebull.67.4.5

In landslide susceptibility assessment studies, which have been developed in recent years, statistical methods have increasingly been applied. Among all, the BLR (Binary Logistic Regression) certainly finds a more extensive application while MARS (Multivariate Adaptive Regression Splines), despite the good performance and the innovation of the strategies of analysis, only recently began to be employed as a statistical tool for predicting landslide occurrence. The purpose of this research was to evaluate the predictive performance and identify possible drawbacks of the two statistical techniques mentioned above, focusing in particular on the prediction of debris flows. To this aim, an inventory of debris flows triggered by the passage of the hurricane IDA and the low-pressure system associated with it 96E, on 7th and 8th November 2009, in an area of about 26 km² close to the Caldera Ilopango, El Salvador (CA), was employed. Two validation strategies have been applied to both statistical techniques, thus obtaining four models – BLR (I), MARS (I), BLR (II), and MARS (II) – to be compared in pairs. Model performance was assessed in terms of AUC (area under the ROC curve), Sensitivity, Specificity, Positive Prediction Value, and Negative Prediction Value. Moreover, to evaluate the robustness of the modelling procedure, 50 replicates were created for each model and the standard deviation was calculated for each of them. The results show that both techniques allow for obtaining good or excellent performances, so it is not possible to define one of the two techniques as absolutely better. However, the validation procedure reveals the slightly better performance of the MARS models, with greater sensitivity and greater discrimination among True Negatives (TNs).

a) Landslide inventory

The landslide archive used in this study is a database of landslide phenomena that occurred in the catchment of Ilopango Caldera at the passage of Ida and 96/E. The archive has already been used in Rotigliano et al. (2019). The recognition of the landslides and their mapping has been carried out remotely, using a high-resolution satellite image available on the Google Earth software, which is dated 11/21/2009 (DigitalGlobe Catalog ID: 101001000AA5D801). This image, acquired only 2 weeks after the passage of Ida-96/E,

allowed the identification and mapping of 2231 debris flows triggered by the aforementioned rainfall event.

Each failure has been mapped by using a landslide identification point (LIP), located at the point of origin of the movement. In the case of evaluation of susceptibility to debris flow, according to Rotigliano et al. (2011), LIPs allow us to obtain the most reliable landslide prediction as their environmental characteristics are those that best represent pre-failure conditions and thus can be considered the best diagnostic areas for calibrating (and validating) landslide predictive models (Rotigliano et al. 2011, Lombardo et al. 2014; Cama et al. 2015). For this reason, it was decided to use the archive without making any changes with respect to the initial characteristics.

b) Model building and validation strategy

Landslide susceptibility assessment requires a validation procedure in order to evaluate the accuracy of the predictive models. This is generally performed in two steps: i) calibration of the models and ii) validation of the models (Chung and Fabbri 2003).

In this study, we evaluated the adaptation, accuracy, and robustness of the models generated with BLR (Binary Logistic Regression) and with MARS (Multivariate Adaptive Regression Splines). To this aim, two validation strategies were developed (Figure 5.2.1), applying a random partition to the same landslide archive.

First, the study area was divided into 249994 10x10m grid cells corresponding to the pixels of the employed DEM. This data set includes 2231 “event” or “positive” cells (i.e., cells hosting at least one LIP) and 247763 “non-event” or “negative” cells (i.e., cells not intersecting any LIP). Through random selection, 50 balanced data sets were created, each of them containing all event cells and an equal number of randomly selected negative cells (Conoscenti et al. 2016), thus including in total of 4462 cells.

The first validation strategy involved the calibration and validation of one model for each of the 50 data sets. Therefore, each data set was exploited both as a learning and validation dataset. In the second validation scheme, each of the 50 data sets was randomly divided into two balanced subsets: a training set, including 75 per cent of the cases, and a test set, including the remaining 25 per cent of the cases.

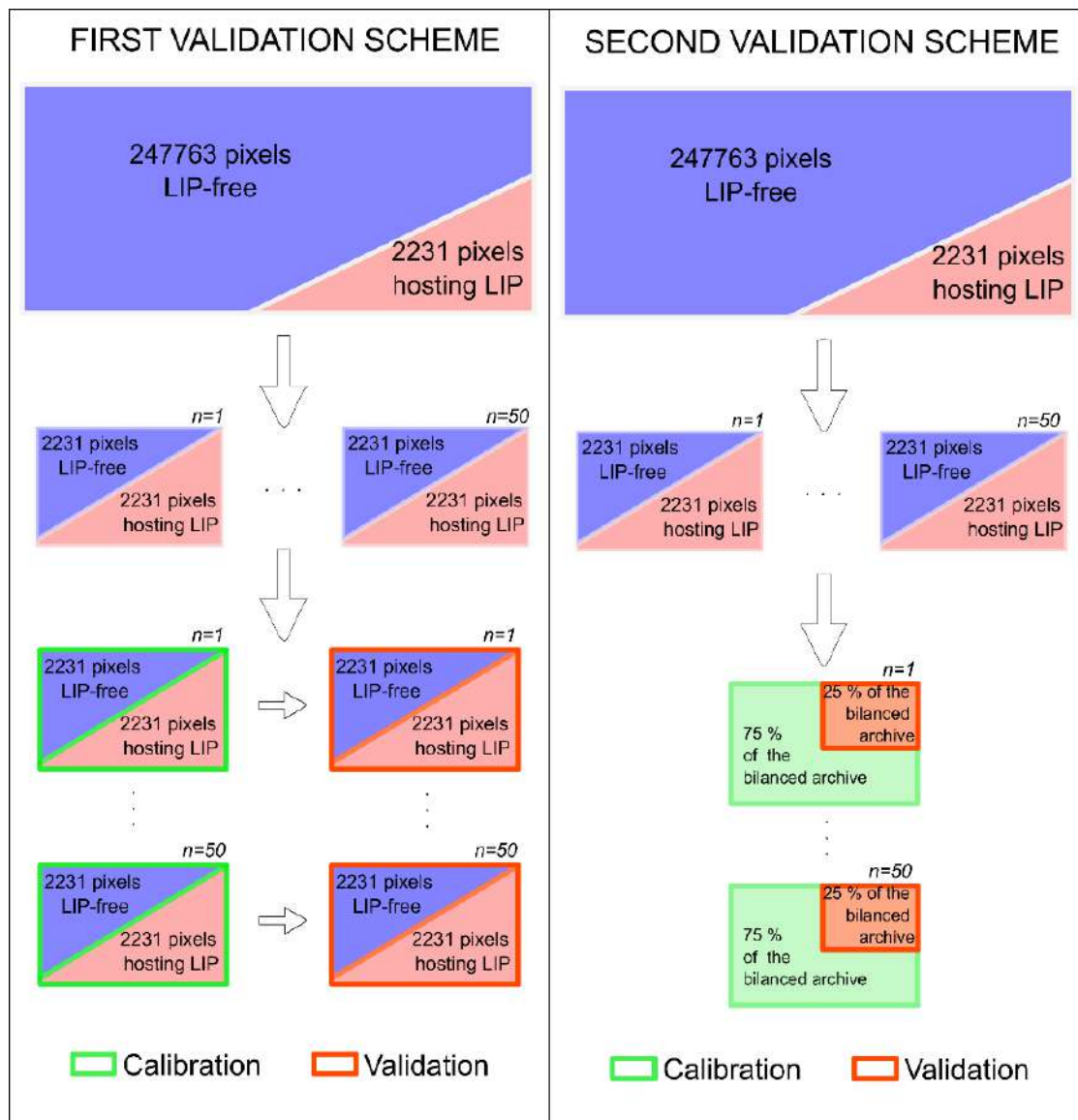


Figure 5.2.1: graphical summary schemes of adopted model building strategies.

For both the validation schemes, it was possible to obtain a pair of models, one generated with the BLR and one with MARS, for each balanced data set. This allowed us to analyse the difference in terms of performance and robustness between the two employed statistical techniques. As training and test datasets were the same, these differences were assumed as due only to the different characteristics of the two statistical techniques. Statistical analyses were carried out to evaluate and quantify the goodness of fit, the prediction skill, and the robustness of the models.

By comparing the prediction image of each model with the spatial occurrence of the event cells, the confusion matrix and thus the number of true positive, true negative, false positive, and false negative cases (TP, TN, FP, and FN, respectively) for each model, applying a Youden index optimized cut-off (Youden 1950).

To evaluate the goodness of fit and prediction skill of the susceptibility models the AUC (area under the receiver operating characteristic [ROC] curve) (Goodenough et al. 1974; Hanley and McNeil 1982; Lasko et al. 2005) was used. A ROC curve plots the true positive rate (sensitivity) against the false negative rate (1 – specificity), at any given cut-off value. For the AUC values, Hosmer and Lemeshow (2000) identified the threshold values of 0.7, 0.8, and 0.9 corresponding to acceptable, excellent, and outstanding predictions respectively.

Finally, to evaluate the robustness of the models, the validation procedures have been applied to all the model runs (50 for BLR and 50 for MARS, for each validation strategy) in order to analyse the accuracy and reliability of the models through the study of the average and standard deviation of the AUC values. These validation tools have already been successfully used in previous studies with the aim of comparing different methods and models (e.g., von Ruetten et al. 2011; Conoscenti et al. 2015, 2016a; Cama et al. 2017).

c) Result

For the description of the developed models and the relative results, a subscript (I) is adopted for those models generated through the first validation strategy, while subscript (II) is used for those created with the second validation strategy.

The mean AUC values of the BLR (I), MARS (I), BLR (II) and MARS (II) models are 0.796, 0.821, 0.789 and 0.811, respectively. According to the classification proposed by Hosmer, and Lemeshow (2000), these values indicate excellent (> 0.8) and acceptable (> 0.7) performance of the models. As shown by the AUC standard deviation values (Table 5.2.1), the performance of both modelling techniques is quite stable. The boxplots of Figure 5.2.2 show a low degree of dispersion in the AUC values, which, as expected, appears slightly higher for the second validation strategy.

MODELS	Accuracy	AUC - mean	AUC - min	AUC - max	AUC Standard Deviation
BLR (I)	0.720	0.796	0.783	0.806	0.005
MARS (I)	0.744	0.8215	0.805	0.833	0.006
BLR (II)	0.716	0.789	0.754	0.815	0.012
MARS (II)	0.736	0.811	0.779	0.836	0.012

Table 5.2.1: characteristics of the AUCs for the four susceptibility models.

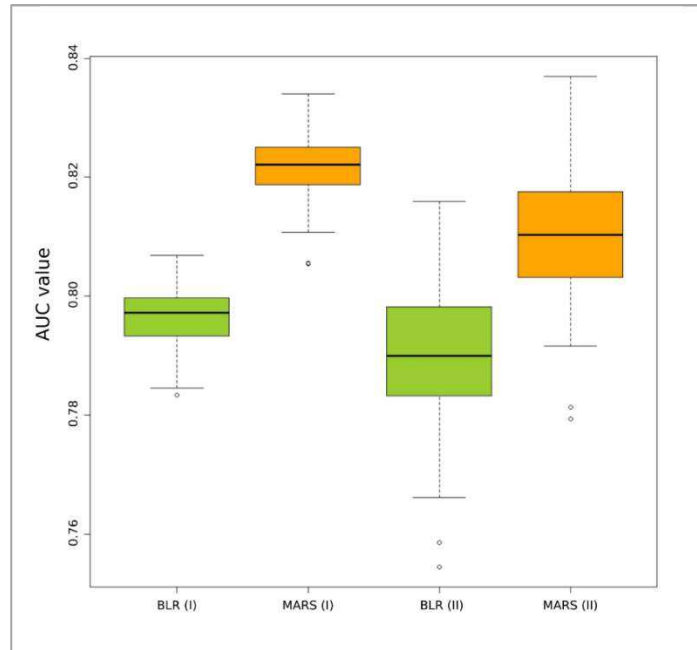


Figure 5.2.2: AUC boxplots for the four models.

Figure 5.2.3 shows the ROC curves obtained from the replicates of each model (grey) while the average ROC curves are plotted in red.

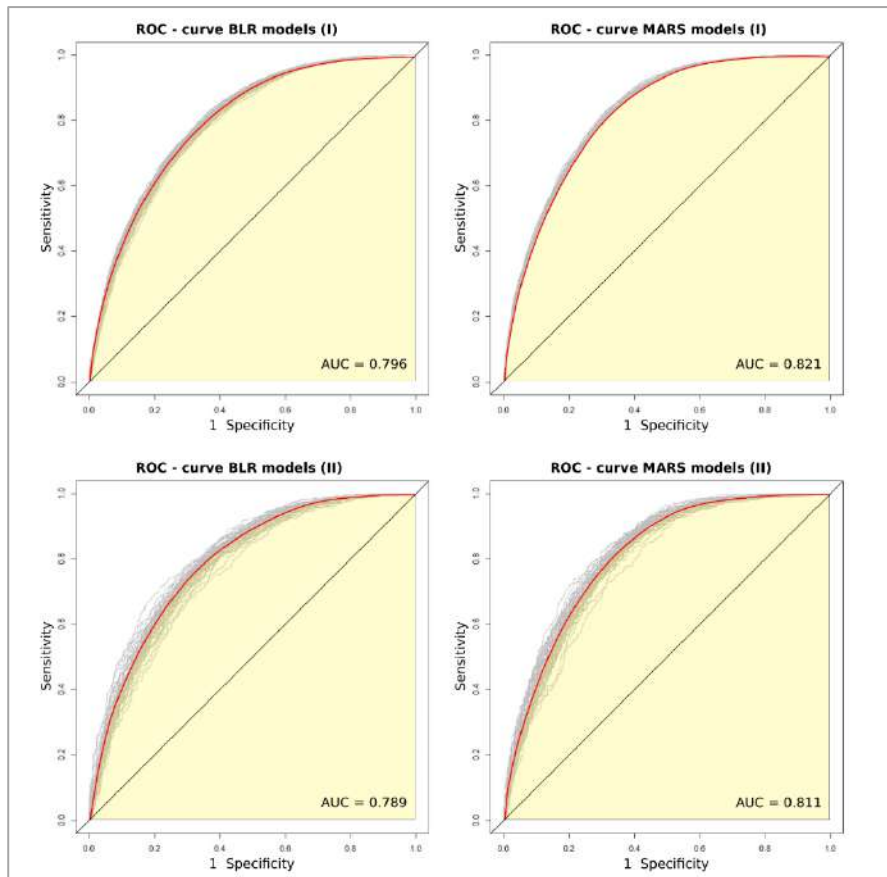


Figure 5.2.3: ROC plots for the four models

Table 5.2.2 shows the cumulative confusion matrices extracted by applying the models to the 50 validation data sets of both validation strategies. Table 5.2.3 shows the average values of sensitivity, specificity, positive prediction value (PPV) and negative prediction value (NPV) and the relative Youden index cut-off.

Confusion matrix BLR (I)				Confusion matrix MARS (I)			
	Reference				Reference		
		0	1			0	1
Prediction	0	74786	25594	Prediction	0	74558	20004
	1	36764	85956		1	36992	91546
Confusion matrix BLR (II)				Confusion matrix MARS (II)			
	Reference				Reference		
		0	1			0	1
Prediction	0	18569	6490	Prediction	0	18453	5234
	1	9331	21410		1	9447	22666

Table 5.2.2: Confusion matrices of the four susceptibility models.

MODELS	Youden index Cut-off	Sensitivity	Specificity	Positive Prediction Value	Negative Prediction Value
BLR (I)	0.48	0.77	0.67	0.70	0.74
MARS (I)	0.46	0.82	0.66	0.71	0.78
BLR (II)	0.48	0.76	0.66	0.69	0.74
MARS (II)	0.46	0.81	0.66	0.70	0.77

Table 5.2.3: Summary of the validation metrics for the four susceptibility models.

The accuracy of the models can be considered good, with values between 0.71 and 0.74. Sensitivity values between 0.76 and 0.82, attest to a good predictive power of positive cases while slightly lower is the ability to discriminate the true negatives (specificity in the range 0.66–0.67). On the other hand, it is noteworthy that the NPV values, which are between 0.74 and 0.78, reveal acceptable predictions of the TNs whereas the PPV values, which are approximately 0.7, attest to a slightly worse ability to predict the TPs.

d) *Discussion*

For the discussion of the results of model validations, we have to take into account that in the first validation strategy (i) the training and the test data sets coincide whereas in the second strategy (ii), the learning and validation sets do not share any pixels and they are randomly extracted from the training/test data sets employed in the first procedure.

Models' validation using the first validation strategy

MARS (I) demonstrate slightly better performance than BLR (I). It should be noted that the difference in terms of AUC is very small, being between 0.02 and 0.05. The accuracy of MARS (I) is only 0.02 higher than the accuracy of BLR (I), whereas the difference of average AUCs is only 0.03. Regarding the ability to predict event cells, a greater difference is recorded: the average sensitivity of MARS (I) is indeed 0.82 whereas that of BLR (I) is 0.77. However, PPV values reveal the same ability for both BLR (I) and MARS (I). On the other hand, although the specificity values suggest similar abilities of BLR (I) and MARS (I) to predict the non-event cells, NPV values demonstrate the better performance of MARS (I) (0.78) compared to that of BLR (I) (0.74).

Models' validation using the second validation strategy

Also, the second validation strategy reveals a slightly better performance of MARS compared to that of BLR, although the observed differences are once again weak. The difference in both accuracy and AUC values is indeed approximately 0.02. Again, the difference in terms of sensitivity between MARS (II) (0.81) and BLR (II) (0.76) does not result in a greater discriminatory power of TP (the difference of PPV is 0.01). Finally, the two techniques show the same specificity (0.66), but the discriminatory ability of TN is higher for MARS (II), with NPV values equal to 0.77 versus 0.74 of BLR (II).

e) *Conclusions*

The use of statistical methods in landslide susceptibility assessment raises the problem of the type of analysis to perform and which one is the best modelling approach and technique. BLR has been proven a useful technique for achieving a reliable assessment of landslide susceptibility. In recent years, however, several other statistical techniques have also demonstrated equally good, and sometimes even better, performance. MARS, which is a relatively new technique, has been employed in a few cases for assessing landslide susceptibility but it has already been demonstrated to provide very good accuracy in

predicting the occurrence of slope failures. However, as far as we know, MARS has never been employed to predict debris flows.

The aim of this study was to highlight the differences in terms of predictive performance between BLR and MARS and, thus, identify the best method for the assessment of debris flow susceptibility in the area of Ilopango Caldera.

The obtained results show that both methods achieve good to excellent predictive performances. Although MARS demonstrated slightly better performance, the difference is too small to be able to define this technique as clearly better than BLR.

Rotigliano et al. (2019) hypothesize that in the 2009 dataset there is a problem related to a second triggering of a number of phenomena due to incision or lateral erosion produced by debris flows activated directly by the storm event. In fact, even in this study, the models obtained are affected by this problem, as shown by the low specificity values. In light of this, however, the performance in terms of NPV is higher than expected. MARS, in fact, with the same dataset, is able to discriminate TN with better ability than BLR. This is probably due to the ability of MARS of identifying different relationships between the dependent and the independent variables, for different regions of the predictors' ranges. This allows MARS to overcome, even if only slightly, the problem of the second triggering of landslides, certainly with a better distinction of cases with respect to BLR. Furthermore, both validation strategies, albeit with subtle results, show a greater ability of MARS to identify positive cases compared to BLR.

In light of this, although the differences are not marked and certainly the results do not allow the definition of a modelling technique as absolutely better than the other, it is possible to identify more merits in the MARS technique than in the BLR.

5.3. Investigating limits in exploiting assembled landslide inventories for calibrating regional susceptibility models: a test in volcanic areas of El Salvador

Submitted to: Applied Sciences – section: Earth Sciences and Geography – Special Issue: Advancing Complexity Research in Earth Sciences and Geography

The research is focused on the evaluation of the reliability of regional landslide susceptibility models obtained by exploiting inhomogeneous (for quality, resolution and/or triggering related type and intensity) collected inventories for calibration. In fact, this is a frequently adopted solution for those areas where the need of preparing basin to regional-scale landslide susceptibility maps for risk management and mitigation collides with the absence of systematic homogenous landslide inventory. At a large-scale glance, merging more inventories can result in good performing models hiding potential strong predictive deficiencies. An example of the limits such kind of models can find is given by a landslide susceptibility study which was carried out for a large sector of the coastal area of El Salvador, where an apparently high performing regional model was obtained by merging the landslide inventories from five volcanic areas (Ilopango and Coatepeque caldera; San Salvador, San Miguel, and San Vicente Volcanoes). A multiscale validation strategy was applied to verify its actual predictive skill on a local base bringing to light the loss in the predictive power of the regional model, with a smooth lowering of ROC_AUC, but strong effects in terms of sensitivity or sensitivity.

a) Landslides inventory and related triggering rainfall events

The main task of this research is to test the suitability of aggregated regional landslides archives in the evaluation of landslide susceptibility assessment. For this reason, a set of independent available debris flows/slides archives were exploited for training and validating a regional landslide susceptibility map. Archives from five different sectors of the El Salvador territory were considered, which, even in the same sector, are to be considered as un-uniform in terms of operators, methods (field/remote), and epoch (which means grouping debris flows/slides linked to multiple and/or different extreme rainfall). In fact, these landslide inventories were prepared in the framework of different studies (master's degree thesis, Ph.D. thesis and so on, see Author Contribution), many of which have been part of the RIESCA project (Proyecto Regional de Formación Aplicada a los Escenarios de Riesgos con Vigilancia y Monitoreo de los Fenómenos Volcánicos, Sísmicos e Hidrogeológicos en

Centro América). For this reason, the study areas are not a priori limited and as mentioned above, they have been restricted to the sectors affected by the activation of the inventoried debris flows: Ilopango (ILO), Coatepeque (COA), San Miguel (SMG), San Vicente (SVC), and San Salvador (SSV) areas.

As above mentioned, the main triggering events for these landslide scenarios are the hurricane Ida and the tropical depression 12E (TD12E). Tropical-humid climate setting of El Salvador produces, in the rainy season between May and October, very high rain-fall amounts (above 1500 mm, on average) that, usually, occur in the form of intense storms. Therefore, rapid saturation of the regolithic mantle and powerful surface runoff can cause the triggering of a huge number of landslides even in the case of a normal rainfall season (Rotigliano et al. 2019).

All the mapped phenomena were individuated by exploiting Google Earth images and the Landslide Identification Point (LIP), which was generated for each of the mapped phenomena corresponding to the highest point along with the landslide crown, was also taken as indicating the area that effectively represents the activation conditions for surface debris flows (Rotigliano et al. 2011, 2018, 2019; Costanzo et al. 2014; Lombardo et al. 2014, 2015; Cama et al. 2015).

The Coatepeque archive includes 1895 debris flows, which have been triggered by the tropical depression (TD) 12E in 2003. The same extreme rainfall event activated the 382 debris flows/slides of the San Salvador dataset. Hurricane Ida is the trigger of the 4975 phenomena mapped in the San Vicente archive, while both TD12E and Ida activated the 38525 debris flows/slides of the Ilopango dataset. Finally, the 233 landslides of the San Miguel archive were triggered by several rainfall events from 2001 to 2018.

b) Model building and validation strategy

i. Predictors and mapping units

The selection of a set of geo-environmental variables potentially expressing the landslide preparatory causes was based on largely adopted geomorphological criteria (Costanzo et al. 2012b; Rotigliano et al. 2018, 2019; Vargas-Cuervo et al. 2019; Martinello et al. 2021, 2022; Mercurio et al. 2021). In particular, outcropping lithology and soil use, were derived from an available thematic map (Weber et al. 1978) and a remote survey, respectively. By processing a 10m pixel digital terrain model (DTM), the following continuous variables were derived: elevation (ELE), steepness (STP), plan (PLN) and profile (PRF) curvatures, topographic wetness index (TWI), and aspect, the latter expressed in terms of easternness

(EASTNS) e northerness (NORTHNS). Besides, the landform classification (LCL) categorical variable was obtained. In this way, a set of three categorical and seven continuous variables was prepared.

Based on the geomechanical expected response, the outcropping lithologies were grouped as soft, medium, hard rocks; very soft, soft, medium, hard soils (Table 5.3.1).

Geomechanical classification	Grouped lithologies	Relative outcropping area	Relative percentage distribution of landslides
Hard soil	c1	18.1%	24.1%
Soft soil	Qf	2.1%	1.2%
Very soft soil	s4	18.1%	57.7%
Hard rock	c3, b3	11.0%	3.1%
Soft rock	b2, s2	23.9%	1.8%
Medium soil	b1, s5a, s1, s5c, s3a	22.3%	7.4%
Medium rock	s3b, s5b, c2	4.5%	4.7%

Table 5.3.1: The geomechanical classes with their corresponding grouped lithologies, relative outcropping area, and relative percentage distribution of landslides into each geomechanical unit.

Table 5.3.1 shows the percentage distribution of landslides in relation to the geomechanical units. On the basis of the landslide distribution in the study areas, soil classes are deeply involved in slope instabilities, with very soft and hard soils accounting for more than 80% of the mapped cases. The very low number of landslides recognized in soft soils has to be ascribed to the very limited extension of the outcropping areas.

All the controlling factors were arranged in 10x10m raster layers.

In order to optimize the final selected predictors that were included in the MARS modelling procedure, the variance inflation factor (VIF) (Naimi 2015) test was performed for multicollinearity analysis through the continuous variables.

The same grid cell structure was then adopted as the susceptibility mapping unit, assigning a stable/unstable status depending on the intersection of LIPs. In fact, according to a number of debris flow susceptibility assessment studies (e.g., Rotigliano et al. 2011; Costanzo et al. 2014; Nicu and Asăndulesei 2018; Mokhtari and Abedian 2019; Sameen et al. 2020; Martinello et al. 2021, 2022; Mercurio et al. 2021; Steger et al. 2021), we considered the instability conditions of each inventoried landslides to be effectively captured in the highest crown 10x10m pixel.

ii. Modelling and validation tools

In this research, Multivariate Adaptive Regression Splines (MARS; Friedman 1991) was applied to regress the outcome (stable/unstable status) onto the covariates set from the controlling factor layers.

MARS statistical modelling of landslide susceptibility conditions requires the random extraction of a sample made of a balanced number of stable and unstable cases to be split into calibration and validation subsets: the first is exploited for regressing the outcome status on the set of covariates that express the adopted controlling factors, while the latter furnishes the unknown-to-model target pattern whose status has to be blindly predicted. In a pixel-based method, where the number of stable cases is typically largely greater than the unstable, balanced samples are obtained by merging all the positives to an equal number of randomly extracted negatives. To account for any potential unrepresentativeness of the extracted negatives, by adopting recurrent random selection routines, multiple samples were produced. Similarly, to control the influence of the specific cases which feed the calibration subsets, multiple (75/25%) calibration/validation splitting was applied to each sample as well. In this way, one-hundred samples were split one-hundred times so that each pixel was classified ten-thousand times allowing to estimate the model resolution and precision. Finally, to fully evaluate the prediction skill of the model, the regression coefficients gained in the calibration/validation subset were applied to the whole investigated area.

Receiver Operating Curve (ROC) (Goodenough et al. 1974; Lasko et al. 2005; Fawcett 2006) and confusion matrices analysis were the tools employed to investigate the model accuracy. In particular, ROC plot analysis is based on evaluating True versus False positive rates for decreasing susceptibility scores, larger Area Under Curve (AUC) (Hanley and McNeil 1982; Hosmer and Lemeshow 2000) attesting for more effective classifications. The score at the maximum gradient of the ROC is then used as optimized cut-off (Youden 1950) for building a binarized (positive/negative-observed/predicted) confusion matrix. In this way, the accuracy of the model can be evaluated both with score independent (ROC_AUC) and dependent (ACC) indices.

iii. Research design and model building strategy

In the following, we will refer to a super area (ALL), considering the one obtained by merging all the positive and negative cases of each of the five sectors (volcanic areas), the latter defining five local datasets (ILO, COA, SMG, SVC, SSV).

It is worth noting that, in light of the number of causes which have been here claimed as responsible for the inventory incompleteness, a different approach from Steger et al. (2017, 2021) was to be designed for evaluating the influence of the bias landslide inventory. In particular, to explore the topic of the research, the following model building procedure was designed, by submitting to a strict validation procedure the hypothesizing of completeness of the inventory.

First, a grand model (ALL) was prepared by applying the typical approach aimed at obtaining a regional model from the available landslide inventories, including in the processed dataframe the whole set of positives and negatives from the five sectors. To have a control on the variability of the negatives and the calibration/validation subset assignment of positives, a suite of one-thousands multiple datasets was obtained by randomly extracting one-hundred sets of negatives and submitting each dataset to ten randomly calibration/validation (75/25%) splitting.

Once the grand model was prepared, it was first validated with respect to the spatial distribution of the landslides in the whole super area (ALL_ALL), according to a self-validation scheme (Chung and Fabbri 2003; Guzzetti et al. 2006; Cama et al. 2015, 2017; Rotigliano et al. 2018, 2019; Vargas-Cuervo et al. 2019; Martinello et al. 2021, 2022). The validation performance of the grand model was then locally evaluated by restricting the validation dataset to a single sector in turn (e.g., ALL_ILO). For comparison, independent local models (e.g., LOC_ILO) were prepared for the five sectors by limiting the application of the modelling procedure to every single dataset and applying a local self-validation scheme. Finally, five one-leave-out models were prepared by applying the same above-described procedure but adopting a 4/1 sectors calibration/validation splitting in the modelling scheme; a local validation was then obtained, by assessing the predictive skill in recognizing the specific positives and negatives of the extracted (left-out) target sector. In the following, these models are referred to as OLO models (e.g., OLO_ILO).

Table 5.3.2 gives a summary of the prepared models, including the specification of the main characteristics.

According to the main task of the research, the ALL_ALL is to be considered as that model one could take as representative for a regional prediction image. At the same time, the imported models (ALL_local), in re-defining the validation set on a local basis, could furnish a useful warning in case the performance of the grand models is actually locally misleading. The local models give an estimation of the reference performance the imported model (ALL or OLO) should achieve to be considered more informative. Finally, the one-leave-out

modelling procedure simulates the results of applying the model to totally unknown sectors (such as a hypothetical sixth unknown volcanic area would result in our research).

<i>type</i>	<i>calibration</i>	<i>validation</i>
ALL_ALL	75% randomly extracted balanced subset from the ALL* dataset	conjugate 25% randomly extracted balanced subset from the ALL dataset
ALL_target	100% randomly extracted balanced subset from the ALL dataset	100% randomly extracted balanced subset from a single target** sector
OLO_target	100% randomly extracted balanced subset from a [ALL-target]** dataset	100% randomly extracted balanced subset from the subtracted target sector
LOC_target	75% randomly extracted balanced subset from a target sector dataset	conjugate 25% randomly extracted balanced subset from a target sector dataset
*ALL: the sum of the positive and negative cases of the five sectors		
**target: the sum of positive and negative cases of a single sector		
***[ALL-target]: the difference between ALL and a target		

Table 5.3.2: Adopted model building scheme for the tested models

c) Results

For each of the models above described, the results of the validation are reported both in Figures 5.3.1-5.3.3, where ROC curves and related AUCs are drawn, and in Table 5.3.3, where binarized positive/negative status comparisons between predicted/observed target cases are given.

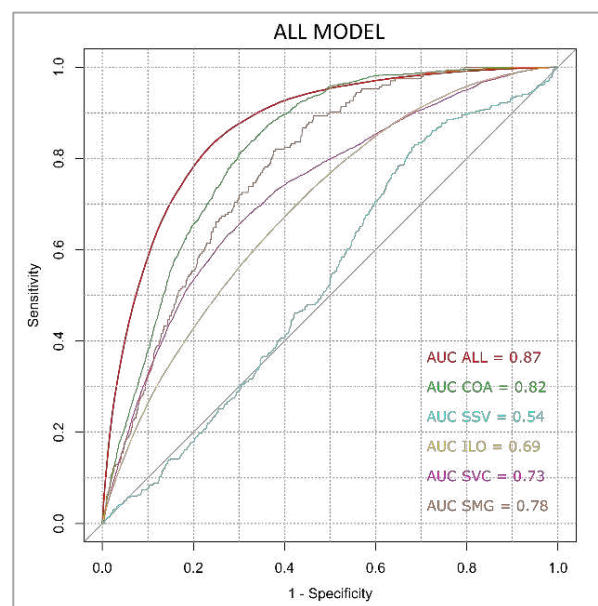


Figure 5.3.1: Roc plots and relative AUC values for the ALL models.

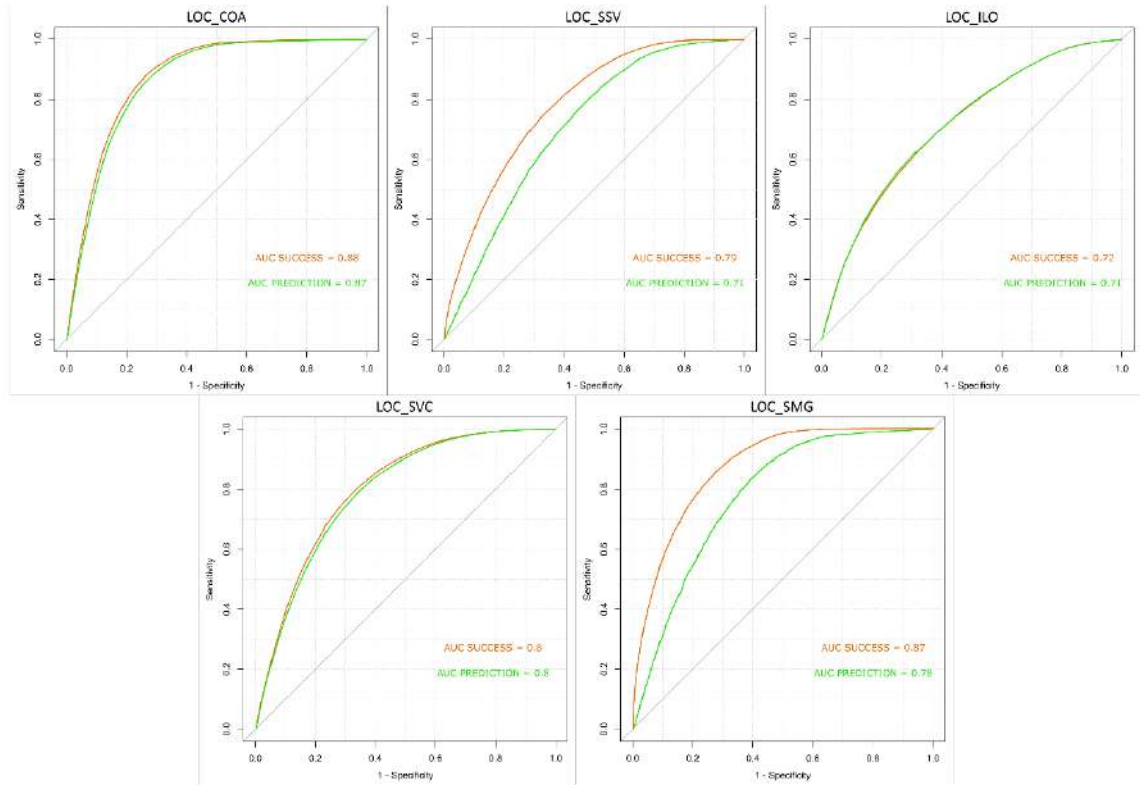


Figure 5.3.2: Roc plots and relative AUC values for the Local models.

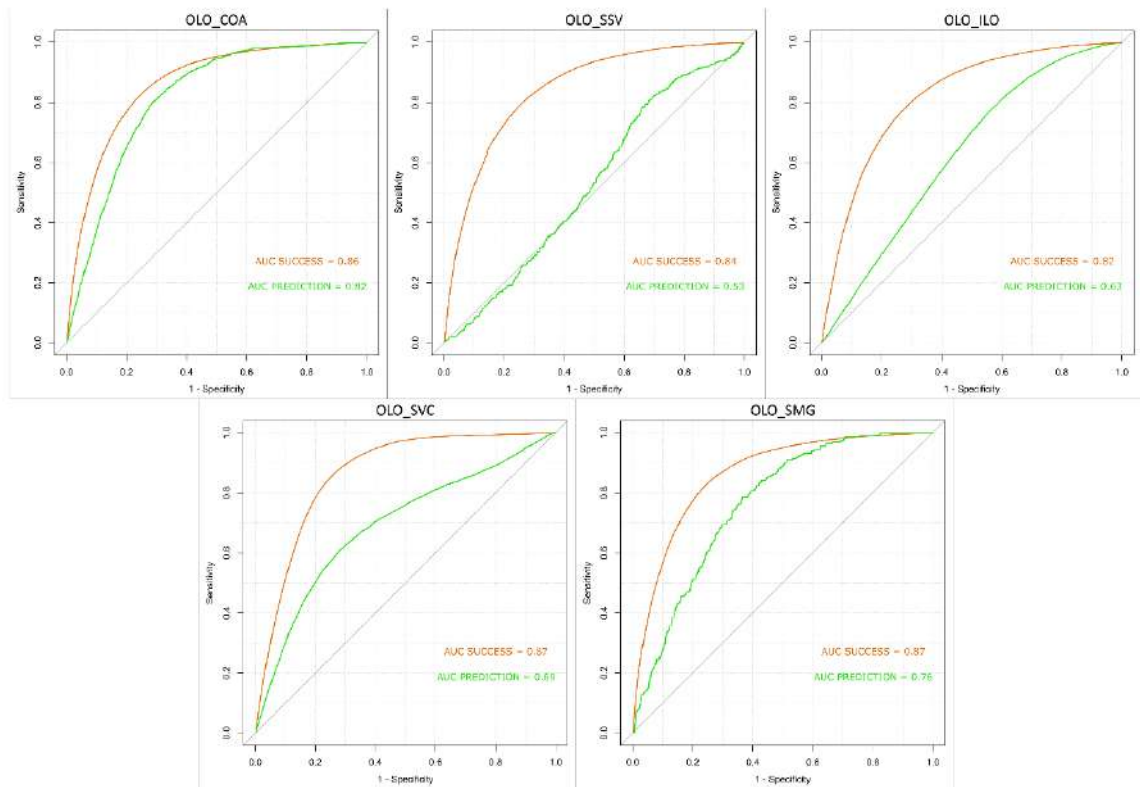


Figure 5.3.3: Roc plots and relative AUC values for the One Leave Out models.

		<i>count</i>	<i>positives</i>	<i>negatives</i>	<i>TN</i>	<i>FN</i>	<i>FP</i>	<i>TP</i>	<i>ACC</i>	<i>Sensitivity</i>	<i>Specificity</i>	<i>AUC</i>
ALL	ALL	6311320	46010	6265310	4786221	8022	1479089	37988	0.76	0.82	0.76	0.87
	COA	806671	1895	804576	698607	967	105969	928	0.87	0.44	0.87	0.82
	SSV	1429050	382	1428668	1369074	367	59594	15	0.96	0.04	0.96	0.54
	ILO	1161436	38525	1122911	378750	4171	744161	34354	0.36	0.89	0.34	0.69
	SVC	2794399	4975	2789424	2221036	2295	568388	2680	0.80	0.54	0.80	0.73
	SMG	119964	233	119731	118754	222	977	11	0.99	0.05	0.99	0.78
LOC	COA	806471	1895	804576	590261	219	214315	1676	0.73	0.88	0.73	0.88
	SSV	1429050	382	1428668	839269	66	589399	316	0.59	0.83	0.59	0.78
	ILO	1161436	38525	1122911	737214	13392	385697	25133	0.66	0.65	0.66	0.72
	SVC	2794399	4975	2789424	1880683	1038	908741	3937	0.67	0.79	0.67	0.80
	SMG	119964	233	119731	79805	25	39926	208	0.67	0.89	0.67	0.87
OLO	COA	806471	1895	804576	622805	562	181771	1333	0.77	0.70	0.77	0.82
	SSV	1429050	382	1428668	1343953	361	84715	21	0.94	0.05	0.94	0.53
	ILO	1161436	38525	1122911	455548	7448	667363	31077	0.42	0.81	0.41	0.63
	SVC	2794399	4975	2789424	2044869	2021	744555	2954	0.73	0.59	0.73	0.69
	SMG	119964	233	119731	119002	229	729	4	0.99	0.02	0.99	0.76

Table 5.3.3: Validation results (confusion matrices) for the sixteen models.

The performance of the ALL_ALL model is very high, with excellent AUC and accuracy (0.87 and 0.76, respectively) and highly satisfactory sensitivity (0.82) and specificity (0.76). If comparing these values to the ones obtained in importing the grand model into the specific sectors (ALL_local) satisfactory to excellent AUC and ACC values still hold, with the exception of ILO and SSV. However, lower sensitivity and higher specificity were recorded for all the models, with the exception of ILO. It is worth to note that only the SVC imported local model still performs with acceptable scores for all the main indices (sensitivity, specificity, ACC, AUC). At the same time, the local models are in general characterized by higher (0.8-0.9) AUC values, with a much more balanced sensitivity/specificity ratio, as a result of higher sensitivity and lower specificity. Again, an opposite behavior is observed for ILO.

Finally, the one-leave-out models confirm the general trend of performance indices variation which was observed for ALL_local validations.

As regards the role of the predictors, the results obtained from the local modelling highlighted two very different responses (Figure 5.3.4): SMG and SSV are fully controlled by elevation and steepness, whilst ILO, COA, and SVC also required the discriminating contribution of either from landform classification (COA and SVC) or outcropping lithology (ILO and SVC) or soil use (for COA and ILO). Elevation, steepness, outcropping lithology, and soil use are all selected by the ALL grand model.

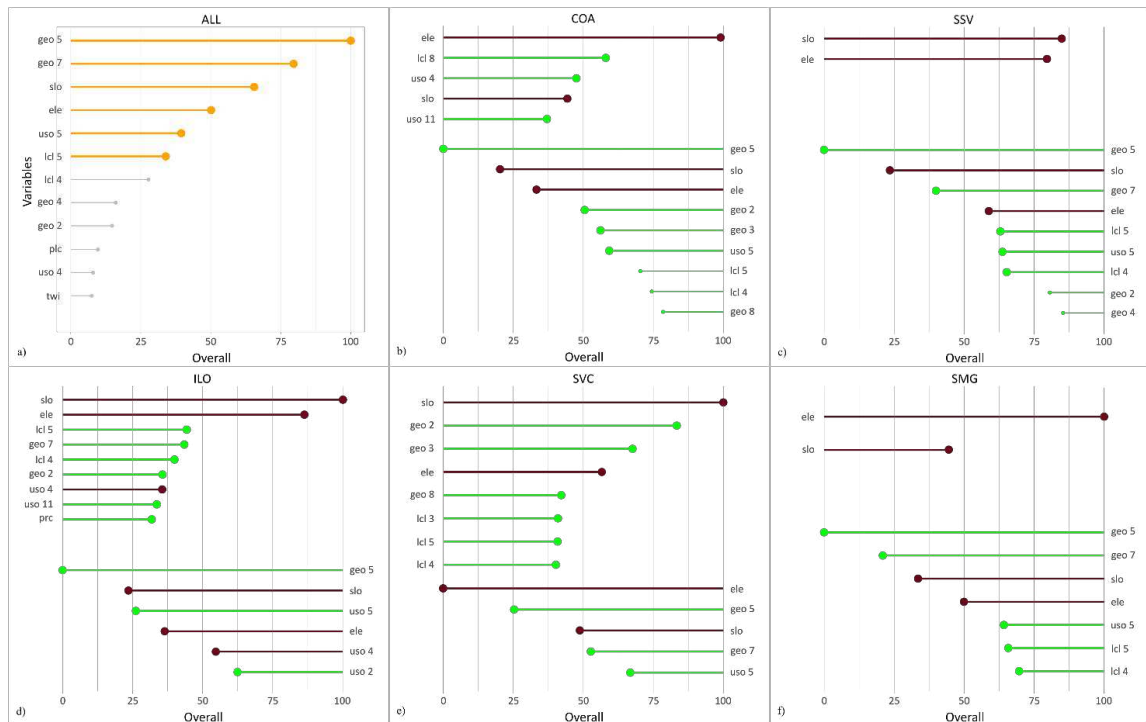


Figure 5.3.4: The most important variables for the ALL model (a) and the LOC (left side) and the OLO (right side) models (b-f). In amaranth, the common variables for the LOC and the OLO models, while in green the different variables. Thin lines are used for variables with a lower overall (minor than 30 out of 100). Here, are the acronyms used: geo 2 = soft rock; geo 3 = hard rock; geo 4 = medium rock; geo 5 = very soft soil; geo 6 = soft soil; geo 8 = medium soil; lcl 3 = valleys; lcl 4 = plains; lcl 5 = open slopes; lcl 8 = midslope ridges; uso 2 = forest; uso 4 = crop and pasture; uso 5 = permanent crop; uso 11 = shrub vegetation.

d) Discussion

The local landslides distribution in five different volcanic sectors was predicted both from imported (both ALL and OLO models) and locally calibrated models. The latter resulted in smoothly (with the exception of SSV) higher AUC values, with a proportional decrease of the cut-off dependent accuracy, but driven by a marked sensitivity increasing and slightly specificity decreasing. In particular, the more the LIP% incidence of a single sector, the higher the TPR decrease recorded for the imported models. A relevant exception that was highlighted by the results is the very odd behaviour of ILO, whose local model produced a worse performance in recognizing its own positives.

The ILO sector includes the very large majority of landslides (83,7%) and, in light of its limited extension (18,4%), the maximum ratio between unstable and stable pixels. When trying to discriminate the status of the ILO pixels, on the base of the ALL or OLO imported model, a better performance arises in positive detection if compared to the skill of the local model. This is due to the undifferentiated presence of positives and negatives in the same geomorphologic conditions and this effect could have been enhanced by the severe

triggering conditions (IDA tropical storm) which activated landslides even in low susceptible areas. In fact, the better performance of ALL and OLO relies on the circumstance that these models take their cases outside ILO, for positive and negative cases of OLO, or prevalently outside ILO, for the negatives of ALL. As a consequence, the local dataset confuses the binary discrimination whilst recurring to the outside pixels allowed to better understand the unstable conditions. At the same time, for a more geomorphologically differentiated setting sub-catchment of ILO (“Arenal de Cujuapa”), Rotigliano et alii (2018; 2019) obtained, with the same MARS modelling approach, higher AUC, and accuracy values (0.83 and 0.73, respectively). Moreover, the same loss in the model performance was observed when trying to temporally predict the landslide inventory of 2003 (produced by a non-extreme rainfall triggering) from the model calibrated with the same 2009 hurricane-induced inventory that was used in the present research.

Once the potentially hampering specific conditions of the ILO sector arose, a new grand model (ALL*) was tested excluding ILO from all sectors (which were reduced to four) and obtaining better locally imported results (Table 5.3.4). With the exception of SSV, these new imported models performed with similar largely satisfactory AUCs to the local models and even higher sensitivity.

	<i>count</i>	<i>positives</i>	<i>negatives</i>	<i>TN</i>	<i>FN</i>	<i>FP</i>	<i>TP</i>	<i>ACC</i>	<i>Sensitivity</i>	<i>Specificity</i>	<i>AUC</i>
ALL*_COA	806471	1895	804576	515857	166	288719	1729	0.64	0.91	0.64	0.85
ALL*_SSV	1429050	382	1428668	1314478	349	114190	33	0.92	0.09	0.92	0.61
ALL*_SVC	2794399	4975	2789424	1813333	1026	976091	3949	0.65	0.79	0.65	0.79
ALL*_SMG	119964	233	119731	37646	8	82085	225	0.32	0.97	0.31	0.75

Table 5.3.4: Validation results (confusion matrices) for the ALL* models.

e) *Conclusions*

On the basis of the obtained results, it is confirmed that grouping landslide inventories from different areas to reach a number high enough to prepare performing susceptibility models can lead to very unreliable results unless further validation tests are carried out. In particular, depending on both the number of landslides and frequency distribution of all the predictors in each of the grouped sectors as well as on their area, the grand model can result as very performing on average, but really misleading and unstable in recognizing positives and/or negatives on a local scale, to the point that locally calibrated models result as more performing even if trained with a lower number of cases. This would typically lead to taking a sense of security and considering the obtained prediction image as reliable for the study area, eventually suggesting also to export the obtained model also to new neighbouring un-recognized sectors, for instance, those between the five mapped ones. In this paper, a new approach was adopted, and related tools were proposed, for verifying the inventory completeness hypothesis. This approach can be involved in any model building procedure so to obtain warnings about the quality of the source data and its influence on the resolution of the derived susceptibility models.

Comparing grand to local models should be a standard procedure when assembling large landslide inventories, even in the case of secondary catchments in large basin-scale studies. The main factors in controlling the skill of the grand model are the number of total pixels and the number of positives and the spatial distribution of the predictors. Two main factors hamper the accuracy and reliability of any grand model, based on a presence/absence method: depending on the relative spatial extension of the classes of each covariate, in light of the need to randomly extract the negatives to prepare balanced datasets, a forcing toward the more diffused classes results for stable conditions; depending on the different completeness of the merged landslide inventories, a forcing toward the unstable conditions coming to light in the sectors or catchments with a higher number of mapped landslides arises. These two effects are much more severe for the categorical variables in the case of un-homogeneous geologic/geomorphologic setting, whilst DTM-derived variables are more unlikely to result as so largely different to mislead the modelling. It is worth noting, that the limits produced by the qualitative and quantitative differences in the landslide inventories suggest as not suitable even the adoption of presence-only methods, in light also of the strong influence that any unrepresentativeness of the landslide inventories produce.

5.4. Optimal slope units partitioning in landslide susceptibility mapping

Published on: Journal of Maps (2021), 17:3, 152-162, DOI: 10.1080/17445647.2020.1805807

In this paper, a test was performed in the Imera Settentrionale river basin (Sicily). MARS (Multivariate Adaptive Regression Splines) modeling was applied to assess rotational/translational landslide susceptibility based on twelve predictors and a 1608 cases database. A pixel-based model was prepared, and the scores were zoned into ten different types of slope units layers, obtained by differently combining two half-basin (HB) and four landslide classification (LCL) coverages. The predictive performance of the ten models was then compared to select the best performing one, whose prediction image was finally modified to take into account also the propagation stage. The final results attest that integrating HB with LCL is more performing than using simple HB classification, with a very limited loss in predictive performance with respect to the pixel-based model.

a) Landslide inventory and landslide conditioning factors

Landslide recognition was carried out using high resolution (0.25m) LIDAR (Light Detection And Ranging) images taken in 2012 by ARTA (Assessorato Regionale al Territorio e all'Ambiente). The inventory includes 1608 rotational/translational slides that, on the whole, affect an area extending for about 26 km² (~8% of the study area). The obtained landslides inventory (Figure 5.4.1) was checked with a randomly hot spots field survey which was carried out in 2019; for each of the mapped landslide polygon, the highest point along the crown (Landslide Identification Point – LIP) was extracted, which several researches (Rotigliano et al. 2011; Lombardo et al. 2014, 2016; Cama et al. 2015) highlighted as an effective diagnostic site for landslide susceptibility evaluation.

In this research, a set of ten topographic predictors was derived by processing with GIS hydro-morphological tools an 8m cell digital elevation model (DEM) obtained from a LIDAR survey in 2008 by ARTA: elevation (ELE), landform classification (LCL), steepness (STP), aspect (expressed as NORTHerness and EASTerness), plan (PLN) and profile (PRF) curvatures, topographic wetness index (TWI), terrain ruggedness index (TRI) and stream power index (SPI).

A bedrock lithology map (LITO) was prepared by grouping the different outcropping lithologies in light of their expected mechanical behavior (see section 4.2.2). The boundaries between the different units were verified and adapted on the basis of remote and field

surveys. The Corine Land Cover 2018 (USE) was also used to classify land use of the Imera Settentrionale river basin.

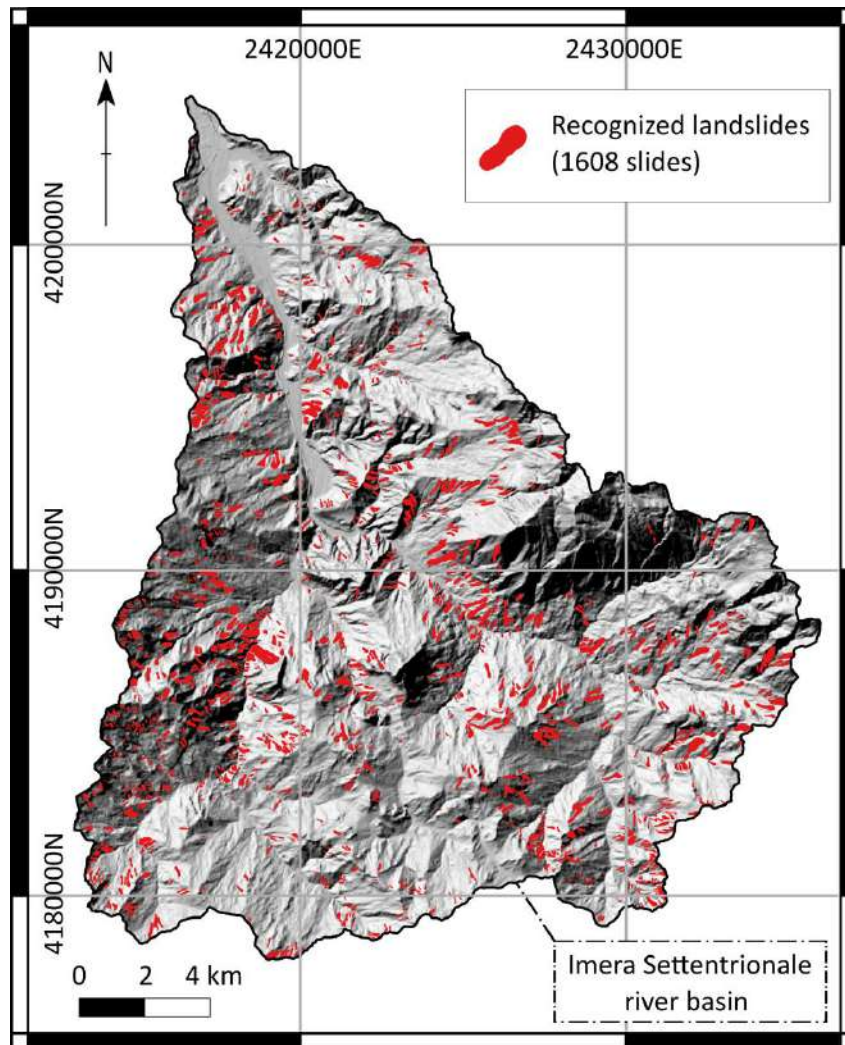


Figure 5.4.1: recognized active rotational/translational slides inventory map.

b) *Model building and validation*

Each 8m pixel was classified as stable or unstable (positive or negative cases) depending on whether or not it hosts at least one LIP and the local values of all the proxy predictors assigned. Thereby, a R dataframe was obtained and exploited to extract a suite of one-hundred balanced (positive/negative) datasets, each including the whole set of positive pixels and an equal number of randomly extracted (without replacement) subsets of negatives. Each dataset was then submitted to a balanced random partition furnishing a 75% subset for calibration and a 25% unknown subset for blind validation tests.

The Multivariate Adaptive Regression Splines (MARS; (Friedman, 1991)) stochastic method was applied to model landslide susceptibility. The model performance was analyzed

in terms of a cut-off independent metric (by AUC: the Area Under the receiver operating Curve) as well as, based on an optimal cut-off (Youden 1950), in terms of TPR and TNR (true positive and negatives rates, respectively) and related accuracy. By exploiting the availability of the one-hundred replicates, each accuracy metric was assessed also in terms of precision.

Each model was tested in predicting the validation test, first, and the whole study area, then. In fact, in evaluating the suitability of the final maps it is of great importance to verify to what extent the forced false positive generation (all the unstable status pixels are inside the calibration/validation subsets) is balanced by the performance in terms of true negative prediction.

c) Slope Units partitioning and scoring

By using two main criteria, ten types of slope-unit partitioning schemes were adopted.

Firstly, two classic hydro-morphological units were obtained by means of contributing area-based procedures: in this way, by exploiting 2000 and 5000 contributing area thresholds, a 2000 half basin (2000_HB_SLU) and a 5000 half basin (5000_HB_SLU) SLU-layers were obtained.

Then, the TPI based Landform Classification (Guisan et al. 1999) SAGA tool was exploited to obtain four different LCL maps from the DEM, by changing the inner/outer radius as 100/1000, 100/2000, 500/1000 and 500/2000 meters. LCL divides and classifies the study area in geomorphological-classes considering the relative vertical position of each pixel.

By intersecting the 2000_HB_SLU and 5000_HB_SLU shapes with the four LCL maps, eight new types of slope-units were obtained (Table 5.4.1), in which each half basin unit was split into several areas having a different geomorphological classification (Figure 5.4.2).

For each of the ten types of obtained slope-unit layers, MEAN (average) and MSTD (mean plus one standard deviation) of the pixel-based scores were zoned for producing ten derived prediction images. A positive (unstable) status was then assigned to the slope-units if containing at least one LIP. In this way, each slope-unit was so characterized by a predicted (derived by MEAN and MSTD scoring) and an observed status, so that Receiver Operating Curve (ROC)-plots and Confusion Matrixes, through a new Youden Index cut-off, were analyzed.

<i>Hydro-morphological units</i>	<i>LCL inner-outer radius</i>	<i>LCL_SLU</i>
2000_HB_SLU	100-1000	211_LCL_SLU
	100-2000	212_LCL_SLU
	500-1000	251_LCL_SLU
	500-2000	252_LCL_SLU
5000_HB_SLU	100-1000	511_LCL_SLU
	100-2000	512_LCL_SLU
	500-1000	551_LCL_SLU
	500-2000	552_LCL_SLU

Table 5.4.1: Characteristics of the LCL_SLU partitioning scheme adopted.

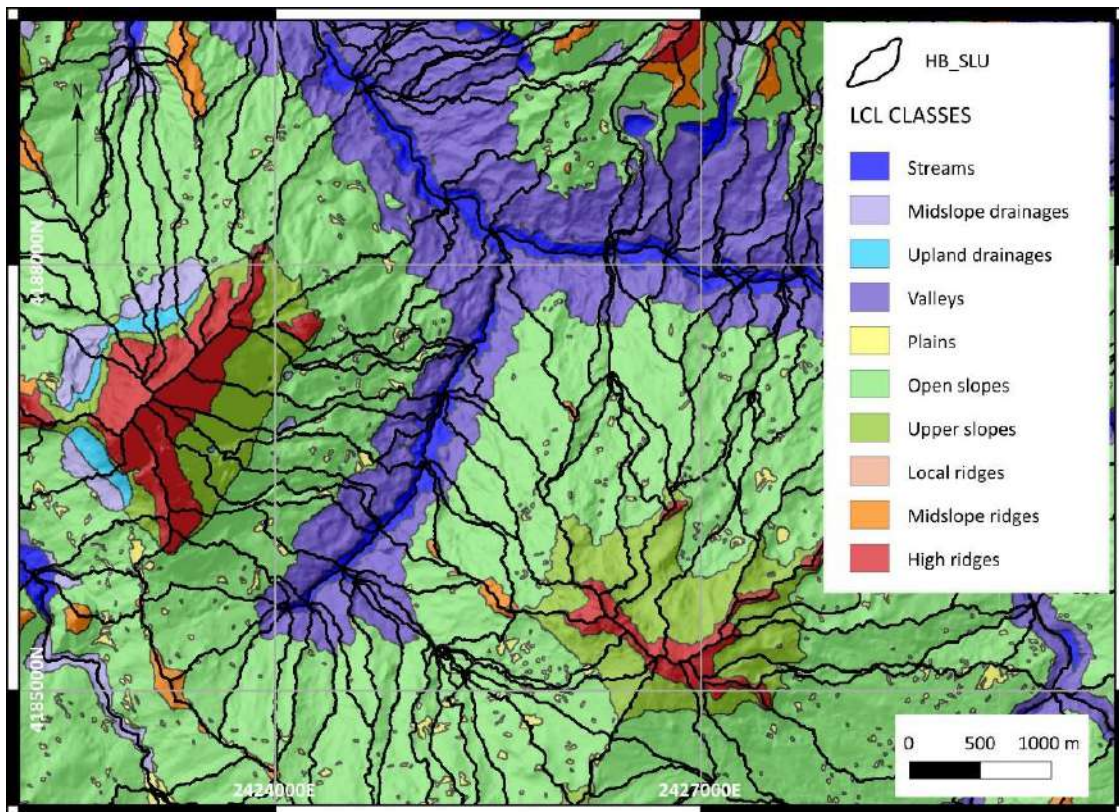


Figure 5.4.2: example of LCL_SLU partition (HB_SLU: 5000 + LCL: 100-2000).

d) Results

The figure 5.4.3a, which shows the ROC-plot of the one-hundred pixel-based models, attests for excellent (Hosmer and Lemeshow 2000) AUC mean values (0.89), associated to very low standard deviations (0.01), and a 0.48 Youden Index cut-off. A similar high performance in terms of prediction accuracy (Figure 5.4.3b) was also obtained from the confusion matrix both for the balanced pixel-based model and the entire area (0.79 to 0.81). Coherently, both

specificity and sensitivity do not change from the balanced datasets (0.83) to the entire area (0.85). On the other hand, while similar (about 0.80) Positive and Negative Predicted Values (PPV and NPV) were achieved by the balanced test, very different results were obtained for the whole area (0.001 and 0.999, respectively).

The figure 5.4.4a shows a graphical resume of the most important selected predictors, by using the nsubsets criterion (Conoscenti et al. 2016; Rotigliano et al. 2019).

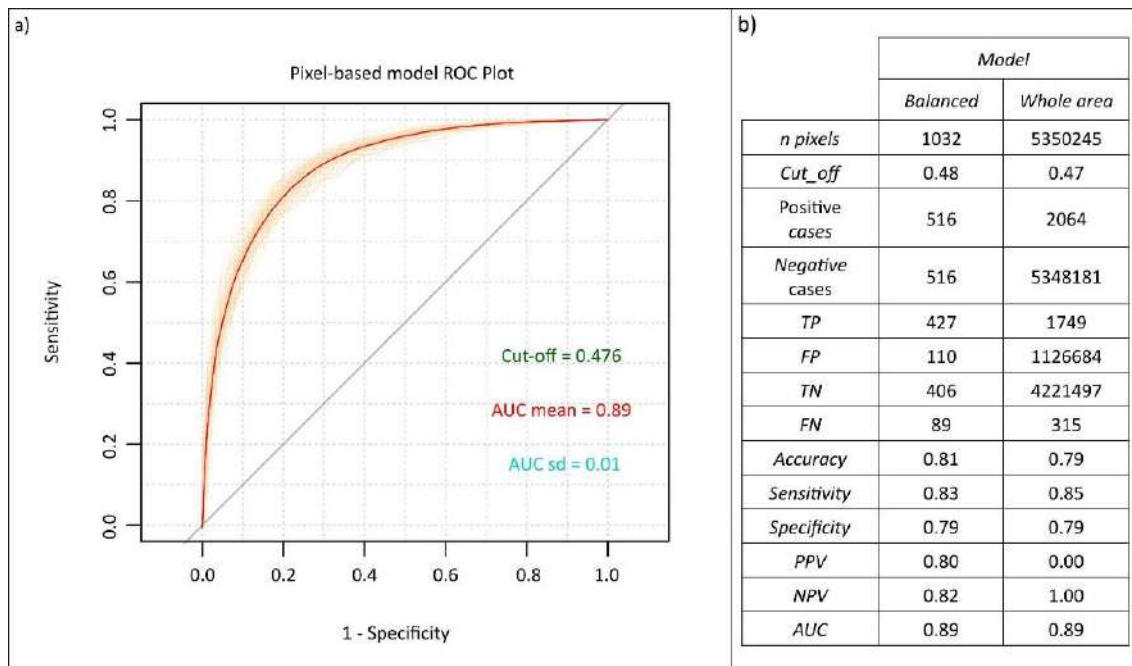


Figure 5.4.3: a) roc plot of pixel-based model (the one-hundred replicates are plotted in orange while the averaged ROC is in red); b) summary of the averaged confusion matrices for the pixel-based model validations (balanced and entire area schemes).

The categorical variables (LCL, LITO, USE) were disassembled into specific classes to analyse their different impact. In this way, 23 out of 45 variables have contributed to discriminate the positive to negative cases but only seven can be considered very important. TRI, SPI, PRF, ELE, SLO and PLN are the most important DEM-derived variables. Between the categorical variables, “lithoid units” and “calcareous and clayey marls” lithology classes, “non-irrigated arable land” and “sclerophyllous vegetation” land use classes and all the LCL classes played a very important role to discriminate the stable/unstable pixels.

The binary correlation between the continuous variables (Figure 5.2.4b) highlights a very high negative correlation between TWI and SLO, TWI and TRI whilst a positive one between SLO and TRI.

In table 5.4.2, the MEAN- and the MSTD-derived LCL_SLU AUCs for the ten types of slope-units are showed. The LCL_SLU AUCs perform always slightly better by using the

MSTD-derived score (>0.84) rather than the MEAN-derived score (> 0.82). A similar behavior is observed also for the HB_SLU models but down-shifted toward less performing results (between 0.74 and 0.78).

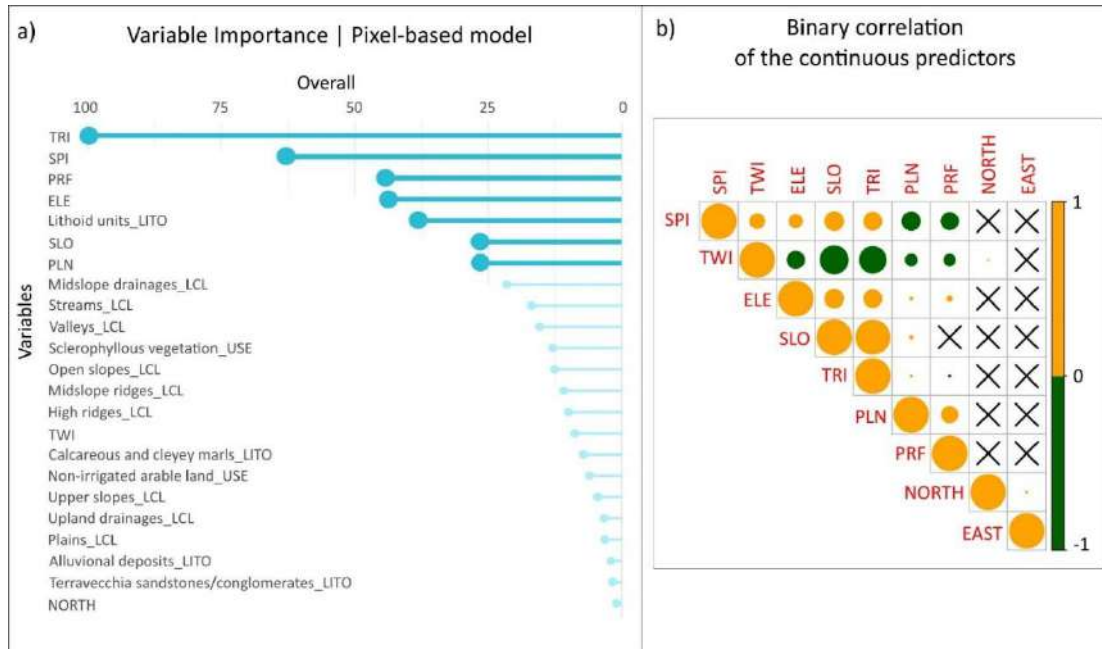


Figure 5.4.4: a) Variables importance for the pixel-based model: the predictors with an overall higher than 25 are plotted in cyan while those with an overall lower than 25 are in light-cyan; b) Binary correlation between the continuous variables: the radius of circle is proportional to the intensity of correlation (between 0 and 1) while the colour is representative to the direction (yellow for positive correlation, green for negative one); the X symbol corresponds to a non-significant correlation (p -value <0.01).

The Youden Index cut-offs are lower than the pixel-based models ones, with a more marked decreasing when passing either from HB_SLU to LCL_SLU or from the MSTD- to the MEAN-derived score.

By using the MSTD-derived score, very high sensitivity values arise for all the LCL_SLU models (>0.90) together with a lower specificity (about 0.7) resulting in a less performing accuracy (about 0.7). On the contrary, the 2000_HB_SLU and the 5000_HB_SLU performances, in spite of a similar (0.81 and 0.78) sensitivity, are affected by a marked decreasing in specificity (0.65 and 0.66) resulting in a just satisfactory accuracy (about 0.7). The principal behaviours of the HB_SLU and LCL_SLU models hold also using the MEAN-derived score, but all the performances result lower than MSTD-derived score: the accuracy fall down (<0.7) due to a marked specificity decreasing (<0.7 , with an extreme value equal to 0.56 for 5000_HB_SLU) while the sensitivity attains good or optimal values (between 0.80 and 0.95).

	model	Number of LCL_SLU or HB_SLU	Cut_off	Positive cases	Negative cases	TP	FP	TN	FN	Accuracy	Sensitivity	Specificity	PPV	NPV	AUC
According to the MSTD	2000_HB_SLU	3519	0.45	783	2736	631	949	1787	152	0.69	0.81	0.65	0.40	0.92	0.78
	5000_HB_SLU	1544	0.46	541	1003	423	337	666	118	0.71	0.78	0.66	0.56	0.85	0.76
	211_LCL_SLU	19165	0.35	979	18178	914	5590	12588	65	0.70	0.93	0.69	0.14	0.99	0.84
	212_LCL_SLU	17443	0.35	953	16482	899	5208	11274	54	0.70	0.94	0.68	0.15	1.00	0.84
	251_LCL_SLU	21398	0.36	1036	20354	962	6484	13870	74	0.69	0.93	0.68	0.13	0.99	0.85
	252_LCL_SLU	19196	0.37	1045	18143	961	5559	12584	84	0.71	0.92	0.69	0.15	0.99	0.85
	511_LCL_SLU	14936	0.35	763	14160	712	4023	10137	51	0.73	0.93	0.72	0.15	0.99	0.85
	512_LCL_SLU	13571	0.35	736	12823	696	3694	9129	40	0.72	0.95	0.71	0.16	1.00	0.84
	551_LCL_SLU	16232	0.35	831	15381	775	4640	10741	56	0.71	0.93	0.70	0.14	0.99	0.85
	552_LCL_SLU	14281	0.37	846	13419	783	3786	9633	63	0.73	0.93	0.72	0.17	0.99	0.86
According to the MEAN	2000_HB_SLU	3519	0.23	783	2736	629	956	1780	154	0.68	0.80	0.65	0.40	0.92	0.77
	5000_HB_SLU	1544	0.20	541	1003	472	441	562	69	0.67	0.87	0.56	0.52	0.89	0.74
	211_LCL_SLU	19165	0.19	979	18178	905	5916	12262	74	0.69	0.92	0.67	0.13	0.99	0.82
	212_LCL_SLU	17443	0.19	933	16482	866	5438	11044	67	0.68	0.93	0.67	0.14	0.99	0.82
	251_LCL_SLU	21398	0.18	1036	20354	965	7088	13266	71	0.67	0.93	0.65	0.12	0.99	0.83
	252_LCL_SLU	19196	0.18	1045	18143	975	6204	11939	70	0.67	0.93	0.66	0.14	0.99	0.84
	511_LCL_SLU	14936	0.18	763	14160	704	4450	9710	59	0.70	0.92	0.69	0.14	0.99	0.82
	512_LCL_SLU	13571	0.17	736	12823	698	4236	8587	38	0.68	0.95	0.67	0.14	1.00	0.82
	551_LCL_SLU	16232	0.18	831	15381	774	5195	10186	57	0.68	0.93	0.66	0.13	0.99	0.83
	552_LCL_SLU	14281	0.19	846	13419	779	4110	9309	67	0.71	0.92	0.69	0.16	0.99	0.84

Table 5.4.2 - Summary of the validation metrics for the ten susceptibility models.

In order to explore the general coherence between pixel- and SLU-based scores for the ten different partitioning adopted criteria, the dispersion of the pixel scores zoned into the SLUs was analysed (Figure 5.4.5). It is worth to note that a less variability arises for HB_SLUs split by LCLs with a minimum internal radius (100m), whilst the maximum variability arises by using the HB_SLUs (especially with the 5000_HB_SLU).

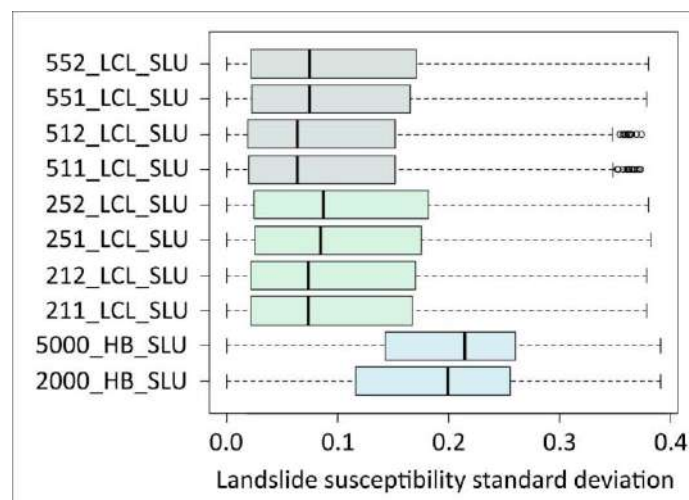


Figure 5.4.5: boxplot of the standard deviation pixel scores zoned into the SLUs.

In Figure 5.4.6, a comparison between the source pixel-based and the final LCL_SLU susceptibility maps is presented for a selected representative sector. In order to objectively reclassify the susceptibility maps, three cut-off values were directly obtained by analysing the ROC-plot. A first main cut-off (*m* cut-off) was first identified on the ROC plot, as the probability value resulting in the maximum difference between false positive (FP) and true

positive (TP) rate (Youden 1950). The same procedure was then applied to the two semi-plots which were obtained by splitting the ROC plot using the m cut-off. In this way, the two secondary cut-off values (l and h) were identified. Exploiting the l , m and h values, the score was finally reclassified into 4 classes depending on the susceptibility interval: NULL (S_0 ; $P < l$), LOW (S_1 ; $l < P < m$), HIGH (S_2 ; (S_1 ; $m < P < h$)) and VERY HIGH (S_3 ; $P > h$).

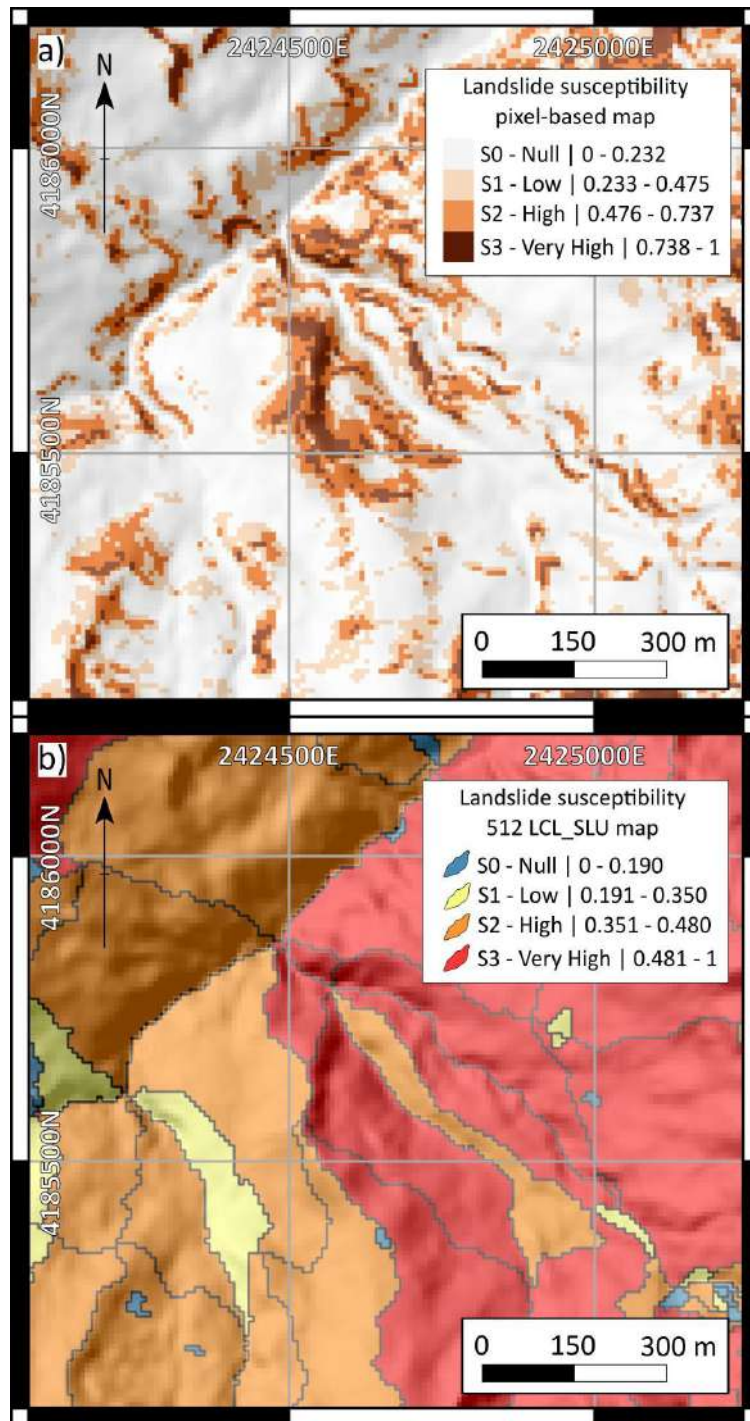


Figure 5.4.6: a) landslide susceptibility pixel-based map; b) landslide susceptibility LCL_SLU-based map

(HB_SLU: 5000 + LCL: 100-2000)

e) *Discussion and conclusions*

The pixel-based model shows excellent performances both in balanced and in the entire validation area. In fact, identical excellent AUC values are obtained for the two tests and the other performance metrics reveal only a slight variation. This proves that the false positive generation in the whole area is widely balanced by the true negative successful prediction. Moreover, the one-hundred replicates demonstrate both high accuracy and precision. In light of the above, the false positive cases potentially are to be expected as future positives (in other words, future landslide initiations) rather than type I errors.

It is worth to note that the variables importance analysis shows that the LCL classes play a very important role in discriminating the landslide initiation areas. This suggests a further slope-units subdivision through the LCL classes as useful for the performant and correct identification of landslide initiation zones and, as a consequence, for developing a zonal environmental subdivision suitable for optimizing the landslide susceptibility map output.

In fact, the results confirmed that the LCL_SLU models produced homogeneous and more easy to interpret prediction images, with a predictive performance higher than HB_SLU, suffering only from a limited performance lowering with respect to the pixel-based model, almost totally dependent on type I errors (false positives); at the same time, the LCL_SLU models resulted in the highest skill in finding/predicting the unstable pixels (sensitivity). In particular, the best LCL_SLU model (HB_SLU: 5000 + LCL: 100-2000) resulted in very high performances (AUC = 0.84; sensitivity = 0.95; specificity = 0.71) and much more readable maps. Moreover, the best LCL_SLU model is characterized by a very low pixel-score variability inside each slope-unit, attesting also for a coherent and stable susceptibility zonation.

Once the best performing susceptibility map was selected, the final step was to connect the propagation stage to the landslide initiation obtained from its prediction images. To this aim, the same morphodynamic meaning of the LCL_SLU was exploited after having dissolved the LCL_SLU smaller than 20000m² (the 3rd quantile of the landslide frequency distribution). A degree of fit plot was then prepared to validate the new integrated susceptibility map in predicting the source landslide polygons, which actually represent the real landslide propagation/arrest areas for the calibration inventory. This plot was then compared to that obtained from a pixel-based model, which differently was calibrated using the same landslide polygons (Figure 5.4.7). The comparison between the two results attested a very more performing behavior of the LCL_SLU integrated model.

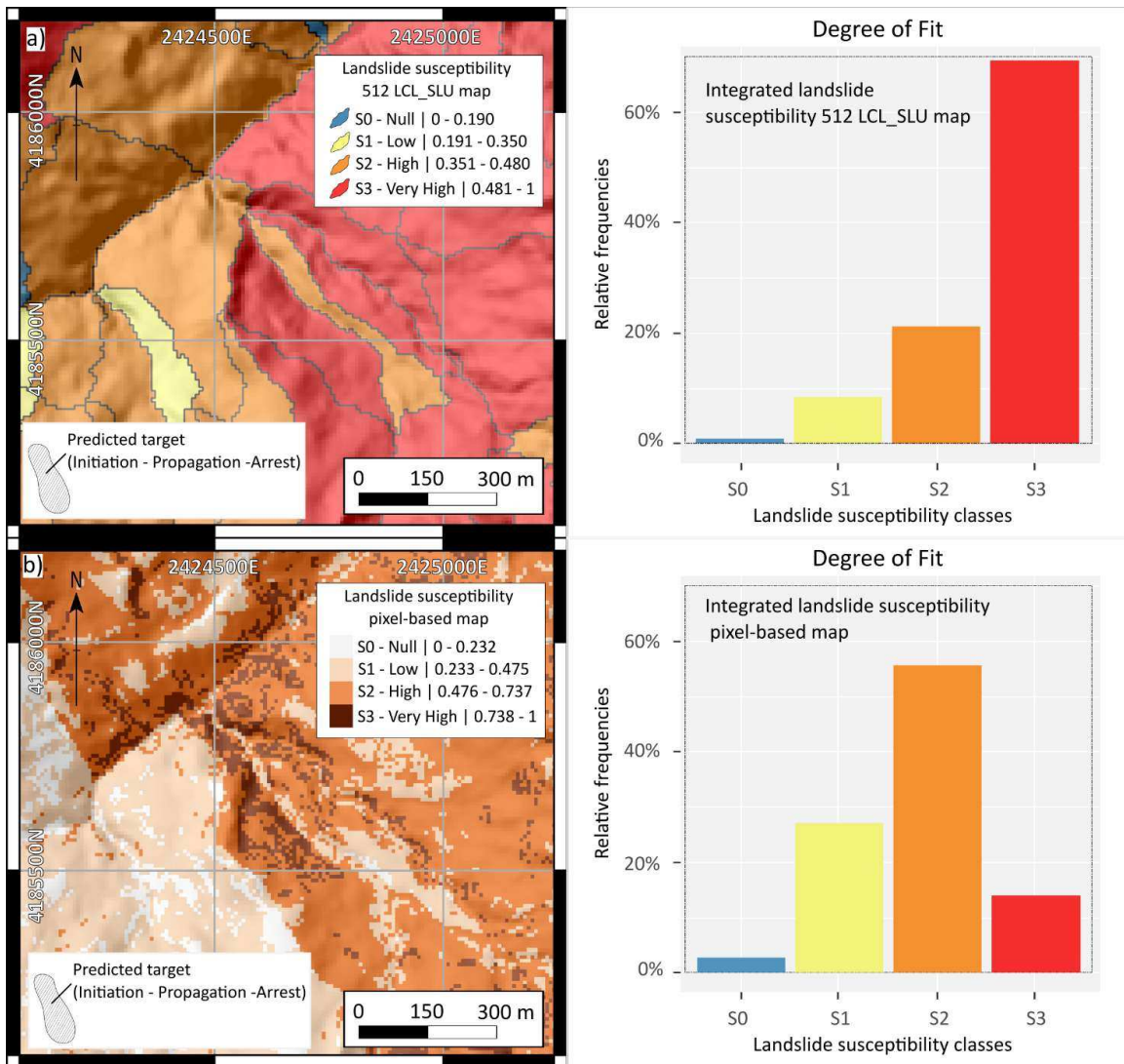


Figure 5.4.7: a) integrated landslide susceptibility LCL_SLU-based map (HB_SLU: 5000 + LCL: 100-2000) and whole basin degree of fit plot; b) landslide polygons calibrated susceptibility pixel-based map and whole basin degree of fit plot.

All the obtained results show that by integrating the classical pixel-based modelling (Figure 5.4.8b) on the LCL_SLU mapping units (Figure 5.4.8c), it is possible to optimize the results of the landslide susceptibility evaluation. The same LCL_SLUs allow also to involve the propagation stage into the predictive images, obtaining easy to interpret high performing integrated susceptibility maps (Figure 5.4.8d).



Optimal slope units partitioning in landslide susceptibility mapping

Chiara Martinello, Chiara Cappadonia, Christian Conoscenti, Valerio Agnesi, Edoardo Rotigliano

Department of Earth and Marine Sciences, University of Palermo, Palermo, Italy

© Journal of Maps, 2020

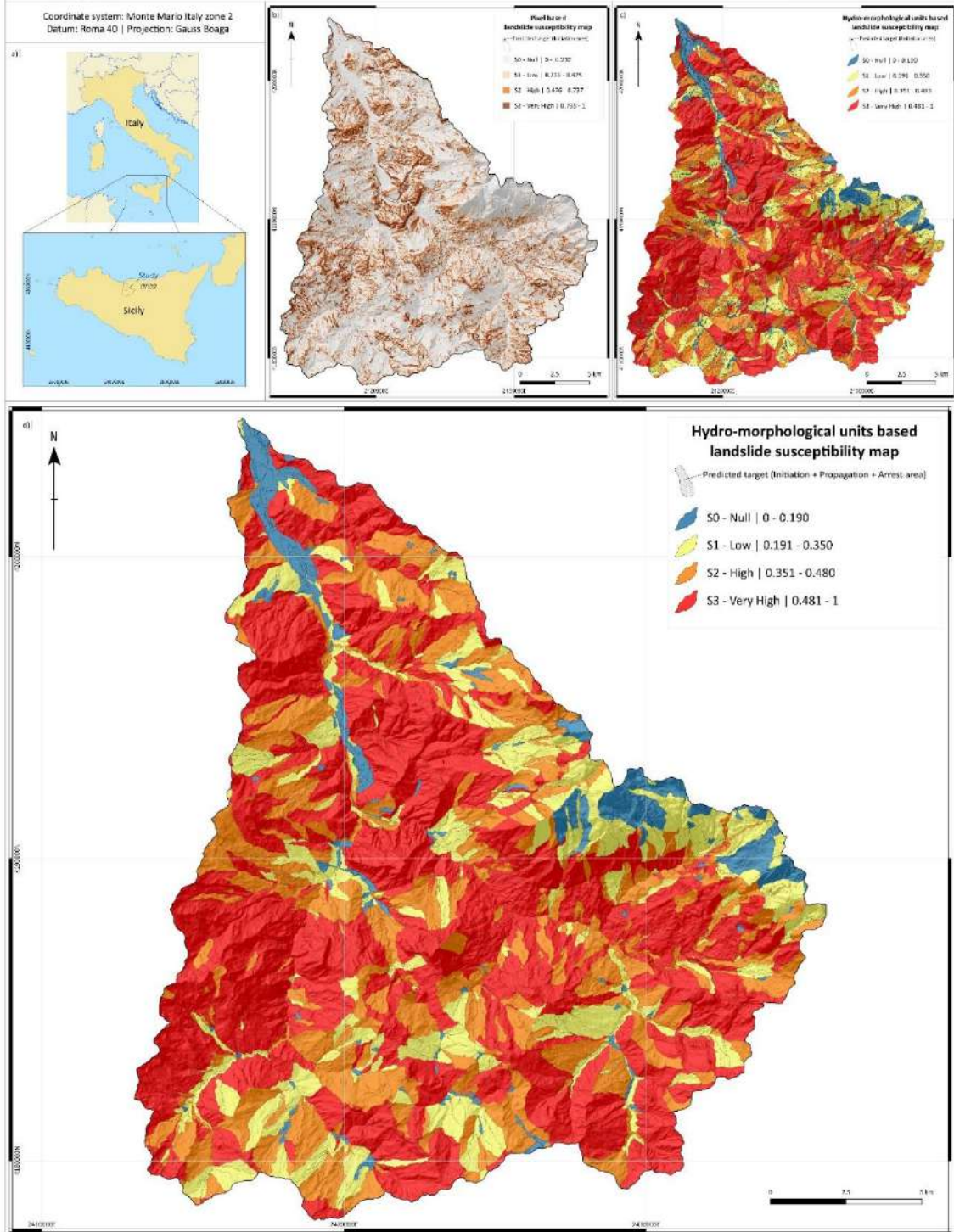


Figure 5.4.8: Main Map. a) Location of the Imera Settentrionale river basin, b) pixel-based landslide susceptibility map, c) integrated pixel-based LCL_SLU landslide susceptibility map, d) final landslide susceptibility map.

5.5. Landform classification: a high performing mapping unit partitioning tool for landslide susceptibility assessment. A test in the Imera river basin (northern Sicily, Italy).

Published on: Landslides (2022), 19:539–553, DOI: 10.1007/s10346-021-01781-8

In this research, landslide susceptibility models were prepared and compared by adopting four different types of mapping units: the largely adopted grid cells (PX); the typical contributing area-controlled slope units (5000_SLU); the recently optimized parameter-free multiscale slope units (PF_SLU); and a new type (LCL_SLU) of slope unit obtained by crossing classic hydrological partitioning with landform classification. At the same time, once a pixel-based model was prepared, four different SLU modelling strategies were applied to each of the obtained slope unit layers, including two different types of pixel score zoning, a pixel score re-modelling and a factor-based SLU re-modelling.

The test was carried out in the Imera river basin, where the spatial relationships between a set of predictors and an inventory of 1608 rotational/translational landslides were analysed using the Multivariate Adaptive Regression Splines (MARS) method.

a) Landslides inventory

The landslide inventory (Figure 5.5.1) employed for this research consists of 1608 rotational/translational slides (Hungr et al. 2014) detected using high resolution (0.25 m) LIDAR (LIght Detection And Ranging) images taken in 2012 by ARTA (Assessorato Regionale al Territorio e all’Ambiente). In terms of landslide risk, the Imera river catchment is very important for Sicily, as its main valley hosts the A19 motorway, which connects the capital (Palermo) to the second largest town (Catania), so that any potential landslides heavily threaten the local and regional economy. This was dramatically demonstrated by the landslide that damaged the pillars of the ‘Imera’ viaduct, causing the interruption of transit from April 2015 to July 2020 (Figure 5.5.2); at the same time, the widespread, landslide-induced poor status of the secondary (national and country) road network has strongly limited any by-pass solution (Figures 5.5.2, 5.5.3).

Translational and rotational landslides in the catchment are mainly associated with the outcropping of the alternation of arenitic and pelitic levels in flysch (Figures 5.5.3g and 5.5.5) or fluvio-delta/transitional deposits (Figure. 5.5.4). Translational slides actively shape moderate to near-dip-slope slopes, while rotational slides typically are associated with horizontally-layered to moderate scarp-slope slopes. In both cases, the presence of an

outcropping hard rock level (calcareous or quartzous arenites) allows the slopes to preserve high steepness. For this reason, large parts of the slopes affected by slide slope-failures are typically long, with a steeper head sector, and they evolve for retrogressive landslide activity distribution. The pelitic levels are typically made of sandy/silty clay, so that the expected failure mechanism is almost systematically linked to rainfall activating infiltration, which causes the neutral pressure to increase and lowers the cohesion. A number of rotational slides in the area are characterized by the typical complex style, with subsequent flow deformation phenomena involving the foot area, down to the failure surface toe. As the susceptibility analysis in this research was focused on the activation phase, all these cases were included in the slide inventory. For the same reason, translational and rotational slides were grouped, with the few surficial regolith/bedrock translational slides being excluded.

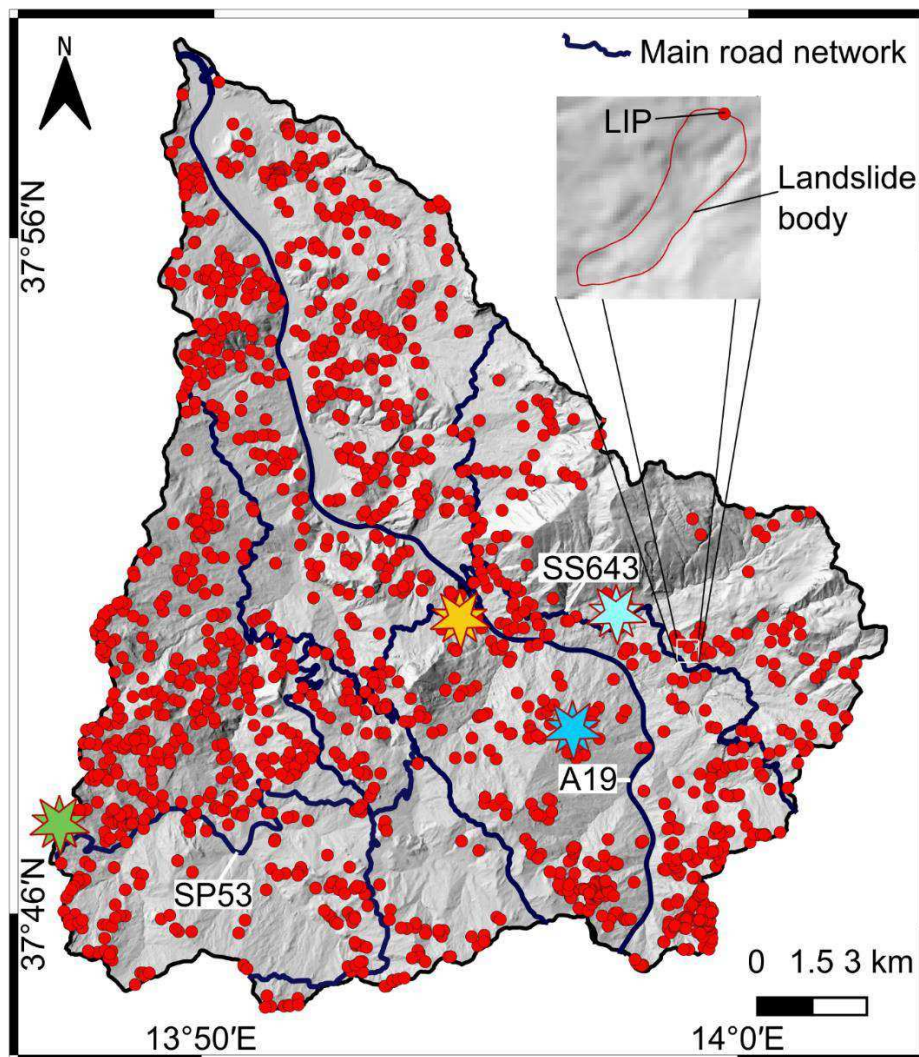


Figure 5.5.1: map of the landslide identification points (LIPs). The stars indicate the sites for the following field examples, with the same colours as the corresponding picture frameworks.



Figure 5.5.2: lateral (b) and main (c) scarps and damaged sectors (d, e, f) at the foot area of the 2015 rotational/flow complex landslide affecting the A19 motorway



Figure 5.2.3: translational slides; main scarp (g) and landslide accumulation (h) of the 2015 rotational slide affecting the SS643 national road.



Figure 5.5.4: damage caused to a wind farm (i, before; j, after) in the head zone of the rotational slide affecting the SP53 country road.



Figure 5.5.2: landslide scarp/head sector of the rotational slide/flow complex landslide in the Suvari area

b) *SLU partitioning*

In this research, three different SLU types were employed and compared: 1) parameter-free slope units (PF_SLUs), obtained using an optimized iterative application of the *r.slopeunits* (Alvioli et al 2020) GRASS GIS module and directly downloaded for the study area from <http://geomorphology.irpi.cnr.it/tools/slope-units>; 2) 5000_SLU half-basins, delimited by applying the *r.watershed* (Ehlschlaeger 1989; Metz et al. 2011) GRASS GIS module with an heuristically set contributing area threshold (5000 cells); 3) LCL_SLU, obtained by intersecting the same 5000_SLU layer with the Topographic Position Index (TPI; 100/2000 inner/outer radius)-based Landform Classification (Guisan et al. 1999; Wisz and Guisan 2009) layer in order to select sub-units with different geomorphological settings (Martinello et al. 2021).

All the slope unit partitioning schemes are controlled by the adopted contributing area threshold the user sets for half-basin recognition. For PF_SLUs, Alvioli et al. (2020) devised a parameter-free iterative nested procedure, which locally optimizes the best combination of the parameters a (minimum planimetric area) and c (circular covariance of the aspect). In this sense, their slope unit coverage is considered optimally scaled, and it is proposed by the authors for applications from the catchment to the national scale. At the same time, we propose here the LCL_SLU partitioning scheme, which is demonstrated to be optimized in the study area for 5000_SLU source half-basin partitions. The latter was also included in the comparative test to highlight potential pros and cons for landform classification-based sub-partitions.

Figure 5.5.6 schematically shows the spatial relations between the three different SLU typologies. In light of their delineation criteria, the number of LCL_SLUs in the same sector is expected to be much higher, and, as a consequence, the mean area of the LCL_SLUs will be lower than that of the 5000_SLUs and PF_SLUs.

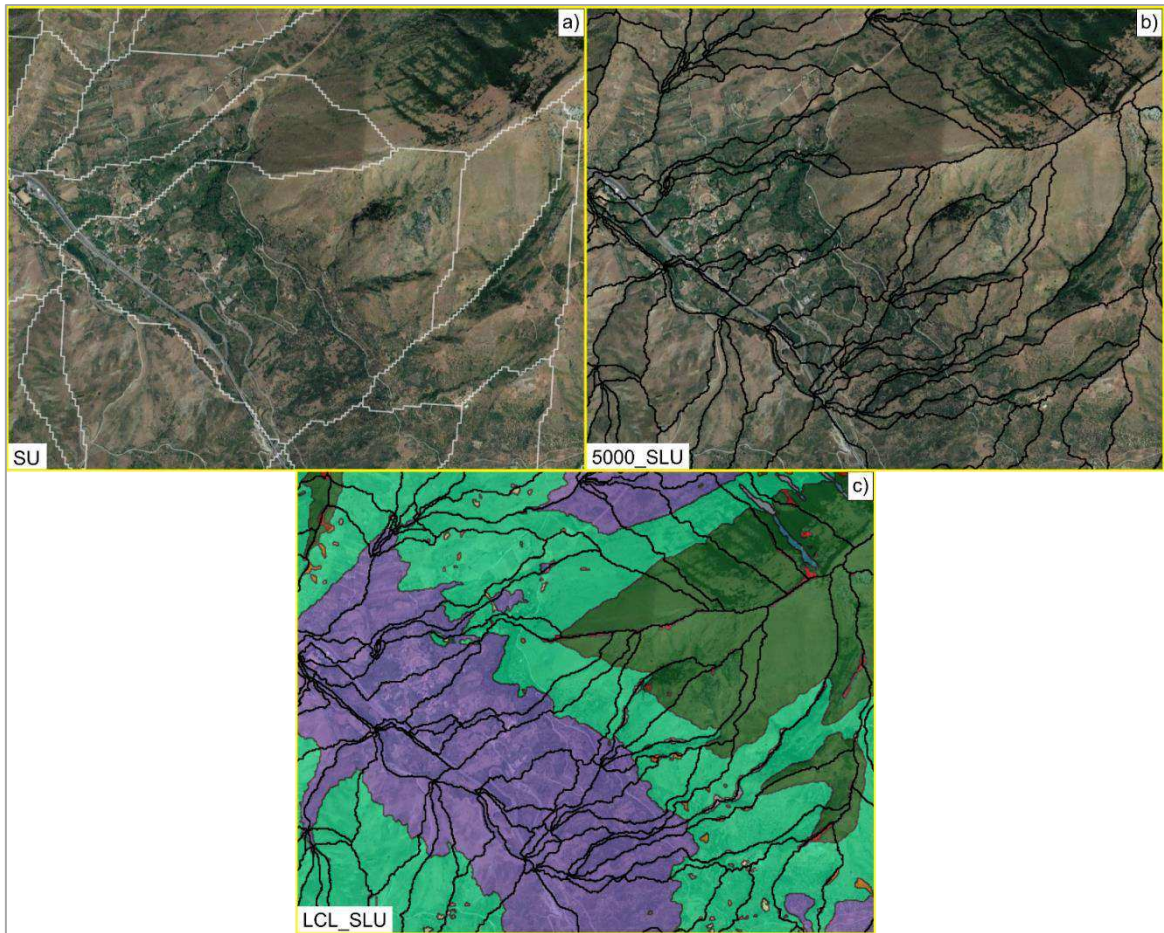


Figure 5.5.6: comparison between PF_SLU (white border), 5000_SLU (black border) and LCL_SLU (red border) partitioning in a representative sector. The different background colours in (c) depict an example of landform classification classes, in particular, 1) midslope drainages, 2) upland drainages, 3) valleys, 4) plains, 5) open slopes, 6) upper slopes, 7) midslope ridges and 8) high ridges

c) Landslide susceptibility assessment

Based on the outcome of previous studies (e.g., Cama et al. 2016), a spatial resolution of 8 m was set for preparing the grid layers of the covariate values and setting the stable/unstable status in the study area. These same layers were then directly used for the pixel-based modelling, while in the case of the slope units, further spatial processing (see below) was performed.

Each of the 1608 landslide mapped polygons was reported in the inventory as a Landslide Identification Point (LIP), which corresponds to the highest point along the crown of the landslide area; here, it is assumed to be diagnostic in potentially marking unstable slope conditions (Rotigliano et al 2011; Lombardo et al 2014; Cama et al 2015; Lombardo et al 2016; Rotigliano et al 2018; Rotigliano et al 2019).

To set the stable/unstable status of the different mapping units, a simple crossing between the LIP vector coverage and the three SLU layers was applied. Therefore, in the case of the pixel partition, the intersection produced the same number of positive cases (1608 cells), while in the case of the SLUs, as a direct consequence of their respective average area, a different number of positive mapping units included more than one LIP, so that 242, 543 and 736 positive cases resulted for the PF_SLU, 5000_SLU and LCL_SLU layers.

Twelve geo-environmental factors were considered as potential predictors for landslide susceptibility modelling: the outcropping lithology (LITO), land use (obtained by the Corine Land Cover 2018 – USE), elevation (ELE), landform classification (LCL), steepness (SLO), aspect (expressed as NORTHerness and EASTerness), plan (PLN) and profile (PRF) curvatures, topographic wetness index (TWI), terrain ruggedness index (TRI) and stream power index (SPI).

d) Statistical method and validation strategy

To detect the relations between the outcome and predictors, the Multivariate Adaptive Regression Splines (MARS; Friedman 1991) method was applied.

MARS modelling was applied to subsets made of the whole set of positive units and an equal number of randomly extracted subsets of negatives. In the case of the PF_SLU slope unit partitioning, which resulted in a greater number of positives than negatives, the regressed dataset was made of all the negatives and an equal number of randomly extracted positives. To test the model's precision and robustness, the extraction of the balanced subsets was repeated one hundred times. Each dataset was then submitted to a balanced random partition: a 75% subset was used for model calibration, while the remaining 25% subset was used for a blind validation test.

The Receiver Operating Curve and confusion matrix analysis were the tools employed to investigate the model accuracy.

In order to exclude redundant predictors from the set of the covariates, a factor multicollinearity analysis was performed before to proceed to the whole modelling procedures, based on the evaluation of the Variance Inflation Factor (VIF; Naimi 2017).

e) Modelling strategy

Together with the pixel-based model, twelve slope unit-based susceptibility models were prepared (Figure 5.5.7) by combining four different procedures with the three SLU-partitioned layers. First, by regressing the pixels' status on the twelve geo-environmental

predictor raster layers, the pixel-based model (PX) was prepared. Then, from the PX-scores, two zoned SLU-models were derived ($-Z_{mstd}$ and $-Z_{cut_off}$, respectively), assuming a mean plus one standard deviation and using the weighted average of the binarized (using the Youden index-derived cut-off) scores to classify the susceptibility of each SLU. At the same time, SLU regression was performed by setting the ten deciles of the PX scores inside each unit as predictors and obtaining the $-REG_{PX}$ model. Finally, a fully PX-score-independent model ($-REG_{FACT}$) was regressed by assigning to the slope units the deciles, for continuous, and the relative frequencies, for categorical, of the source predictor values (obtaining a total of 127 variables). In this way, for each of the three adopted slope units, a suite of four models was obtained. The two zoned models can simply be considered the result of direct SLU reclassifications, as they aggregate the pixel-based maps differently; on the contrary, the two regressed models are based on new regression procedures, with one maintaining a link with the pixel susceptibility scores and one set back to the factor source domain.

In analysing the results of the SLU-based models, predictive performance indices (accuracy, precision, and robustness) and geomorphological adequacy, together with the coherence with the PX model (i.e., the ability to recognize the same site score or predicted status), were considered.

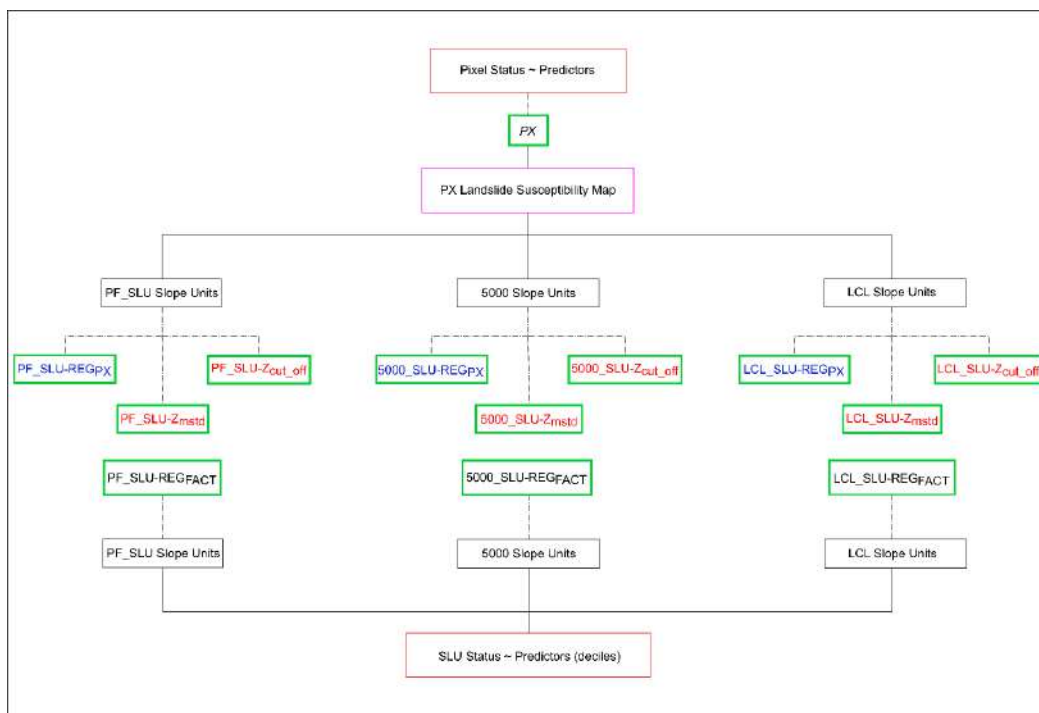


Figure 5.5.7: adopted model building scheme for the thirteen tested models (in green), with the red and blue labels indicating zoned and regressed models, respectively. Grey boundary boxes specify the adopted mapping units. The pixel-based landslide susceptibility map is shown in pink

f) Results

The AUC values that were obtained for each model are synthetically shown in Figure 5.5.8, where violin plots allow us to compare the resulting accuracy and robustness. The PX model can be defined as excellent (near outstanding), with an average AUC value equal to 0.89 and a very limited dispersion, while, among the SLU-based models, the LCL_SLU and the 5000_SLU suites achieved very high AUC accuracy and precision. In particular, the highest performances were systematically achieved by the LCL_SLU suite, while the PF_SLU models had largely lower performances, with AUCs well below the excellence threshold (with the exception of PF_SLU-REG_{PX}, which nearly reaches an AUC of 0.8) and significantly larger dispersions. More specifically, for the LCL_SLU suite, the -REG_{PX} and the -REG_{FACT} models attain the same outstanding AUC (0.95), above the PX performance, while slightly lower but excellent values were observed for the two zoned models (0.85 for -Z_{mstd} and 0.83 for -Z_{cut_off}). A similar but down-scaled trend can be observed for the 5000_SLU suite, with a slight AUC lowering (0.86 for the -REG_{PX} and -REG_{FACT} models and 0.76 for the two zoned models), together with a smaller difference between the 5000_SLU- and PF_SLU-zoned models.

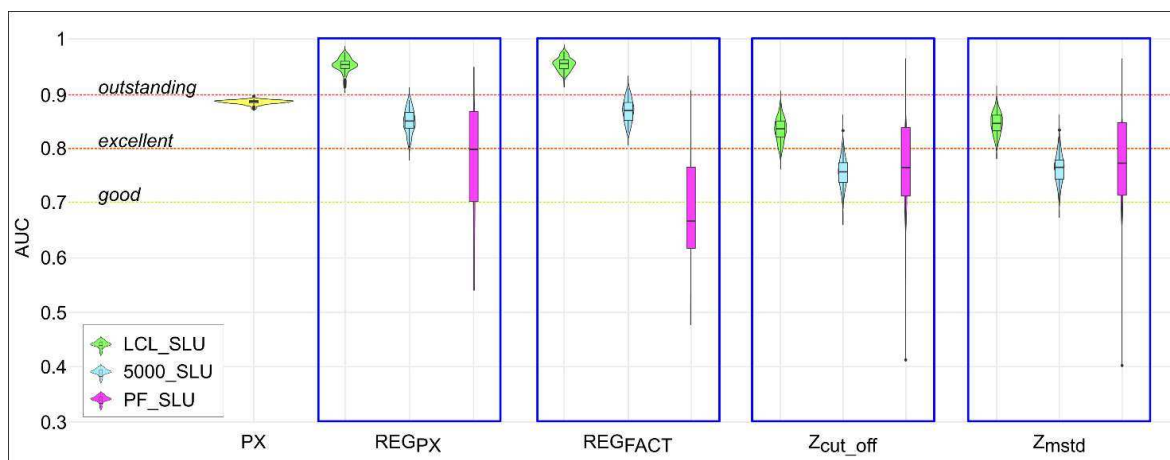


Figure 5.5.8: validation results (AUC values) for the thirteen models

By projecting each model from the modelling subset to the entire study area, confusion matrices based on the Youden index cut-off binarization were obtained (Table 5.5.1). Again, the LCL_SLU models achieved very high accuracy values, balanced in terms of sensitivity and specificity: additionally, in this case, an excellent performance is achieved by -REG_{PX} (0.88) and -REG_{FACT} (0.86). It is worth noting that, in contrast to what was observed for the AUCs, the PF_SLU models show the highest accuracies out of the zoned models and a near perfect predictive performance (0.98) for -REG_{FACT}. However, these results are associated

with the marked inverse prevalence of positive cases (242 out of 296) for the PF_SLU partition, so that, with the exception of -REG_{FACT} (whose AUC value, conversely, is below the acceptance threshold), lower sensitivities and specificities were observed. For the LCL_SLU suite, -REG_{PX} and -REG_{FACT} obtained very similar high performances, with the same numbers of True Positives (TP = 706) and False Negatives (FN = 30) and very similar True Negative and False Positive cases (FP = 1685 and 1804 and TN = 11156 and 11010 for -REG_{PX} and -REG_{FACT}, respectively).

	model	Number of cases	Cut_off	Positive cases	Negative cases	TP	FP	TN	FN	Accuracy	Sensitivity	Specificity	PPV	NPV
	PX	5350245	0.48	1607	5348638	1361	1180709	4167929	246	0.78	0.85	0.78	0.00	0.99
LCL_SLU	REG _{PX}	13550	0.45	736	12814	706	1658	11156	30	0.88	0.96	0.87	0.3	0.99
	REG _{FACT}	13550	0.46	736	12814	706	1804	11010	30	0.86	0.96	0.86	0.28	0.99
	Z _{cut_off}	13550	0.51	736	12814	708	3807	9007	28	0.72	0.96	0.7	0.15	0.89
	Z _{mstd}	13550	0.51	736	12814	703	3771	9043	33	0.72	0.96	0.71	0.15	0.99
5000_SLU	REG _{PX}	1544	0.49	543	1001	466	264	737	77	0.78	0.86	0.74	0.64	0.91
	REG _{FACT}	1544	0.45	543	1001	492	268	733	51	0.8	0.91	0.73	0.65	0.93
	Z _{cut_off}	1544	0.55	543	1001	469	438	563	74	0.67	0.86	0.56	0.51	0.88
	Z _{mstd}	1544	0.44	543	1001	444	373	626	99	0.69	0.82	0.63	0.54	0.86
PF_SLU	REG _{PX}	296	0.44	242	54	205	14	40	37	0.83	0.85	0.74	0.93	0.52
	REG _{FACT}	296	0.41	242	54	236	1	53	6	0.98	0.98	0.98	0.99	0.9
	Z _{cut_off}	296	0.55	242	54	192	20	34	50	0.76	0.79	0.62	0.9	0.4
	Z _{mstd}	296	0.43	242	54	188	18	36	54	0.76	0.78	0.63	0.9	0.4

Table 5.5.1: validation results (confusion matrices) for the thirteen models

In order to investigate those variables playing a central role in determining the stable/unstable conditions of the SLUs, the importance of the predictors for the better performing 5000_SLU-REG_{FACT} and LCL_SLU-REG_{FACT} models was analysed and compared to PX (Table 5.5.2). On average, PX selected 16 factors through the replicates, while the two different slope unit-based models had the same lower number of predictors (10); 14, 9 and 6 factors have a mean predictor importance higher than 10/100 for PX, 5000_SLU and the more parsimonious LCL_SLU models, respectively. Focusing on the variables that were selected the most, the 5000_SLU model is required to include two LCL classes (midslope ridges and high ridges, the first and fifth variables), together with the eastward aspect, high topographic ruggedness, and convex plan curvature, in order of importance. Conversely, the LCL_SLU model included the profile convex curvature, the northward aspect, high steepness, and the eastward aspect, in order of importance, out of the 6 most selected predictors.

Variable	Models		
	PX	5000_SLU	LCL_SLU
E (10 th decile)	/	47	20
N (10 th decile)	/	2	38
ELE*	43	/	/
ELE (first decile)	/	14	1
LCL - High ridges	9	33	4
LCL - Midslope Drainages	21	4	0
LCL - Midslope ridges	11	58	12
LCL - Open slopes	11	0	0
LCL - Streams	16	4	6
LCL - Upland drainages	14	0	0
LITO - "Terravecchia" pelites	37	13	15
PLC*	26	/	/
PLC (10 th decile)	/	41	1
PRF*	41	/	/
PRF (10 th decile)	/	5	70
SLO*	29	/	/
SLO (10 th decile)	/	17	37
SLO (9 th decile)	/	14	2
SPI*	63	/	/
TRI*	100	/	/
TRI (10 th decile)	/	43	5
TWI*	10	/	/
USE - Transitional woodland-shrub	12	3	4

Table 5.5.2: most important variables (at least 10/100) for PX, 5000-SLU and LCL_SLU –REGFACT models. *for the PX model, DTM-derived factors were not reclassified into decile intervals

g) Discussion

The main task of this research was to evaluate four different types of mapping units by comparing the predictive performances of their derived models on a basin-scale landslide susceptibility analysis.

One basic issue to be solved in analysing the results of the research was to estimate the potential trivial influence on the model performances of the differences in terms of the number of positive/negative cases resulting from the different spatial resolutions of the compared mapping units. In particular, there was a need to verify to what extent, if any, the higher number of cases produced by the LCL_SLU partition was responsible for making more accurate and precise derived models, so all modelling procedures were repeated after having reduced to the same number of cases the compared models. The obtained results (Figure 5.5.9) highlighted how the observed differences in performance still hold even after having dramatically scaled the LCL_SLU positive/negative balanced cases to $543 \times 2 = 1086$

and $54 \times 2 = 108$, for comparison to 5000_SLU and PF_SLU, respectively. More specifically, the comparison tests allowed us to recognize that the LCL_SLU partitioning scheme is very robust to case reduction, with a marked high performance (still well above the outstanding threshold) for -REG_{PX}. In this sense, it is also worth highlighting that the LCL_SLU partitioning in the two reduced versions, despite its lower spatial resolution (area of LCL_SLUs equal to 2.5 ha on average) and related number of positive cases, maintained a higher predictive performance with respect even to the pixel-based model.

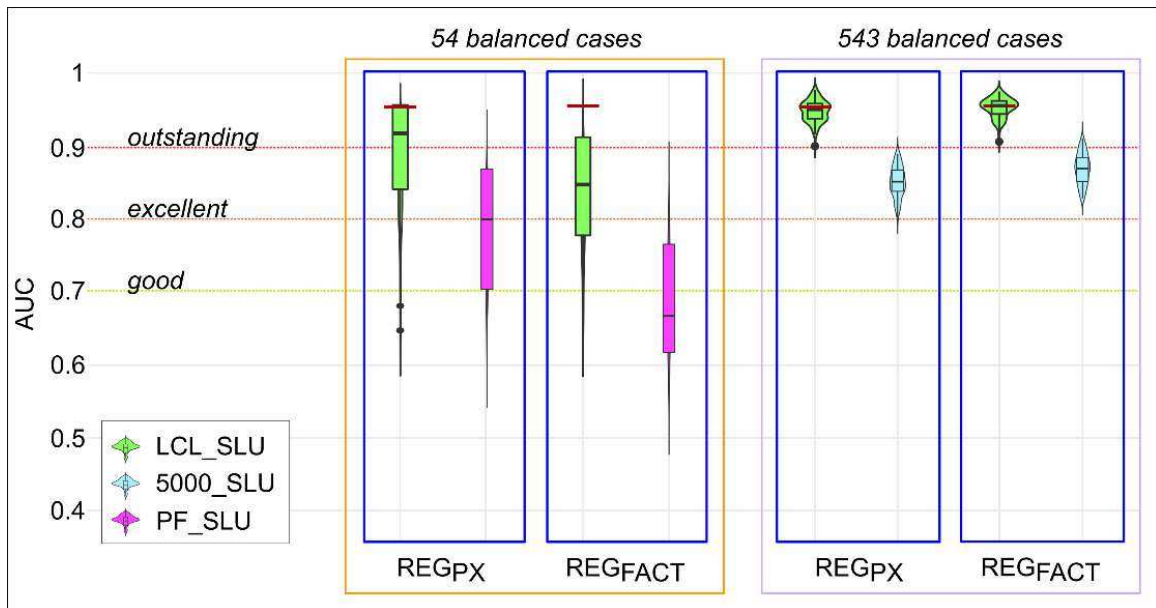


Figure 5.5.9: Comparison of AUC values obtained for regressed models with equal case numbers: LCL_SLU Vs. PF_SLU and 5000_SLU Vs. LCL_SLU (543 cases). The red lines are the corresponding AUC values of LCL_SLU models calibrated with the 736 positive cases

A further deep analysis of the relation between the accuracy and slope unit characteristics was carried out by comparing the two better-performing -REG_{PX} models, obtained for 5000_SLU and LCL_SLU partitioning of the study area, respectively. In particular, analysing the spatial relations between the source (mother) 5000_SLUs and the sub-partitioned derived (sons) LCL_SLUs, the reasons for the higher performance of the latter were investigated. In this way, it was possible to verify if the higher accuracy of LCL_SLU was ascribable to a trivial 5000_SLU multi-splitting-induced true case replication, rather than to geomorphological adequateness and more accurate prediction. Table 5.5.3 shows in detail the relation between the SLU type and predictive performance from each 5000_SLU mother to its LCL_SLU sons. In general, from the 1544 mother SLUs, 13550 son elements were produced, with a ratio of mothers to sons, or prolificity rate (prlf. rate), of 8.8. The 737 true negative 5000_SLUs produced 3511 LCL_SLUs, with 3117 TN confirmations (prlf.

rate = 4.2) and 394 reclassifications into false positive cases. It is definitely worth noting that the 2478 LCL_SLU sons derived from 264 false positive mother SLUs were confirmed only in 583 cases, while 1895 conversions to true negative conditions (prlf. rate = 7.2) were gained. Many of the 6639 son slope units generated from the 466 true positive mothers (prlf. rate = 14.2) instead received a true negative classification (5227; prlf. rate = 11.2), together with 766 false positive cases and 637 true positive confirmations (prlf. rate = 1.4). It is worth noting, together with the relevant increase in true negatives, the skill of the LCL_SLU model in discriminating true positive islands inside a number of multi-LIP positive 5000_SLUs, with the exception of only 9 false negative cases. In particular, the 77 false negative 5000_SLUs were converted into 922 sons (prlf. rate = 12), which were correctly classified as 771 true negative (prlf. rate = 10), 69 true positive cases, 61 false positives and only 21 false negatives. This suggests that LCL partitioning is capable of discriminating between true positives and negatives inside the 5000_SLU portion.





		Confusion matrix results				
		TOT	TN	FP	TP	FN
5000_SLU mother		1544	737 (47.7%)	264 (17.1%)	466 (30.2%)	77 (5%)
						
		13550 [8.8]	3511 [4.8] (25.9%)	2478 [9.4] (18.3%)	6639 [14.2] (49%)	922 [12.0] (6.8%)
Confusion matrix results	TN		3117 [4.2]	1895 [7.2]	5227 [11.2]	771 [10.0]
	FP		394 [0.53]	583 [2.2]	766 [1.6]	61 [0.79]
	TP		/	/	637 [1.37]	69 [0.90]
	FN		/	/	9 [0.02]	21 [0.27]
	LCL_SLU sons					

Table 5.5.3: Scheme for the relationships between the source 5000_SLU mother, framed in light green, and the derived LCL_SLU sons (REGPX model), framed in cyan. Percent number (round brackets) and prolificity rate (square brackets) for mother and son units: total (TOT), true negative (TN), false positive (FP), true positive (TP), false negative (FN) cases

In light of the points summarized above, LCL_SLU partitioning performs better, and this performance is not trivially related to an increase in true cases generated by multiple sub-partitions: its outstanding accuracy is robust to strong case reduction and higher than the accuracy obtained from the pixel-based model. By comparing the prolificity ratios and the derived generation of true/false positive/negative cases in the son mapping units, it is clear that the LCL_SLU splitting more specifically recognizes the susceptibility conditions inside the single 5000_SLUs, increasing TNs and TPs without increasing prediction costs in terms of FPs and FNs.

Regarding the geomorphological adequacy of the LCL_SLU partitioning, a further analysis was carried out in terms of those slope unit characteristics (outcropping lithology and soil use) that are independent of the landform classification, as they are not DTM-derived (Figure 5.5.10). For both of these attributes, LCL_SLU partitioning actually allowed the investigated area to be simplified into more homogeneous spatial domains. On the contrary, the mother 5000_SLUs show a marked right asymmetry toward the multi-class cases: almost 80% of the LCL_SLUs are characterized by only one type of LITO or USE class, while the majority of the remaining slope units have two classes and just a few have more than two. More specifically, to investigate the geomorphological conditions of the LCL_SLUs responsible for the higher performance of the modelling based on this type of slope unit, true cases not correctly classified by the 5000_SLU-REG_{PX} model were analysed.

Figure 5.5.11 clearly highlights that the true negative successes are linked to homogeneous LCL_SLUs, while true positive cases are mainly related to sectors with no more than 3 classes of outcropping lithology or soil use. Therefore, LCL_SLU partitioning has been demonstrated to immediately explain those simple and more diffused geomorphological settings responsible for the known mapped landslides: north- to east-facing, highly steep and convex slopes, which are typically set where arenite/pelite alternation outcrop (e.g., Figure 5.5.3g and Figure 5.5.5). In fact, the areas where rotational/translational slides were activated are characterized by the outcroppings at the heads of arenite caps, so that convex and steeper slopes can be preserved from erosion *lato sensu*. In the investigated area, these conditions are more frequently recognized on the north- to east-facing slopes. Moreover, the geologic setting of the area is marked by northeast-vergent structures, and the north-facing slopes are characterized by a slightly scarp-slope / near-horizontal-to-dip-slope strata attitude, which are the more typically required conditions for rotational and translational slides, respectively.

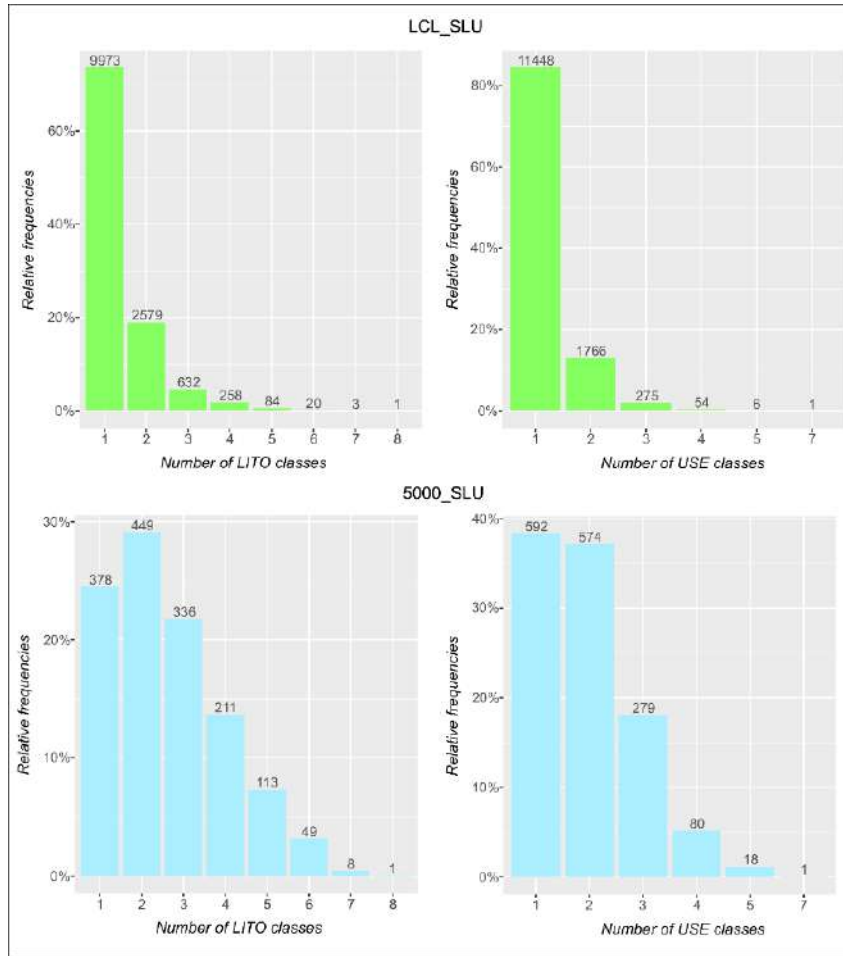


Figure 5.5.10: Analysis of the homogeneity of LCL_SLUs and 5000_SLUs for outcropping lithology and soil use predictors

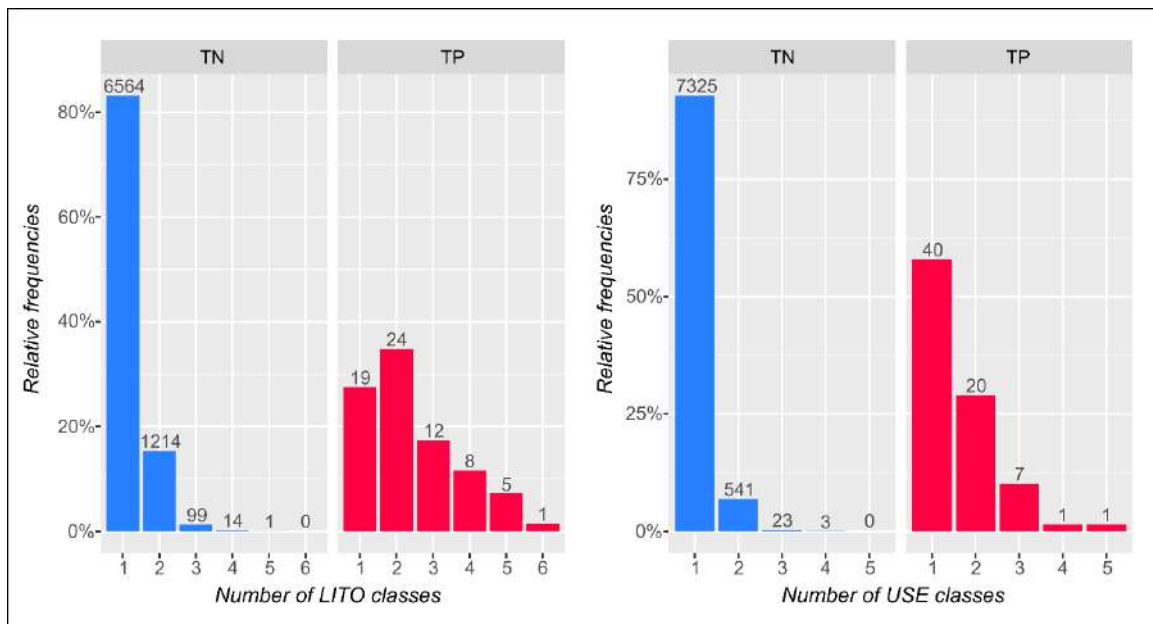


Figure 5.5.11: Analysis of the distribution of true cases with respect to the number of LITO and USE classes in each LCL_SLU

In terms of SLU modelling strategy, the regressed models performed better than the zoned models, suggesting that it is more correct, when passing from pixel- to SLU-based susceptibility mapping, to adopt new modelling procedures that are rooted in partitioning the same mapping units rather than statistically zoning the pixel-based scores. Additionally, the skill in coherently recognizing the pixel-based status of all the pixels in the study area was also assessed by comparing the number of matching cases to the PX predicted status for the two best performing models: LCL_SLU-REG_{PX} and -REG_{FACT}. The histogram in Figure 5.5.12 displays, for the four PX predicted/observed statuses, the difference in terms of matching between the -REG_{PX} and -REG_{FACT} models, highlighting how the former supports a higher number (303033 pixels = 19.4 km²) of TNs. At the same time, the slightly higher number of FNs can be considered negligible (9 pixels).

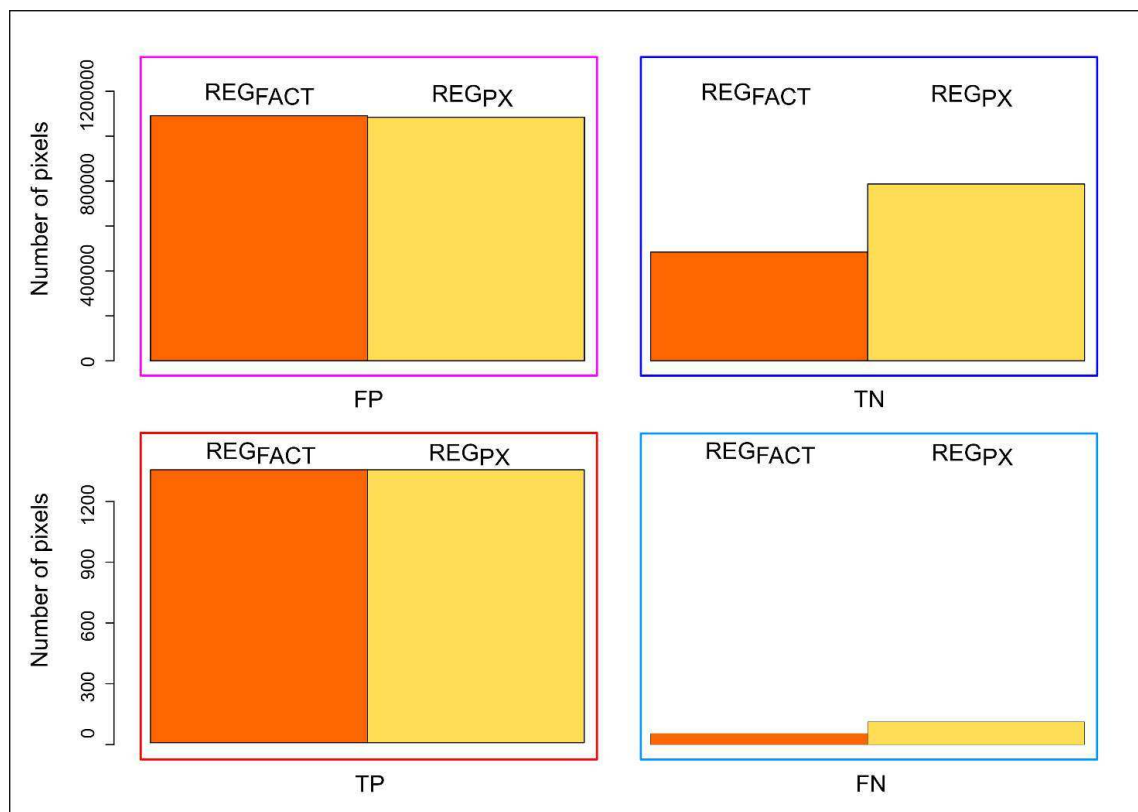


Figure 5.5.12: Matching TP, TN, FP and FN cases between PX, LCL_SLU-REG_{FACT} and LCL_SLU-REG_{PX}

Figure 5.5.13 shows a representative zoomed sector extracted from the susceptibility maps obtained by PX, 5000_SLU-REG_{PX} and LCL_SLU-REG_{PX}. The pixel-based MARS model, which was confirmed to be suitable for high performing predictive modelling, results in a derived prediction image that typically shows scattered score spatial patterns (e.g., Figure 5.5.13b). Conversely, the LCL_SLUs, which resulted in the best AUC performance and cut-

off-based accuracy, produced susceptibility maps in which clustered homogeneous pixels were correctly aggregated and classified (Figure 5.5.13c). The 5000_SLU model performance indices assumed intermediate values, with related susceptibility maps denoting larger units resulting in a lower resolution than LCL_SLU (Figure 5.5.13d).

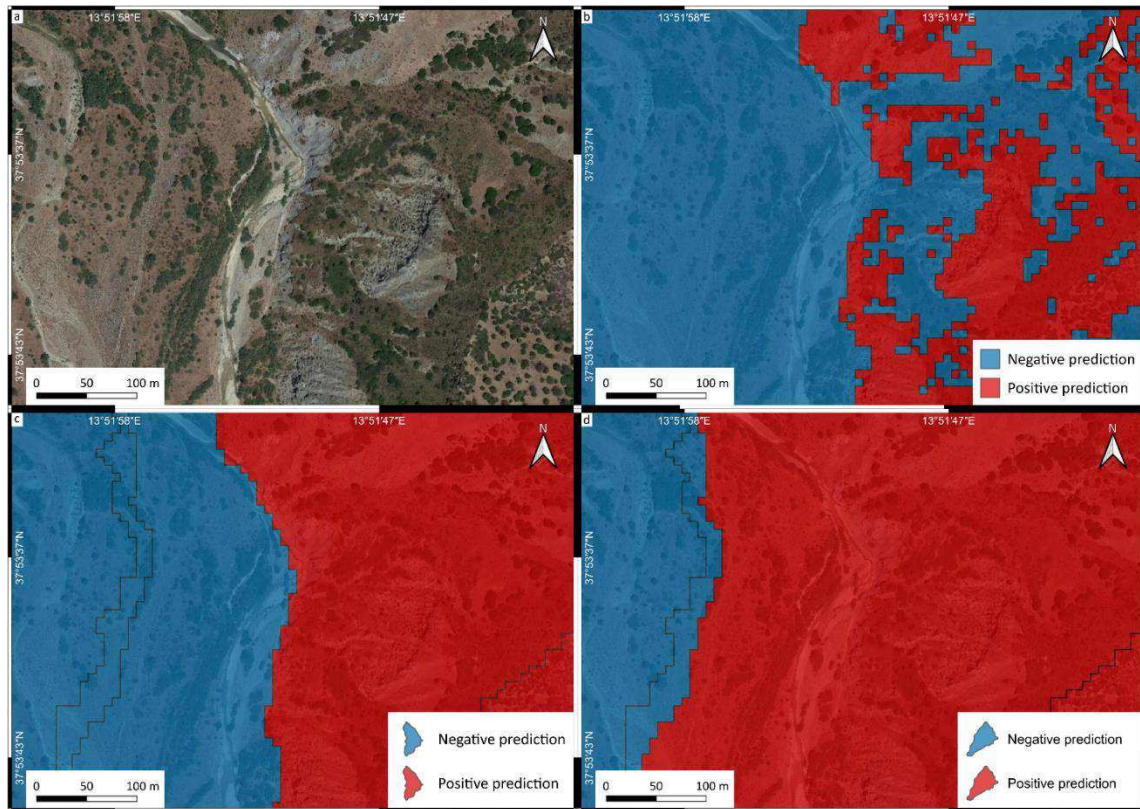


Figure 5.5.13: (a) Geomorphological setting of a representative sector and corresponding (b) pixel-based, (c) LCL_SLU-based and (d) 5000_SLU-based landslide susceptibility assessments

h) Conclusions

MARS modelling is confirmed to be suitable for a very high-performing landslide susceptibility assessment using either pixel- or slope unit-based models. Regarding the mapping units, based on the test we carried out in the Imera river basin, LCL_SLU modelling seems to be the optimal compromise between high-performing but scattered and smoothed but lower-performing prediction images, which were obtained from pure pixel-based and hydrologic SLU-based modelling, respectively. In particular, we demonstrated that the higher performance of LCL_SLU models is not trivially related to their smaller area, but rather is strictly dependent on their suitability for capturing the spatial pattern of the slope failure conditioning factors. Additionally, in terms of geomorphological adequacy (outcropping lithology, soil use and landform classification), the LCL_SLU partition was

much more suitable for recognizing those settings for which a homogeneous morphodynamic response can be expected. Furthermore, the LCL_SLU-based modelling is capable of producing SLU scores that match the source pixel score, confirming that their boundaries reflect an optimized spatial aggregation pattern for landslide susceptibility assessment. At the same time, landform classification was confirmed to be a powerful proxy for selecting homogeneous mapping units in terms of outcropping lithology and soil use. As a consequence, LCL_SLU partitioning is the basis for correctly defining more/less landslide-prone mapping unit conditions in terms of all the controlling factors: together with a more parsimonious selection of the important variables, LCL_SLUs are more geomorphologically interpretable with respect to either the scattered or too-smoothed prediction images obtained from pixel rasterization and slope unit partitioning, respectively.

Regarding the optimal LCL_SLU modelling strategy, a difference between the better-performing -REG_{PX} and -REG_{FACT} arose, due to the fact that -REG_{PX} takes the score as a summary-oriented indicator of slope instability proneness in a more simple way, while in the case of -REG_{FACT}, a very large fan of predictors (typically, more than one hundred) has to be generated. Moreover, if a pixel factor characterization seems to be too local, especially for slide-type landslides, extracting deciles from slope units that are too large could be geomorphologically misleading if morphodynamically disconnected pixels contribute to the same susceptibility class. In this sense, LCL_SLU partitioning seems to be a very promising solution, as it delimits much more restricted units that share a very basic common feature: their landform classification.

LCL_SLU partitioning and -REG_{PX} modelling are proposed here as a high-performing solution in basin scale translational/rotational slide susceptibility assessment. The susceptibility maps we obtained in this research were set to predict landslide initiation conditions and would need to be integrated into a complete susceptibility model that also includes the propagation phase. To this end, the landform classification-based slope unit partitioning approach we propose here seems to contain potential tools for correctly routing/chaining landslide susceptibility through the slopes.

6. Concluding remarks

As specific conclusions regarding the applications which have been carried out in this PhD research project have been already given in chapter 5, in the following some summary concluding remarks are given so as to link the experimental activity to the theoretical design of the thesis.

GIS-based statistical modelling is a powerful approach for landslide susceptibility assessment in multiscale studies up to a high-resolution basin scale. However, in spite of the more and more increasing source data availability and high performing statistical modelling techniques, some issues related to the very theoretical structure of the stochastic approach still require insights and innovative solutions.

In this thesis, some of these topics have been faced with the aim of investigating the limits of standard methods and eventually selecting strategies for giving some solutions to these. In particular, the studies which have been carried out in El Salvador allowed exploring a topic potentially hampering the basic key principle (the past is the key to the future) the stochastic approach relies on. In fact, in non-stationary conditions such as the ones produced by climate changes, calibrating models by exploiting landslide inventories produced by standard rainfall events could lead to underestimating the susceptibility conditions or prediction images which could be produced by extreme events. In this sense, it is important to exploit areas where extreme events are typically recurrent as this is the scenario which, on a more local scale, is going to prevail also into Mediterranean areas. In these areas, very local and intense phenomena (named *Medicanes*) can strike small hilly/mountain coastal sectors in autumn (during the westerlies falldown) triggering thousands of landslides in a few square kilometres. In this case, the susceptibility map calibrated with normal seasonal rainfall demonstrates to underestimate of the susceptibility of some multivariate conditions, suggesting as a better solution to calibrate the models in the small sectors already hit by past storms. This approach has been confirmed as suitable in the test we carried out in the Ilopango caldera.

As regards, the implementation of effective regional/basin approaches, two big issues have been here faced: mapping units and incomplete inventories. These two topics are strictly connected to the real possibility of completing the technological transfer to the public authority so that stochastic susceptibility modelling could be taken (as indicated at a communitarian level) as the reference approach for land-use planning and civil protection. In fact, the incompleteness of the inventories is one of the main limits for accepting as

time/cost-effective this approach for systematic application to regional territories. However, the research we carried out in El Salvador allowed defining a method for obtaining indexes suitable to warn the user about the false sense of completeness, when highly populated regional inventories are obtained just by merging sparse data. At the same time, solutions for integrating the data have been tested in Sicily (Torto basin), so to optimize the efforts in landslide recognition to integrate poor inventories.

As regards the topic of mapping units, in this research project efforts have been put into searching for optimal solutions both for susceptibility modelling and mapping. In particular, by crossing terrain units automatically obtained by means of hydrologic tools with the landform classification classes based on the topographic position index, a much more refined susceptibility zoning has been obtained. In fact, LCL-SLUs are allowed to split those Rock/Scarp to Clayey/Slope sequences which are undistinguished in normal terrain units-based modelling. At the same time, adopting slope units for susceptibility reclassification and mapping demonstrated to results in much more final user-friendly maps, where the alarm of high scores is eventually not dispersed into unconnected pixels. Moreover, in light of their morphodynamic meaning, LCL-SLUs allow also to extend the interpretation of the susceptibility maps from a simple image of where is more likely new landslides will trigger from, also including the propagation phase.

The comparison between binary logistic regression and MARS allowed highlighting the importance of maintaining a strict link between the statistical and the geomorphological modelling. MARS indeed is capable of more strictly fitting the model, resulting in more performing prediction. However, efforts are required to explain in geomorphological terms the role of factors, as these are split into intervals which can escape from a simple interpretation. In this thesis, a strong focus has been always kept on the analysis of the role of the controlling factors, devising tools for making direct the reading for the user.

Finally, all throughout the experimental tests which have been carried out, severe validation procedures have been applied with the aim of suggesting a standard for outputs in the public territory administration. A large part of this research was carried out in the framework of a project (SUFRA) requiring the preparation of susceptibility maps for the whole Sicilian territory and as such, standardizing analysis, and map design, as well as validation strategies and tools was among the final tasks of the research.

Much more efforts are to be put into solving or even exploring the limits of stochastic approaches for landslide susceptibility modelling. However, in the present research, some

contributions have been given and the related solutions made available both to the scientist and territorial administrative-technical levels.

References

- Abate B, Catalano R, D'argenio B, et al (1982) Carta geologica delle Madonie orientali.
- Abate B, Pescatore T, Renda P, Tramutoli M (1988) Schema geologico dei Monti di Termini Imerese e delle Madonie Occidentali (Sicilia). *Mem Soc Geol Ital* 41:465–474
- Accaino F, Catalano R, di Marzo L, et al (2011) A crustal seismic profile across Sicily. *Tectonophysics* 508:52–61. <https://doi.org/10.1016/j.tecto.2010.07.011>
- Agnesi V, Camarda M, Conoscenti C, et al (2005) A multidisciplinary approach to the evaluation of the mechanism that triggered the Cerda landslide (Sicily, Italy). *Geomorphology* 65:101–116. <https://doi.org/10.1016/j.geomorph.2004.08.003>
- Agnesi V, Cosentino P, di Maggio C, et al (1997) The great landslide at Portella Colla (Madonie, Sicily). *Geografia Fisica e Dinamica Quaternaria* 19:273–280
- Agnesi V, de Cristofaro D, di Maggio C, et al (2000) Morphotectonic setting of the Madonie area (central northern Sicily). *Mem Soc Geol Ital* 55:373–379
- Agnesi V, Macaluso T (1997) Mass movements in Sicily and their role in slope evolution. *Mathematica* 42:51–61
- Agostini S, Corti G, Doglioni C, et al (2006) Tectonic and magmatic evolution of the active volcanic front in El Salvador: insight into the Berlín and Ahuachapán geothermal areas. *Geothermics* 35:368–408. <https://doi.org/10.1016/j.geothermics.2006.05.003>
- Alvioli M, Guzzetti F, Marchesini I (2020) Parameter-free delineation of slope units and terrain subdivision of Italy. *Geomorphology* 358:107124. <https://doi.org/10.1016/j.geomorph.2020.107124>
- Alvioli M, Marchesini I, Reichenbach P, et al (2016) Automatic delineation of geomorphological slope units with r.slopeunits v1.0 and their optimization for landslide susceptibility modeling. *Geoscientific Model Development* 9:3975–3991. <https://doi.org/10.5194/gmd-9-3975-2016>
- Amanti M, Chiessi V, Bertolini G, et al (2001) Guida alla compilazione della scheda frane IFFI (Inventario Fenomeni Franosi in Italia). Allegato 1 al Progetto IFFI.
- Amato G, Eisank C, Castro-Camilo D, Lombardo L (2019) Accounting for covariate distributions in slope-unit-based landslide susceptibility models. A case study in the alpine environment. *Engineering Geology* 260:105237. <https://doi.org/10.1016/j.enggeo.2019.105237>

- Auslander M, Nevo E, Inbar M (2003) The effects of slope orientation on plant growth, developmental instability and susceptibility to herbivores. *Journal of Arid Environments* 55:405–416. [https://doi.org/10.1016/S0140-1963\(02\)00281-1](https://doi.org/10.1016/S0140-1963(02)00281-1)
- Avellone G, Barchi MR, Catalano R, et al (2010) Interference between shallow and deep-seated structures in the Sicilian fold and thrust belt, Italy. *J Geol Soc London* 167:109–126. <https://doi.org/10.1144/0016-76492008-163>
- Avila LA, Cangialosi J (2010) Tropical Cyclone Report Hurricane Ida (AL112009) 4-10 November 2009
- Ba Q, Chen Y, Deng S, et al (2018) A comparison of slope units and grid cells as mapping units for landslide susceptibility assessment. *Earth Science Informatics* 11:373–388. <https://doi.org/10.1007/s12145-018-0335-9>
- Basilone L (2012) Litostratigrafia della Sicilia. Arti Grafiche Palermitane s.r.l.
- Bates RL, Jackson JA (1984) Glossary of geology. American Geological Institute, Falls Church, Virginia
- Beven KJ, Kirkby MJ (1979) A physically based, variable contributing area model of basin hydrology / Un modèle à base physique de zone d'appel variable de l'hydrologie du bassin versant. *Hydrological Sciences Bulletin* 24:43–69. <https://doi.org/10.1080/02626667909491834>
- Bordoni M, Galanti Y, Bartelletti C, et al (2020a) The influence of the inventory on the determination of the rainfall-induced shallow landslides susceptibility using generalized additive models. *Catena (Amst)* 193:104630. <https://doi.org/10.1016/j.catena.2020.104630>
- Bordoni M, Vivaldi V, Lucchelli L, et al (2020b) Development of a data-driven model for spatial and temporal shallow landslide probability of occurrence at catchment scale. *Landslides*. <https://doi.org/10.1007/s10346-020-01592-3>
- Borrelli L, Cofone G, Coscarelli R, Gullà G (2015) Shallow landslides triggered by consecutive rainfall events at Catanzaro strait (Calabria–Southern Italy). *Journal of Maps* 11:730–744. <https://doi.org/10.1080/17445647.2014.943814>
- Brabb EE (1984) Innovative approaches to landslide hazard and risk mapping. In: *Proceedings 4th International Symposium on Landslides*. . Toronto, Canada, pp 307–324
- Brabb EE (1991) The Word Landslide Problem. *Episodes* 14:

- Brandolini P, Pepe G, Capolongo D, et al (2018) Hillslope degradation in representative Italian areas: Just soil erosion risk or opportunity for development? *Land Degradation and Development* 29:3050–3068. <https://doi.org/10.1002/ldr.2999>
- Brennan M (2011) Tropical Depression One-E Advisory 1. National Oceanic and Atmospheric Administration.
- Brenning A (2005) Spatial prediction models for landslide hazards: review, comparison and evaluation. *Natural Hazards and Earth System Sciences* 5:853–862
- Buccolini M, Coco L, Cappadonia C, Rotigliano E (2012) Relationships between a new slope morphometric index and calanchi erosion in northern Sicily, Italy. *Geomorphology* 149–150:41–48. <https://doi.org/10.1016/j.geomorph.2012.01.012>
- Burrough PA, McDonnell RA (1998) *Principle of Geographic Information Systems*
- CODRA-Creating Opportunities to Develop Resilient Agriculture View project
- Groundwater Governance in the Arab World: Taking Stock and Addressing the Challenges View project
- Cama M, Conoscenti C, Lombardo L, Rotigliano E (2016) Exploring relationships between grid cell size and accuracy for debris-flow susceptibility models: a test in the Giampileri catchment (Sicily, Italy). *Environmental Earth Sciences* 75:1–21. <https://doi.org/10.1007/s12665-015-5047-6>
- Cama M, Lombardo L, Conoscenti C, et al (2015) Predicting storm-triggered debris flow events: Application to the 2009 Ionian Peloritani disaster (Sicily, Italy). *Natural Hazards and Earth System Sciences* 15:1785–1806. <https://doi.org/10.5194/nhess-15-1785-2015>
- Cama M, Lombardo L, Conoscenti C, Rotigliano E (2017) Improving transferability strategies for debris flow susceptibility assessment Application to the Saponara and Itala catchments (Messina, Italy). *Geomorphology* 288:52–65. <https://doi.org/10.1016/j.geomorph.2017.03.025>
- Camilo DC, Lombardo L, Mai PM, et al (2017) Handling high predictor dimensionality in slope-unit-based landslide susceptibility models through LASSO-penalized Generalized Linear Model. *Environmental Modelling and Software*. <https://doi.org/10.1016/j.envsoft.2017.08.003>
- Cappadonia C, Coco L, Buccolini M, Rotigliano E (2016) From Slope Morphometry to Morphogenetic Processes: An Integrated Approach of Field Survey, Geographic Information System Morphometric Analysis and Statistics in Italian Badlands. *Land Degradation and Development* 27:851–862. <https://doi.org/10.1002/ldr.2449>

- Cappadonia C, Conoscenti C, Rotigliano E (2011) Monitoring of erosion on two calanchi fronts-Northern Sicily (Italy). *Landform Analysis* 17:21–25
- Carrara A, Cardinali M, Guzzetti F, Reichenbach P (1995) Gis Technology in Mapping Landslide Hazard. 135–175. https://doi.org/10.1007/978-94-015-8404-3_8
- Catalano R, Avellone G, Basilone L, et al (2011) Note illustrative della Carta Geologica d'Italia alla scala 1: 50.000 del Foglio 609 “Termini Imerese”, con allegata carta geologica in scala 1: 50.000
- Catalano R, Stefano P di, Sulli A, Vitale FP (1996) Paleogeography and structure of the central Mediterranean: Sicily and its offshore area
- CEPAL (2011) Evaluación de daños y pérdidas en El Salvador ocasionados por la depresión tropical 12E
- CEPAL (2010) El Salvador : impacto socioeconómico, ambiental y de riesgo por la baja presión asociada a la tormenta tropical ida en noviembre de 2009
- Chen W, Pourghasemi HR, Panahi M, et al (2017) Spatial prediction of landslide susceptibility using an adaptive neuro-fuzzy inference system combined with frequency ratio, generalized additive model, and support vector machine techniques. *Geomorphology* 297:69–85. <https://doi.org/10.1016/j.geomorph.2017.09.007>
- Cheng L, Zhou B (2018) A new slope unit extraction method based on improved marked watershed. *MATEC Web of Conferences* 232:04070. <https://doi.org/10.1051/mateconf/201823204070>
- Chiarabba C, Jovane L, DiStefano R (2005) A new view of Italian seismicity using 20 years of instrumental recordings. *Tectonophysics* 395:251–268. <https://doi.org/10.1016/j.tecto.2004.09.013>
- Chung CJF, Fabbri AG (2003) Validation of spatial prediction models for landslide hazard mapping. *Natural Hazards* 30:451–472. <https://doi.org/10.1023/B:NHAZ.0000007172.62651.2b>
- Clerici A, Perego S, Tellini C, Vescovi P A procedure for landslide susceptibility zonation by the conditional analysis method
- Conoscenti C, Agnesi V, Cama M, et al (2018) Assessment of Gully Erosion Susceptibility Using Multivariate Adaptive Regression Splines and Accounting for Terrain Connectivity. *Land Degradation and Development* 29:724–736. <https://doi.org/10.1002/ldr.2772>
- Conoscenti C, Ciaccio M, Caraballo-Arias NA, et al (2015) Assessment of susceptibility to earth-flow landslide using logistic regression and multivariate adaptive regression

- splines: A case of the Belice River basin (western Sicily, Italy). *Geomorphology* 242:49–64. <https://doi.org/10.1016/j.geomorph.2014.09.020>
- Conoscenti C, di Maggio C, Rotigliano E (2008a) GIS analysis to assess landslide susceptibility in a fluvial basin of NW Sicily (Italy). *Geomorphology* 94:325–339. <https://doi.org/10.1016/j.geomorph.2006.10.039>
- Conoscenti C, Maggio C, Rotigliano E (2008b) Soil erosion susceptibility assessment and validation using a geostatistical multivariate approach: A test in Southern Sicily. *Natural Hazards* 46:287–305. <https://doi.org/10.1007/s11069-007-9188-0>
- Conoscenti C, Martinello C, Alfonso-Torreño A, Gómez-Gutiérrez Á (2021) Predicting sediment deposition rate in check-dams using machine learning techniques and high-resolution DEMs. *Environmental Earth Sciences* 80:1–19. <https://doi.org/10.1007/s12665-021-09695-3>
- Conoscenti C, Rotigliano E, Cama M, et al (2016) Exploring the effect of absence selection on landslide susceptibility models: A case study in Sicily, Italy. *Geomorphology* 261:222–235. <https://doi.org/10.1016/j.geomorph.2016.03.006>
- Conrad O, Bechtel B, Bock M, et al (2015) System for Automated Geoscientific Analyses (SAGA) v. 2.1.4. *Geoscientific Model Development* 8:1991–2007. <https://doi.org/10.5194/gmd-8-1991-2015>
- Corti G, Carminati E, Mazzarini F, Garcia MO (2005) Active strike-slip faulting in El Salvador, Central America. *Geology* 33:989–992. <https://doi.org/10.1130/G21992.1>
- Costanzo D, Cappadonia C, Conoscenti C, Rotigliano E (2012a) Exporting a Google Earth™ aided earth-flow susceptibility model: A test in central Sicily. *Natural Hazards* 61:103–114. <https://doi.org/10.1007/s11069-011-9870-0>
- Costanzo D, Chacón J, Conoscenti C, et al (2014) Forward logistic regression for earth-flow landslide susceptibility assessment in the Platani river basin (southern Sicily, Italy). *Landslides* 11:639–653. <https://doi.org/10.1007/s10346-013-0415-3>
- Costanzo D, Rotigliano E, Irigaray C, et al (2012b) Factors selection in landslide susceptibility modelling on large scale following the gis matrix method: Application to the river Beiro basin (Spain). *Natural Hazards and Earth System Science* 12:327–340. <https://doi.org/10.5194/nhess-12-327-2012>
- Crone AJ, Baum RL, Lidke DJ, et al (2001) *Landslides Induced by Hurricane Mitch in El Salvador - An Inventory and Descriptions of Selected Features*
- Crozier MJ (1986) *Landslides: Causes, Consequences and Environment*. London

- Cruden DM, Varnes DJ (1996) Landslide types and processes. Transportation Research Board, U.S. National Academy of Sciences, Special Report, 247: 36-75
- Diebold J, Driscoll N (1999) Chapter 19 New insights on the formation of the caribbean basalt province revealed by multichannel seismic images of volcanic structures in the Venezuelan basin. *Sedimentary Basins of the World* 4:561–589. [https://doi.org/10.1016/S1874-5997\(99\)80053-7](https://doi.org/10.1016/S1874-5997(99)80053-7)
- Doglioni C, Gueguen E, Harabaglia P, Mongelli F (1999) On the origin of west-directed subduction zones and applications to the western Mediterranean. Geological Society, London, Special Publications 156:541–561
- Dull RA, Southon JR, Sheets P (2001) VOLCANISM, ECOLOGY AND CULTURE: A REASSESSMENT OF THE VOLCAN ILOPANGO TBJ ERUPTION IN THE SOUTHERN MAYA REALM
- Ehlschlaeger C (1989) Using the AT search algorithm to develop hydrologic models from digital elevation data. *International Geographic Information Systems (IGIS) Symposium* 275–281
- Erener A, Düzgün HSB (2012) Landslide susceptibility assessment: What are the effects of mapping unit and mapping method? *Environmental Earth Sciences* 66:859–877. <https://doi.org/10.1007/s12665-011-1297-0>
- Fabbri AG, Chung C-J On Blind Tests and Spatial Prediction Models. <https://doi.org/10.1007/s11053-008-9072-y>
- Faccenna C, Piromallo C, Crespo-Blanc A, et al (2004) Lateral slab deformation and the origin of the western Mediterranean arcs. *Tectonics* 23:. <https://doi.org/10.1029/2002TC001488>
- Fawcett T (2006) An introduction to ROC analysis. *Pattern Recognition Letters* 27:861–874. <https://doi.org/10.1016/j.patrec.2005.10.010>
- Florinsky I v (2012) DIGITAL TERRAIN ANALYSIS IN SOIL SCIENCE AND GEOLOGY
- Friedman JH (1991) Multivariate Adaptive Regression Splines. *The Annals of Statistics* 19:1–67
- García-Rodríguez MJ, Havenith HB, Benito B (2008) Evaluation of earthquake-triggered landslides in El Salvador using a gis- based newmark model
- García-Rodríguez MJ, Malpica JA (2010) Assessment of earthquake-triggered landslide susceptibility in El Salvador based on an artificial neural network model. *Natural*

- Hazards and Earth System Science 10:1307–1315. <https://doi.org/10.5194/nhess-10-1307-2010>
- Goodenough DJ, Rossmann K, Lusted LB (1974) Radiographic Applications of Receiver Operating Characteristic (ROC) Curves I Diagnostic Radiology
- GRASS Development Team (2022) Geographic Resources Analysis Support System (GRASS) Software, Version 8.0. Open Source Geospatial Foundation.
- Gugliotta C, Agate M, Sulli A (2013) Sedimentology and sequence stratigraphy of wedge-top clastic successions: Insights and open questions from the upper Tortonian Terravecchia Formation of the Scillato Basin (central-northern Sicily, Italy). *Marine and Petroleum Geology* 43:239–259. <https://doi.org/10.1016/j.marpetgeo.2013.02.004>
- Guisan A, Weiss SB, Weiss AD (1999) GLM versus CCA Spatial Modeling of Plant Species Distribution. *Plant Ecology* 143:107–122
- Gupta V, Kumar S, Kaur R, Tandon RS (2022) Regional-scale landslide susceptibility assessment for the hilly state of Uttarakhand, NW Himalaya, India. *Journal of Earth System Science* 131:. <https://doi.org/10.1007/s12040-021-01746-4>
- Guzzetti F (2005) Landslide hazard and risk assessment. Thesis Doctoral 373. <https://doi.org/10.1002/9780470012659>
- Guzzetti F, Carrara A, Cardinali M, Reichenbach P (1999) Landslide hazard evaluation: A review of current techniques and their application in a multi-scale study, Central Italy. *Geomorphology* 31:181–216. [https://doi.org/10.1016/S0169-555X\(99\)00078-1](https://doi.org/10.1016/S0169-555X(99)00078-1)
- Guzzetti F, Reichenbach P, Ardizzone F, et al (2006) Estimating the quality of landslide susceptibility models. *Geomorphology* 81:166–184. <https://doi.org/10.1016/j.geomorph.2006.04.007>
- Guzzetti F, Reichenbach P, Cardinali M, et al (2005) Probabilistic landslide hazard assessment at the basin scale. *Geomorphology* 72:272–299. <https://doi.org/10.1016/j.geomorph.2005.06.002>
- Hanley JA, McNeil BJ (1982) The Meaning and Use of the Area under a Receiver Operating Characteristic (ROC) Curve1
- Hart WJ, Steen-McIntyre V (1983) Terra Blanca tephra. Archeology and volcanism in central America 93:1143–1154
- Hosmer DW, Lemeshow Stanley (2000) Applied logistic regression. John Wiley & Sons, Inc.

- Hua Y, Wang X, Li Y, et al (2020) Dynamic development of landslide susceptibility based on slope unit and deep neural networks. *Landslides*. <https://doi.org/10.1007/s10346-020-01444-0>
- Huang F, Cao Z, Guo J, et al (2020) Comparisons of heuristic, general statistical and machine learning models for landslide susceptibility prediction and mapping. *Catena (Amst)* 191:.. <https://doi.org/10.1016/j.catena.2020.104580>
- Hungr O, Leroueil S, Picarelli L (2014) The Varnes classification of landslide types, an update. *Landslides* 11:167–194
- Hutchinson JN (1995) Keynote Paper: Landslide Hazard Assessment. In: *Landslides*, Bell, Ed., Balkema, Rotterdam
- IAEG Commission on Landslides (1990) Suggested Nomenclature for Landslides. In: *Bulletin of the International Association of Engineering Geology*. pp 13–16
- Jacobs L, Kervyn M, Reichenbach P, et al (2020) Regional susceptibility assessments with heterogeneous landslide information: Slope unit- vs. pixel-based approach. *Geomorphology* 356:107084. <https://doi.org/10.1016/j.geomorph.2020.107084>
- Jibson RW, Crone AJ (2001) Observations and Recommendations Regarding Landslide Hazards Related to the M-7.6 El Salvador Earthquake Open-File Report 01-141 Paper Edition
- Jibson RW, Crone AJ, Harp EL, et al (2004a) Landslides triggered by the 13 January and 13 February 2001 earthquakes in El Salvador. In: Rose WI, Bommer JJ, López DL, et al. (eds) *Natural Hazards in El Salvador*. Geological Society of America, p 0
- Jibson RW, Crone AJ, Harp EL, et al (2004b) Landslides triggered by the 13 January and 13 February 2001 earthquakes in El Salvador. In: Rose WI, Bommer JJ, López DL, et al. (eds) *Natural Hazards in El Salvador*. Geological Society of America, p 0
- Lasko TA, Bhagwat JG, Zou KH, Ohno-Machado L (2005) The use of receiver operating characteristic curves in biomedical informatics. *Journal of Biomedical Informatics* 38:404–415. <https://doi.org/10.1016/j.jbi.2005.02.008>
- Lay US, Pradhan B, Yusoff ZBM, et al (2019) Data Mining and Statistical Approaches in Debris-Flow Susceptibility Modelling Using Airborne LiDAR Data. *Sensors* 19:3451. <https://doi.org/10.3390/s19163451>
- Leroueil S., Locat A., Eberhardt E., Kovacevic N. (2012) Progressive failure in natural and engineered slopes. *Landslides and Engineered Slopes. Proceedings, 11th International Symposium on Landslides, Banff*

- Lexa J, Šebesta J, Chavez JA, et al (2011) Geology and volcanic evolution in the southern part of the San Salvador Metropolitan Area. *Journal of Geosciences* 56:105–140. <https://doi.org/10.3190/jgeosci.088>
- Lombardo L, Bachofer F, Cama M, et al (2016) Exploiting Maximum Entropy method and ASTER data for assessing debris flow and debris slide susceptibility for the Giampileri catchment (north-eastern Sicily, Italy). *Earth Surface Processes and Landforms* 41:1776–1789. <https://doi.org/10.1002/esp.3998>
- Lombardo L, Cama M, Conoscenti C, et al (2015) Binary logistic regression versus stochastic gradient boosted decision trees in assessing landslide susceptibility for multiple-occurring landslide events: application to the 2009 storm event in Messina (Sicily, southern Italy). *Natural Hazards* 79:1621–1648. <https://doi.org/10.1007/s11069-015-1915-3>
- Lombardo L, Cama M, Maerker M, Rotigliano E (2014) A test of transferability for landslides susceptibility models under extreme climatic events: Application to the Messina 2009 disaster. *Natural Hazards* 74:1951–1989. <https://doi.org/10.1007/s11069-014-1285-2>
- Lücke OH, Lücke OH, Arroyo IG (2015) Density structure and geometry of the Costa Rican subduction zone from 3-D gravity modeling and local earthquake data. *Solid Earth* 6:1169–1183. <https://doi.org/10.5194/sed-7-1941-2015>
- Major JJ, Schilling SP, Major JJ, et al (2003) Volcanic debris flows in developing countries-The extreme need for public education and awareness of debris-flow hazards Hydrogeomorphic responses to eruptions View project Synthesizing physical and ecological responses to dam removal View project Volcanic debris flows in developing countries-the extreme need for public education and awareness of debris-flow hazards
- Mandal B, Mandal S (2017) Landslide susceptibility mapping using modified information value model in the Lish river basin of Darjiling Himalaya. *Spatial Information Research* 25:205–218. <https://doi.org/10.1007/s41324-017-0096-4>
- Mao Z, Shi S, Li H, et al (2022a) Landslide susceptibility assessment using triangular fuzzy number-analytic hierarchy processing (TFN-AHP), contributing weight (CW) and random forest weighted frequency ratio (RF weighted FR) at the Pengyang county, Northwest China. *Environmental Earth Sciences* 81:. <https://doi.org/10.1007/s12665-022-10193-3>
- Mao Z, Shi S, Li H, et al (2022b) Landslide susceptibility assessment using triangular fuzzy number-analytic hierarchy processing (TFN-AHP), contributing weight (CW) and

- random forest weighted frequency ratio (RF weighted FR) at the Pengyang county, Northwest China. *Environmental Earth Sciences* 81:.. <https://doi.org/10.1007/s12665-022-10193-3>
- Mao Z, Shi S, Li H, et al (2022c) Correction to: Landslide susceptibility assessment using triangular fuzzy number-analytic hierarchy processing (TFN-AHP), contributing weight (CW) and random forest weighted frequency ratio (RF weighted FR) at the Pengyang county, Northwest China (*Environ. Environmental Earth Sciences* 81:.. <https://doi.org/10.1007/s12665-022-10300-4>
- Marineros-Orantes EA, García-González M (2021) Los desastres naturales en El Salvador, una descripción cronológica de sus impactos, 1900-2020. *Revista Iberoamericana de Bioeconomía y Cambio Climático* 7:1610–1935. <https://doi.org/10.5377/ribcc.v7i14.12585>
- MARN (2010a) Síntesis de los informes de evaluación técnica de las lluvias del 7 y 8 de noviembre 2009 en El Salvador: Análisis del impacto físico natural y vulnerabilidad socio ambiental
- MARN (2011) Depresión Tropical 12E/sistema depresionario sobre El Salvador y otros eventos extremos del Pacífico
- MARN (2004) Memoria técnica para el mapa de susceptibilidad de deslizamientos de tierra en El Salvador
- MARN (2010b) 7 y 8 de noviembre 2009 en El Salvador : Análisis del impacto físico natural y vulnerabilidad socio ambiental ” Comisión Técnico Científica : Coordina el Ministerio de Medio Ambiente y Recursos
- Martinello C, Cappadonia C, Conoscenti C, et al (2021) Optimal slope units partitioning in landslide susceptibility mapping. <https://doi.org/10.1080/17445647.2020.1805807>
- Martinello C, Cappadonia C, Conoscenti C, Rotigliano E (2022) Landform classification: a high-performing mapping unit partitioning tool for landslide susceptibility assessment—a test in the Imera River basin (northern Sicily, Italy). *Landslides* 19:539–553. <https://doi.org/10.1007/s10346-021-01781-8>
- McCalpin JP (1984) Preliminary age classification of landslides for inventory mapping
- Meijerink AMJ (1988) Data acquisition and data capture through terrain mapping units. *ITC Jour* 1:23–44
- Mercurio C, Martinello C, Rotigliano E, et al (2021) Mapping Susceptibility to Debris Flows Triggered by Tropical Storms: A Case Study of the San Vicente Volcano Area (El Salvador, CA). *Earth* 2:66–85. <https://doi.org/10.3390/earth2010005>

- Metz M, Mitasova H, Harmon RS (2011) Efficient extraction of drainage networks from massive, radar-based elevation models with least cost path search. *Hydrology and Earth System Sciences* 15:667–678. <https://doi.org/10.5194/hess-15-667-2011>
- Milborrow S (2014) Notes on the earth package. 1–60
- Mokhtari M, Abedian S (2019) Spatial prediction of landslide susceptibility in Taleghan basin, Iran. *Stochastic Environmental Research and Risk Assessment* 33:. <https://doi.org/10.1007/s00477-019-01696-w>
- Morticelli MG, Valenti V, Catalano R, et al (2015) Deep controls on foreland basin system evolution along the Sicilian fold and thrust belt. *Bulletin de la Societe Geologique de France* 186:273–290. <https://doi.org/10.2113/gssgfbull.186.4-5.273>
- Naimi B (2015) Usdm: Uncertainty Analysis for Species Distribution Models. R Package Version 1.1-15. Usdm: Uncertainty Analysis for Species Distribution Models
- Naimi B (2017) Package “usdm”. Uncertainty Analysis for Species Distribution Models. R-Cran 18
- National Research Council (2004) Partnerships for Reducing Landslide Risk: Assessment of the National Landslide Hazards Mitigation Strategy. National Academies Press
- NGI (2013) Landslide Hazard and Risk Assessment in El Salvador Norwegian Geotechnical Institute (NGI) Background Paper Prepared for the Global Assessment Report on Disaster Risk Reduction 2013
- Nhu VH, Shirzadi A, Shahabi H, et al (2020) Shallow landslide susceptibility mapping by Random Forest base classifier and its ensembles in a Semi-Arid region of Iran. *Forests* 11:. <https://doi.org/10.3390/F11040421>
- Nicu IC, Asăndulesei A (2018) GIS-based evaluation of diagnostic areas in landslide susceptibility analysis of Bahluiet River Basin (Moldavian Plateau, NE Romania). Are Neolithic sites in danger? *Geomorphology* 314:27–41. <https://doi.org/10.1016/j.geomorph.2018.04.010>
- Ohlmacher GC (2007) Plan curvature and landslide probability in regions dominated by earth flows and earth slides. *Engineering Geology* 91:117–134. <https://doi.org/10.1016/j.enggeo.2007.01.005>
- Panahi M, Gayen A, Pourghasemi HR, et al (2020) Spatial prediction of landslide susceptibility using hybrid support vector regression (SVR) and the adaptive neuro-fuzzy inference system (ANFIS) with various metaheuristic algorithms. *Science of the Total Environment* 741:. <https://doi.org/10.1016/j.scitotenv.2020.139937>

- Persichillo MG, Bordoni M, Meisina C, et al (2017) Shallow landslides susceptibility assessment in different environments. *Geomatics, Natural Hazards and Risk* 8:748–771. <https://doi.org/10.1080/19475705.2016.1265011>
- Petschko H, Brenning A, Bell R, et al (2014) Assessing the quality of landslide susceptibility maps - Case study Lower Austria. *Natural Hazards and Earth System Sciences* 14:95–118. <https://doi.org/10.5194/nhess-14-95-2014>
- Poiraud A (2014) Landslide susceptibility-certainty mapping by a multi-method approach: A case study in the Tertiary basin of Puy-en-Velay (Massif central, France). *Geomorphology* 216:208–224. <https://doi.org/10.1016/j.geomorph.2014.04.001>
- Pourghasemi HR, Gayen A, Edalat M, et al (2020) Is multi-hazard mapping effective in assessing natural hazards and integrated watershed management? *Geoscience Frontiers* 11:1203–1217. <https://doi.org/10.1016/j.gsf.2019.10.008>
- Pourghasemi HR, Rossi M (2017) Landslide susceptibility modeling in a landslide prone area in Mazandarn Province, north of Iran: a comparison between GLM, GAM, MARS, and M-AHP methods. *Theoretical and Applied Climatology* 130:609–633. <https://doi.org/10.1007/s00704-016-1919-2>
- Pulice I, Cappadonia C, Scarciglia F, et al (2012) Geomorphological, chemical and physical study of “calanchi” landforms in NW Sicily (southern Italy). *Geomorphology* 153–154:219–231. <https://doi.org/10.1016/j.geomorph.2012.02.026>
- QGIS.org (2022) QGIS Geographic Information System
- Qin S, Lv J, Cao C, et al (2019) Mapping debris flow susceptibility based on watershed unit and grid cell unit: a comparison study. *Geomatics, Natural Hazards and Risk* 10:1648–1666. <https://doi.org/10.1080/19475705.2019.1604572>
- Regmi AD, Poudel K (2016) Assessment of landslide susceptibility using GIS-based evidential belief function in Patu Khola watershed, Dang, Nepal. *Environmental Earth Sciences* 75:. <https://doi.org/10.1007/s12665-016-5562-0>
- Regmi AD, Yoshida K, Pourghasemi HR, et al (2014) Landslide susceptibility mapping along Bhalubang — Shiwapur area of mid-Western Nepal using frequency ratio and conditional probability models. *Journal of Mountain Science* 11:1266–1285. <https://doi.org/10.1007/s11629-013-2847-6>
- Reichenbach P, Rossi M, Malamud BD, et al (2018) A review of statistically-based landslide susceptibility models. *Earth-Science Reviews* 180:60–91. <https://doi.org/10.1016/j.earscirev.2018.03.001>

- Riley SJ, DeGloria SD, Elliot R (1999) Terrain_Ruggedness_Index.pdf. *Intermountain Journal of Science* 5:23–27
- Rolo R, Bommer JJ, Houghton BF, et al (2004) Geologic and engineering characterization of Tierra Blanca pyroclastic ash deposits. *Special Paper of the Geological Society of America* 375:55–67. <https://doi.org/10.1130/0-8137-2375-2.55>
- Rotigliano E, Agnesi V, Cappadonia C, Conoscenti C (2011) The role of the diagnostic areas in the assessment of landslide susceptibility models: A test in the sicilian chain. *Natural Hazards* 58:981–999. <https://doi.org/10.1007/s11069-010-9708-1>
- Rotigliano E, Cappadonia C, Conoscenti C, et al (2012) Slope units-based flow susceptibility model: Using validation tests to select controlling factors. *Natural Hazards* 61:143–153. <https://doi.org/10.1007/s11069-011-9846-0>
- Rotigliano E, Martinello C, Agnesi V, Conoscenti C (2018) Evaluation of debris flow susceptibility in El Salvador (CA): a comparison between Multivariate Adaptive Regression Splines (MARS) and Binary Logistic Regression (BLR). *Hungarian Geographical Bulletin* 67:361–373. <https://doi.org/10.15201/hungeobull.67.4.5>
- Rotigliano E, Martinello C, Hernández MA, et al (2019) Predicting the landslides triggered by the 2009 96E/Ida tropical storms in the Ilopango caldera area (El Salvador, CA): optimizing MARS-based model building and validation strategies. *Environmental Earth Sciences* 78:. <https://doi.org/10.1007/s12665-019-8214-3>
- RStudio Team (2020) RStudio: Integrated Development for R.
- Rubin DB (1987) Multiple imputation for nonresponse in surveys. Wiley
- Sajadi P, Sang Y-F, Gholamnia M, et al (2022) Evaluation of the landslide susceptibility and its spatial difference in the whole Qinghai-Tibetan Plateau region by five learning algorithms. *Geoscience Letters* 9:. <https://doi.org/10.1186/s40562-022-00218-x>
- Sameen MI, Pradhan B, Bui DT, Alamri AM (2020) Systematic sample subdividing strategy for training landslide susceptibility models. *Catena (Amst)* 187:. <https://doi.org/10.1016/j.catena.2019.104358>
- Schmidt-Thomé M (1975) The geology in the San Salvador area (El Salvador, Central America), a basis for city development and planning
- Sinharay S (2010) An overview of statistics in education. *International Encyclopedia of Education* 1–11. <https://doi.org/10.1016/B978-0-08-044894-7.01719-X>
- Skempton AW, Hutchinson JN (1969) Stability of natural slopes and embankment foundations. *Proceedings, 7th. International conference of soil mechanics and foundation engineering* 291–340

- Steger S, Brenning A, Bell R, Glade T (2017) The influence of systematically incomplete shallow landslide inventories on statistical susceptibility models and suggestions for improvements. *Landslides* 14:1767–1781. <https://doi.org/10.1007/s10346-017-0820-0>
- Steger S, Mair V, Kofler C, et al (2021) Correlation does not imply geomorphic causation in data-driven landslide susceptibility modelling – Benefits of exploring landslide data collection effects. *Science of the Total Environment* 776:.. <https://doi.org/10.1016/j.scitotenv.2021.145935>
- Stoiber RE, Carr MJ (1973) Quaternary volcanic and tectonic segmentation of Central America. *Bulletin Volcanologique* 37:304–325. <https://doi.org/10.1007/BF02597631>
- Sujatha ER, Kumaravel P, Rajamanickam GV (2014) Assessing landslide susceptibility using Bayesian probability-based weight of evidence model. *Bulletin of Engineering Geology and the Environment* 73:147–161. <https://doi.org/10.1007/s10064-013-0537-9>
- Sun X, Chen J, Han X, et al (2020) Application of a GIS-based slope unit method for landslide susceptibility mapping along the rapidly uplifting section of the upper Jinsha River, South-Western China. *Bulletin of Engineering Geology and the Environment* 79:533–549. <https://doi.org/10.1007/s10064-019-01572-5>
- Swanston D.N. (1974) Slope stability problems associated with timber harvesting in mountainous regions of the Southwestern United States, U. S. . Washington, DC
- Terzaghi K (1950) Mechanism of Landslides. . In: *Application of Geology to Engineering Practice*. Geological Society of America, pp 83–123
- The World Bank Group (2021) Climate Change Knowledge Portal. <https://climateknowledgeportal.worldbank.org/>. Accessed 14 Apr 2022
- van den Eeckhaut M, Hervás J, Jaedicke C, et al (2012) Statistical modelling of Europe-wide landslide susceptibility using limited landslide inventory data. *Landslides* 9:357–369. <https://doi.org/10.1007/s10346-011-0299-z>
- Van Den Eeckhaut M, Reichenbach P, Guzzetti F, et al (2009) Combined landslide inventory and susceptibility assessment based on different mapping units: An example from the Flemish Ardennes, Belgium. *Natural Hazards and Earth System Science* 9:507–521. <https://doi.org/10.5194/nhess-9-507-2009>
- van Westen CJ, Rengers N, Terlien MTJ, Soeters R (1997) Prediction of the occurrence of slope instability phenomena through GIS-based hazard zonation. 86:404–414
- Vargas-Cuervo G, Rotigliano E, Conoscenti C (2019) Prediction of debris-avalanches and -flows triggered by a tropical storm by using a stochastic approach: An application to

- the events occurred in Mocoa (Colombia) on 1 April 2017. *Geomorphology* 339:31–43. <https://doi.org/10.1016/j.geomorph.2019.04.023>
- Varnes D. J (1984) *Landslide Hazard Zonation: A Review of Principles and Practice*. Paris
- Varnes David J. (1978) Slope Movement Types and Processes. In: R.L. Schuster and R.J. Krizek (ed) *Special Report 176*. National Research Council, Washington, D.C.
- von Ruettele J, Papritz A, Lehmann P, et al (2011) Spatial statistical modeling of shallow landslides-Validating predictions for different landslide inventories and rainfall events. *Geomorphology* 133:11–22. <https://doi.org/10.1016/j.geomorph.2011.06.010>
- Wang Q, Li W, Wu Y, et al (2016) A comparative study on the landslide susceptibility mapping using evidential belief function and weights of evidence models
- Wilson JP, Gallant JC (2000a) *Terrain Analysis: Principles and Applications*
- Wilson JP, Gallant JC (2000b) Primary Topographic Attributes. In: Wilson JP, Gallant JC (eds) *Terrain Analysis: Principles and Applications*. John Wiley & Sons
- Wisz MS, Guisan A (2009) Do pseudo-absence selection strategies influence species distribution models and their predictions? An information-theoretic approach based on simulated data. *BMC Ecology* 9:1–13. <https://doi.org/10.1186/1472-6785-9-8>
- Xie Z, Chen G, Meng X, et al (2017) A comparative study of landslide susceptibility mapping using weight of evidence, logistic regression and support vector machine and evaluated by SBAS-InSAR monitoring: Zhouqu to Wudu segment in Bailong River Basin, China. *Environmental Earth Sciences* 76:. <https://doi.org/10.1007/s12665-017-6640-7>
- Youden WJ (1950) Index for rating diagnostic tests. *Cancer* 3:32–35. [https://doi.org/10.1002/1097-0142\(1950\)3:1<32::AID-CNCR2820030106>3.0.CO;2-3](https://doi.org/10.1002/1097-0142(1950)3:1<32::AID-CNCR2820030106>3.0.CO;2-3)
- Youssef AM, Pourghasemi HR, Pourtaghi ZS, Al-Katheeri MM (2016) Landslide susceptibility mapping using random forest, boosted regression tree, classification and regression tree, and general linear models and comparison of their performance at Wadi Tayyah Basin, Asir Region, Saudi Arabia. *Landslides* 13:839–856. <https://doi.org/10.1007/s10346-015-0614-1>
- Zevenbergen LW, Thorne CR (1987) Quantitative analysis of land surface topography. *Earth Surface Processes and Landforms* 12:47–56. <https://doi.org/https://doi.org/10.1002/esp.3290120107>

- Zêzere JL, Pereira S, Melo R, et al (2017) Mapping landslide susceptibility using data-driven methods. *Science of the Total Environment* 589:250–267.
<https://doi.org/10.1016/j.scitotenv.2017.02.188>
- Zhang T, Han L, Han J, et al (2019) Assessment of landslide susceptibility using integrated ensemble fractal dimension with Kernel logistic regression model. *Entropy* 21:.
<https://doi.org/10.3390/e21020218>

*The only way to do great work
is to love what you do*

Steve Jobs

Alla fine di un percorso lungo e sicuramente non semplice, ringraziare chi mi ha portato al traguardo è la minima cosa che possa fare.

Sono stati tre anni particolari in cui la mia vita è cambiata radicalmente sotto tanti punti di vista.

Fare ricerca è complicato... Poche prospettive e tanti bastoni tra le ruote.

Ma sono una piccola ricercatrice fortunata io.

Ho trovato una piccola famiglia che mi ha accolto (il DiSTeM), un tutor che mi è stato accanto e tanti colleghi e amici che mi hanno accompagnato nel percorso.

Ho trovato una guida che poi si è rivelata anche una carissima amica, che sopporta ogni giorno me e la mia esultanza per ogni piccola cosa.

E poi, ho trovato un mentore che ha creduto in me (e chissà perché) dal primo anno di magistrale e mi ha supportato e sopportato fino all'ultimo giorno di questo percorso. Se qualcosa di buono ho fatto, è solo perché ho un gran maestro.

At least but not last, ho un consigliere, amico e marito fantastico, un piccolo ometto arrivato proprio in corsa, una madre meravigliosa, un fratello e una sorella che ogni giorno tifano per me e i miei successi, che con i loro sorrisi e abbracci mi sollevano dai momenti difficili.

L'ho già detto che sono una piccola ricercatrice fortunata?

Grazie

Chiara